

Distribution Agreement

In presenting this thesis or dissertation as a partial fulfillment of the requirements for an advanced degree from Emory University, I hereby grant to Emory University and its agents the non-exclusive license to archive, make accessible, and display my thesis or dissertation in whole or in part in all forms of media, now or hereafter known, including display on the world wide web. I understand that I may select some access restrictions as part of the online submission of this thesis or dissertation. I retain all ownership rights to the copyright of the thesis or dissertation. I also retain the right to use in future works (such as articles or books) all or part of this thesis or dissertation.

Signature:

Felicia Annette Fullilove

Date

In Situ Kinetic Studies of Reactions Involving Dirhodium(II) Donor/Acceptor Carbenes

By
Felicia Annette Fullilove
Doctor of Philosophy
Chemistry

Dr. Huw M. L. Davies
Advisor

Dr. Simon Blakey
Committee Member

Dr. Frank McDonald
Committee Member

Accepted:

Lisa A. Tedesco, Ph.D.
Dean of the James T. Laney School of Graduate Studies

Date

***In Situ* Kinetic Studies of Reactions Involving Dirhodium(II) Donor/Acceptor
Carbenes**

By
Felicia Annette Fullilove
B.S. Butler University, 2008

Advisor: Huw M. L. Davies, PhD

An abstract of
A dissertation submitted to the Faculty of the
James T. Laney School of Graduate Studies of Emory University
in partial fulfillment of the requirements for the degree of
Doctor of Philosophy
in Chemistry
2014

Abstract

In Situ Kinetic Studies of Reactions Involving Dirhodium(II) Donor/Acceptor Carbenes

By Felicia Annette Fullilove

The exceptional reactivity of dirhodium(II) donor/acceptor carbenes has made them key intermediates in organic synthesis. New reaction development and application to natural products synthesis has displayed the power of dirhodium(II) donor/acceptor carbenes. The breadth of transformations that can be conducted include C-H functionalization, ylide formation, cyclopropanation, N-H, O-H and Si-H insertion. Moreover, the advent of chiral catalysts has rendered many of these transformations asymmetric. These catalysts are extremely active and in special cases are capable of very high turnover numbers. However, the high turnover capability is very dependent on the substrates used, and a general problem is the occurrence of a major drop in the levels of enantioselectivity when low catalyst loadings are used. Research to date has not pinpointed the cause of the catalyst failure, and this seriously limits the practical utility of such an expensive catalyst and its application as an immobilized catalyst or in flow chemistry. The purpose of the work described in this thesis is to gain a better understanding of the factors that govern catalysts activity and stability, especially under high turnover conditions.

The two major goals of the thesis are to (1) explore modes of catalyst deactivation/ decomposition *via* kinetic analysis and (2) demonstrate how kinetic understanding can aid in natural product synthesis. These goals have been undertaken through detailed kinetic analysis for three classic dirhodium(II) carbenoid reactions and application of the kinetic knowledge gained to a synthetic approach for a complex natural product. Particular interest has focused on cyclopropanation of styrene. The selectivity of this standard reaction and ability for the catalyst to achieve high turnover numbers under solvent-free conditions has been extensively studied; however, the stability of the catalyst is not well understood. A more challenging reaction, C-H insertion into activated and unactivated C-H bonds was explored because high TONs have yet to be achieved for these reactions. Si-H insertion is a reaction that has shown to be very robust for dirhodium(II) carbenoid catalysis. Therefore, understanding factors attributing the high activity of the catalyst is integral. Finally, application of the kinetic analysis to address relative rate challenges in a project directed towards the synthesis of phorbol was undertaken. The introductory chapter will outline critical background material for understanding the motivation behind the kinetic studies.

***In Situ* Kinetic Studies of Reactions Involving Dirhodium(II) Donor/Acceptor
Carbenes**

By
Felicia Annette Fullilove
B.S. Butler University, 2008

Advisor: Huw M. L. Davies, PhD

A dissertation submitted to the Faculty of the
James T. Laney School of Graduate Studies of Emory University
in partial fulfillment of the requirements for the degree of
Doctor of Philosophy
in Chemistry
2014

Acknowledgements

The past five years have been a remarkable experience. In this section, I would like to acknowledge the individuals that have assisted my professional and personal growth both directly and indirectly.

First, I would like to thank my advisor, Dr. Huw Davies, for accepting me into his research group. Dr. Davies gave me the freedom to explore areas of science outside of traditional synthetic organic chemistry and I will be forever grateful for that opportunity. I have learned a great deal from him and his ability to undertake immense challenges. Dr. Davies always has a positive outlook and his role as a leader has helped me grow as a scholar and scientist.

During my time at Emory, there are several professors whom have impacted my professional development. First, I would also like to thank my committee members Dr. Simon Blakey and Dr. Frank McDonald. Both have been extremely supportive throughout this process and have challenged me to be a more critical thinker. Additionally, I would like to thank Dr. Cora MacBeth and Dr. Patria Marsteller, whom have both acted as mentors. Special thanks to Dr. MacBeth who allowed for me to write my dissertation in her laboratory!

I have had the opportunity to make a number of lifelong connections at Emory, both professionally and personally. Thank you to all of the members of the Davies group for their support and memories. Special thanks to past and present Davies group members Kathryn Chepiga, Dr. Pablo Guzman, Dr. Nicholas Brunelli, Dr. Yajing Lian, Dr. Etienne Nadeau, Dr. Fred Briones, and Changming Qin for being great friends and colleagues.

None of this would have been possible without your in-lab support. Additionally, thanks to Dr. Daniel Morton, who in many ways taught me how to be a leader in the laboratory. Friends outside of the Davies lab, including Jen Bon, Clay Owens, and Omar Villanueva thank you for listening to my crazy antics and giving me feedback when necessary.

One of the most memorable parts of my graduate experience has been my involvement with the NSF Center for Selective C-H Functionalization. Through the Center, I have had the opportunity to collaborate and connect with numerous students and professors outside of Emory University. Specifically, my involvement with Dr. Donna Blackmond at the Scripps Research Institute has truly been a highlight. The opportunity to learn reaction kinetics from the world's expert is an opportunity I will never forget. The ability to travel to another laboratory was an amazing experience, and I hope other students take advantage of all the Center can offer. Special thanks to the Blackmond research group for all of their help throughout the final year of my PhD.

I would like to thank my friends and family for their love and support. None of this would have been possible without the support of great friends and family. To my grandmother and aunt whom sparked my interest in science, thank you! I also would like to thank my best friend, Tia, for constantly giving me words of encouragement. The silly things we talk about have made this experience so much easier.

Finally, I have to thank my parents and brother, Hollis. Without my family, I do not think I would have made it to this point. I can only hope that I make you all proud. Thank you mom and dad for supporting me in being a life-long learner.

For God, mom, dad and Hollis

TABLE OF CONTENTS

CHAPTER 1: Introduction to Dirhodium(II) Carbene Chemistry	1
1.1 Description of Chapter.....	1
1.2 Classes of Metallocarbenoids	2
1.3 Dirhodium (II) Catalysts.....	4
1.4 Reactivity of Dirhodium(II) Carbenoids.....	6
1.5 Site- and Chemo-selectivity of Dirhodium Donor/Acceptor Carbenoids for C-H Functionalization.....	8
1.6 Mechanistic Studies of Dirhodium(II) Carbenoid Carbenes.....	11
1.6.1 Proposed Mechanism.....	11
1.6.2 Isolation of the Dirhodium(II) Carbene.....	12
1.6.3 KIE Analysis.....	13
1.6.4 Hammett Analysis	15
1.6.5 Computational Analysis.....	17
1.6.6 Michealis-Menten Kinetics.....	18
1.7 Coordination to the Dirhodium Core and Catalyst Decomposition.....	20
1.8 Technique: Reaction Progress Kinetic Analysis	21
1.9 Description of Thesis	32
CHAPTER 2: Kinetic Studies on the Donor/Acceptor Dirhodium(II) Carbene Cyclopropanation of Styrene	42
2.1 Background.....	42
2.1.1 Dirhodium Catalysts High TON.....	43
2.2 Results.....	45
2.2.1 Dirhodium(II) Catalyst Screening.....	47
2.2.2 RPKA Studies.....	56
2.2.3 Mechanism and Rate Law.....	64
2.2.4 Reaction Calorimetry.....	69
2.2.5 Addition Experiments.....	74
2.2.6 Unusual Kinetics for methyl <i>p</i> -methoxy-phenyldiazoacetate.....	82
2.3 Discussion and Conclusions.....	88
2.4 Experimental.....	94
CHAPTER 3: Kinetic Studies on Donor/Acceptor Dirhodium(II) Carbene C-H Functionalization	112
3.1 Background.....	112

3.2 Results.....	113
3.2.1 RPKA for C-H insertion into 1,4-Cyclohexadiene.....	113
3.2.2 High TON for C-H Insertion into 1,4-Cyclohexadiene.....	122
3.2.3. Reaction Calorimetry.....	124
3.2.4 Bridging vs. Non Bridging Catalysts	125
3.2.5 Exploration of MK-1-235.....	129
3.2.6 C-H insertion into Cyclohexane.....	131
3.3 Discussion and Conclusions.....	133
3.4 Experimental.....	135
CHAPTER 4: Kinetic Studies on Donor/Acceptor Dirhodium(II) Carbene Si-H Insertion.....	144
4.1 Background.....	144
4.2 Project Logic.....	146
4.3 Results.....	147
4.3.1. Si-H Kinetic Studies.....	147
4.3.2 Reaction Calorimetry	151
4.3.3 Further Kinetic Screening for Si-H Insertion.....	158
4.4 Discussion and Conclusions.....	165
4.5 Experimental.....	166
CHAPTER 5: Kinetic Studies for the Dirhodium(II) Mediated Reactions of a Chemically Non-equivalent Bis-Diazo Compound.....	171
5.1 Background.....	171
5.1.1 Bis-Diazo Compounds.....	172
5.2 Dr. Guzman's Results.....	176
5.3 Goals of This Work.....	179
5.4 Results.....	180
5.4.1 Kinetic Experiments of Diazo Compounds 31, 32, 33.....	180
5.4.2 Competition Studies.....	184
5.4.3 Kinetic Studies of the Bis-Diazo Compounds.....	192

5.5 Discussion and Conclusions	197
5.6 Experimental	199

LIST OF FIGURES

Figure 1.1: Functional group modification compared to C-H functionalization.....	2
Figure 1.2: Classes of Diazo Compounds.....	3
Figure 1.3 Various Dirhodium Catalysts used for C-H Functionalization.....	4
Figure 1.4: Inherent Reactivity of Transient Metal Carbenoids.....	7
Figure 1.5: ^{13}C KIE for Cyclopropanation of Styrene.	13
Figure 1.6: Hammett Plot for Cyclopropanation of Styrene Analogs with Diazoacetate 1	15
Figure 1.7: Traditional Kinetic Plots.....	22
Figure 1.8: Same Excess Plot.....	27
Figure 1.9: Different Excess Plot.....	28
Figure 2.1: Three-dimensional FTIR spectrum of diazo compound 1 recorded with a Mettler Toledo ReactIR TM 45M.....	46
Figure 2.2: Dirhodium(II) catalysts screened in the cyclopropanation of styrene.....	47
Figure 2.3: Plot generated from ReactIR TM data depicting time(min) versus concentration of 1 for reaction of 2 (3.0 M) catalyzed by $\text{Rh}_2(\text{S-DOSP})_4$ (0.005 mol%) in hexanes at 0 °C.	49
Figure 2.4: Plot of the reaction rate (v (M/min)) versus concentration of 1 for reaction of 2 (3.0 M) catalyzed by $\text{Rh}_2(\text{S-DOSP})_4$ (0.005 mol%) in hexanes at 0 °C.....	60

Figure 2.5: Kinetic activity of chiral dirhodium(II) catalysts screening in reaction of **1** (0.3 M) with **2** (3.0 M) at 0.005 mol% of Rh(II) catalyst in hexanes at 0 °C.....52

Figure 2.6: Kinetic activity of achiral dirhodium(II) catalysts in the reaction of **1** (0.3 M) and **2** (3.0 M) with 0.005 mol% of Rh(II) catalyst in hexanes at 0 °C.....55

Figure 2.7: Reaction rate ν (M/min) versus concentration of **1** for the reaction of **2** with Rh₂(*S*-DOSP)₄ in hexanes at 0 °C. The concentration of [Rh] is varied.....58

Figure 2.8: Reaction rate ν (M/min) versus time (min) for the reaction of **1** with **2**(3.0 M) with Rh₂(*S*-DOSP)₄ (0.005 mol%) in hexanes at 0 °C. The concentration of **1** is varied.59

Figure 2.9: Reaction rate ν (M/min) versus concentration of **1** for the reaction of **1** (0.3 M) with **2** catalyzed by Rh₂(*S*-DOSP)₄ (0.005 mol%). The dependence on **2** was varied.....60

Figure 2.10: Reaction rate ν (M/min) versus concentration **1** in reaction with **2** catalyzed by Rh₂(*S*-DOSP)₄ (0.005 mol%) in hexanes at 0 °C.....62

Figure 2.11: Reaction rate ν (M/min) versus concentration of **1** (0.3M) in reaction with **2** (3.0M) catalyzed by Rh₂(*S*-DOSP)₄ in hexanes at 0 °C.....63

Figure 2.12: On-cycle and Off-cycle elementary steps for the cyclopropanation of **2** (3.0 M) with **1** (0.3 M) catalyzed by $\text{Rh}_2(\text{S-DOSP})_4$ (0.005 mol%) in hexanes at 0 °C.....66

Figure 2.13: Standard heat flow (mW) versus time (min) for reaction of **1** (1.0 M) with **2** (15.0 M) catalyzed by $\text{Rh}_2(\text{S-DOSP})_4$ (0.007 mol%) in dichloromethane at 10 °C.....70

Figure 2.14: Heat flow (mW) versus time (min) for five successive injections of **1** (1.0 M) in the reaction of **2** (15.0 M) catalyzed by $\text{Rh}_2(\text{S-DOSP})_4$ (0.007 mol%) in dichloromethane at 10 °C.....71

Figure 2.15: Heat flow (mW) versus time (min) for 10 successive injections of **1** (1.0 M) in the reaction of **2** (15.0 M) catalyzed by $\text{Rh}_2(\text{S-DOSP})_4$ (0.0007 mol%) in dichloromethane at 10 °C.....72

Figure 2.16: Heat flow (mW) versus time (min) for five successive 1.0 M injections of **1** into a 5.0M solution of **2** catalyzed by $\text{Rh}_2(\text{S-DOSP})_4$ (0.007 mol%) in dichloromethane at 10 °C.....73

Figure 2.17: Baseline addition plot. Concentration of **1**(M) versus time (min) for the catalyst free addition of **1** (0.5 M) with **2** (3.0 M) in hexanes at 25 °C.....75

Figure 2.18: Concentration of **1** (M) and % ee of **3** versus time (min) for the slow addition of a 2:1 mixture of **2** and **1** to a solution of Rh₂(*S*-DOSP)₄ (0.001 mol%) in hexanes at 25 °C.....77

Figure 2.19: Concentration of **1** (M) and % ee of **3** versus time (min) for the slow addition of **1** (0.5 M) into a solution of **2** (3.0 M) and Rh₂(*S*-DOSP)₄ (0.001 mol%) in hexanes at 25 °C.....79

Figure 2.20: Concentration of **1** (M) and % ee of **3** versus time (min) for the slow addition of **1** (0.5 M) into a solution of **2** (3.0 M) and Rh₂(*S*-DOSP)₄ (0.001 mol%) in hexanes at 68 °C.....81

Figure 2.21: Relative rate of reaction for *p*-substituted aryl diazo compounds.....84

Figure 2.22: Reaction rate comparison for **1a** and **1b** under high TON conditions of 0.3 M (**1a** or **1b**) in reaction with **2** (3.0 M) catalyzed by Rh₂(*S*-DOSP)₄ (0.005 mol%) in hexanes at 0 °C.....85

Figure 2.23: Reaction rate comparison for diazo compound **1b** (0.3 M) in reaction with **2** (0.6 M = blue, 1.5 M = green, 3.0M = pink, 6.0 M = teal) catalyzed by Rh₂(*S*-DOSP)₄ (0.005 mol%) in hexanes at 0 °C.....87

Figure 2.24: UV-Vis titration of the catalyst with styrene, conducted by Dr. Nicholas Brunelli.....	91
Figure 2.25: Plot of the peak height (A.U.) versus relative time (hh:mm:ss) of 1 for reaction of 2 (3.0 M) catalyzed by $\text{Rh}_2(\text{S-DOSP})_4$ (0.005 mol%) in hexanes at 0 °C.....	99
Figure 2.26: Calibration Curve for Methyl Phenyl diazoacetate	100
Figure 2.27: Plot generated from ReactIR TM data depicting concentration of 1a versus time (min) for reaction of 2 (3.0 M) catalyzed by $\text{Rh}_2(\text{S-DOSP})_4$ (0.005 mol%) in hexanes at 0 °C.....	102
Figure 2.28: Plot of the reaction rate (v (M/min)) versus concentration of 1 for reaction of 2 (3.0 M) catalyzed by $\text{Rh}_2(\text{S-DOSP})_4$ (0.005 mol%) in hexanes at 0 °C.....	103
Figure 2.29: Tau corrected plot for multiple injection experiment (raw data). Heat flow (mW) versus time (min) for 10 successive injections of 1 (1.0 M) in the reaction of 2 (15.0 M) catalyzed by $\text{Rh}_2(\text{S-DOSP})_4$ (0.0007 mol%) in dichloromethane at 10 °C.....	105
Figure 3.1: Standard kinetic plots for the reaction of 1 (0.3 M) with 2 (0.3 M) catalyzed by $\text{Rh}_2(\text{S-DOSP})_4$ (0.01 mol%) in hexanes at 0 °C.....	114

Figure 3.2: Influence of increasing concentration of **2** for the reaction of **1** (0.3 M blue and green) with **2** (0.3 M blue, 0.6M green) catalyzed by $\text{Rh}_2(\text{S-DOSP})_4$ (0.01 mol%) in hexanes at 0 °C.....115

Figure 3.3: Influence of decreasing concentration of $\text{Rh}_2(\text{S-DOSP})_4$ for the reaction of **1** (0.3 M blue and red) with **2** (0.3 M blue, and green) catalyzed by $\text{Rh}_2(\text{S-DOSP})_4$ (0.005 mol% -Red, 0.01 mol% - Blue) in hexanes at 0 °C.....116

Figure 3.4: Influence of decreasing concentration of **1** for the reaction of **1** (0.3 M blue and 0.15 M purple) with **2** (0.3 M blue, and purple) catalyzed by $\text{Rh}_2(\text{S-DOSP})_4$ (0.01 mol% - blue and purple) in hexanes at 0 °C.....117

Figure 3.5: Same excess experiment for the reaction of **1** (0.3 M blue and 0.6 M teal) with **2** (0.3 M blue, and 0.6 M teal) catalyzed by $\text{Rh}_2(\text{S-DOSP})_4$ (3.0×10^{-5} M - blue and teal) in hexanes at 0 °C.....118

Figure 3.6: Product doping experiment containing **3** (0.3 M for brown curve, 0.0 M for blue) for the reaction of **1** (0.3 M blue and brown) with **2** (0.3 M blue and brown) catalyzed by $\text{Rh}_2(\text{S-DOSP})_4$ (3.0×10^{-5} M - blue and brown) in hexanes at 0 °C.....119

Figure 3.7: Concentration of **1** (M) and % ee of **2** versus time (min) for the slow addition of **1** (0.375M) to a solution of **5** (3.0 M) catalyzed by $\text{Rh}_2(\text{S-DOSP})_4$ (0.001 mol%) in hexanes at 25 °C.....123

Figure 3.8: Heat flow (mW) versus time (min) for 10 successive injections of 1 (1.0 M) in the reaction of 5 (15.0 M) catalyzed by Rh ₂ (S-DOSP) ₄ (0.0007 mol%) in dichloromethane at 10 °C.....	124
Figure 3.9 Dirhodium(II) catalysts screened.....	126
Figure 3.10: Peak height of 1 (A.U.) versus relative time (hh:mm:ss) for the TOF comparison between nonbridged dirhodium(II) catalyst Rh ₂ (S-PTAD) ₄ (0.005 mol%) and bridging catalyst KWF-V-049 (0.005 mol%) for the reaction of 1 (0.3 M) with 5 (1.5 M) in dichloromethane at 25 °C.....	128
Figure 3.11: Du Bois' catalyst MK-1-235.....	129
Figure 3.12: Kinetic profile of MK-1-235 (0.005 mol%) for the reaction of 1 (0.3 M) with 5 (1.5 M).....	130
Figure 3.13: Plot of the peak height (A.U.) versus relative time (hh:mm:ss) of 1 for reaction of 2 (3.0 M) catalyzed by Rh ₂ (S-DOSP) ₄ (0.005 mol%) in hexanes at 0°C.....	136
Figure 4.1: The initial rate of the reaction (v (M/s)) for the first 5 sec versus concentration of silane 4 (0.2-2.5 M) for the reaction of 3 (0.6 M) catalyzed by Rh ₂ (S-DOSP) ₄ (0.005 mol%) in dichloromethane at 10 °C.....	148

Figure 4.2: The initial rate of the reaction (v (M/s)) for the first 5 sec versus concentration of **3** (0.2-0.9 M) for the reaction of **4** (1.2 M) catalyzed by $\text{Rh}_2(\text{S-DOSP})_4$ (0.005 mol%) in dichloromethane at 10 °C.....149

Figure 4.3: The initial rate of the reaction (v (M/s)) for the first 5 sec versus concentration of $\text{Rh}_2(\text{S-DOSP})_4$ (0.00001-0.000045 M) for the reaction of **4** (1.2 M) and **3** (0.4 M) in dichloromethane at 10 °C.....150

Figure 4.4: Multiple injection calorimetry. The heat flow of the reaction (mW) versus reaction time (min) for the reaction of **4** (1.2 M) with 0.2 mL injections of **3** (7.5 M) catalyzed by $\text{Rh}_2(\text{S-DOSP})_4$ (0.007 mol%) in dichloromethane at 10 °C.....152

Figure 4.5: The heat flow of the reaction (mW) versus reaction time (min) for the reaction of **4** (1.2 M) with one 0.2 mL injection of **3** (4.5 mmol) catalyzed by $\text{Rh}_2(\text{S-DOSP})_4$ (0.007 mol%) in dichloromethane at 10 °C.....144

Figure 4.6: The heat flow of the reaction (mW) versus reaction time (min) for the reaction of **4** (1.2 M) with 0.2 mL injections of **3** (7.5 M) and additive **6** (7.5M) in the reaction mixture. The reaction is catalyzed by $\text{Rh}_2(\text{S-DOSP})_4$ (0.007 mol%) in dichloromethane at 10 °C.....156

Figure 4.7: Potential reaction mechanism for dirhodium(II) carbenoid Si-H insertion into dimethylphenylsilane.....158

Figure 4.8: Two runs of Peak Height (A.U.) versus time (sec) for the first 5 seconds in the reaction of 4 (1.2 M) and 3 (0.4 M) catalyzed by Rh ₂ (S-DOSP) ₄ (0.0005 mol%) in dichloromethane at 10 °C.....	167
Figure 5.1: Generic Bis-Diazo Compound.....	171
Figure 5.2: Bis-diazo compounds synthesized by Dr. Guzman for model study.....	172
Figure 5.3: Diazo compounds explored in this study.....	173
Figure 5.4: Plot of Abs vs Time for 31 (0.6 M) and 33 (0.6 M) in the presence of furan (6.0 M) and Rh ₂ (S-PTAD) ₄ (0.01 mol%)	184
Figure 5.5: The competition reaction between 32 (0.6 M) and 33 (0.6 M) with furan (6.0 M) in the presence of (Rh ₂ (S- PTAD) ₄) 0.01 mol%	185
Figure 5.6: The competition reaction between 31 (0.6 M) and 34 (0.6 M) in the presence of furan (6.0 M) and Rh ₂ (S-PTAD) ₄ (0.01 mol%)	186
Figure 5.7: The competition reaction between 32 (0.6 M) and 34 in (0.6 M) the presence of furan (6.0 M) and Rh ₂ (S-PTAD) ₄ (0.01 mol%).....	187

Figure 5.8: The competition reaction between **31** (0.6 M) and **34** (0.6 M) in the presence of diene **26** (6.0 M) and $\text{Rh}_2(\text{S-PTAD})_4$ (0.01 mol%).....189

Figure 5.9: The competition reaction between diazo compound **31** (0.6 M) and **34** (0.6 M) in the presence of **26** (6.0 M), and 0.01 mol% 1:1 $\text{Rh}_2(\text{S-DOSP})_4$: pyrazole solution.191

Figure 5.10: Reaction of 0.3 M of the bis-diazo compound **24** with 3.0 M furan in the presence of 0.01 mol% $\text{Rh}_2(\text{S-PTAD})_4$ and pyrazole additive.....193

Figure 5.11: Reaction of 0.3 M of the bis-diazo compound **24** with 3.0 M furan in the presence of 0.01 mol% $\text{Rh}_2(\text{S-DOSP})_4$195

Figure 5.12: Reaction of 0.3 M of the bis-diazo compound **25** with 3.0 M furan in the presence of 0.01 mol% $\text{Rh}_2(\text{S-DOSP})_4$196

LIST OF SCHEMES

Scheme 1.1: Competition Study of Common Substrates for C-H Functionalization.....	8
Scheme 1.2: Site Selectivity for Donor/Acceptor Carbenoid C-H Functionalization.....	9
Scheme 1.3: Dirhodium Carbenoid Cyclopropanation and C-H Insertion.....	10
Scheme 1.4: General Mechanism for Carbenoid Insertion.....	11
Scheme 1.5: Isolation of Rhodium Carbenoid.....	12
Scheme 1.6: Mechanism for Cyclopropanation of Styrene with Diazoacetate 1 and 2	17
Scheme 1.7: Generic Enzymatic Catalytic Cycle.....	18
Scheme 1.8: Arbitrary catalytic reaction.....	24
Scheme 1.9: Yu's C-H Olefination.....	29
Scheme 1.10: Mechanism for Yu's Pd(II) Olefination.....	30
Scheme 2.1: Dirhodium(II) catalyzed cyclopropanation of 2 with donor/acceptor diazo compound 1	47
Scheme 2.2: Mechanism for cyclopropanation of styrene.....	65
Scheme 2.3: Rh ₂ (S-DOSP) ₄ (0.10 mol%) catalyzed cyclopropanation of styrene with <i>p</i> -substituted aryldiazoacetates in dichloromethane at -10 °C.....	83
Scheme 2.4: Substrate coordination to the dirhodium(II) catalyst.....	90
Scheme 2.5: Product coordination to the dirhodium(II) catalyst.....	92
Scheme 3.1: Solvent-free C-H insertion into 1,4 cyclohexadiene.....	112
Scheme 3.2: Mechanism for C-H insertion.....	121

Scheme 3.3: C-H insertion into cyclohexane.....	132
Scheme 3.4: Kinetic results for C-H insertion into cyclohexane.....	132
Scheme 3.5: Proposed mechanism for azine formation.....	133
Scheme 4.1: Vinyl and aryl dirhodium(II) and copper(I) carbenoids are commonly utilized in the synthesis of chiral silanes.....	138
Scheme 4.2: Dirhodium donor/acceptor carbenoid mediated Si-H insertion reaction explored for the kinetic studies in this work.....	141
Scheme 5.1: Reactions that can be conducted with dirhodium(II) carbenoids.....	171
Scheme 5.2: Krimise's photochemical ring constriction of a bis-diazo compound.....	173
Scheme 5.3: Tomioka's approach to photochemical selective photochemical decomposition of a bis-diazo compound.	173
Scheme 5.4: Moody's selective decomposition of non-equivalent diazo compounds within a bis-diazo compound.	175
Scheme 5.5: Muthusamy's selective C-alkylation and cycloaddition.....	176
Scheme 5.6: Retrosynthesis of phorbol.....	177
Scheme 5.7: Reactivity of 23 with acyclic diene 26	178
Scheme 5.8: Formation of the pyrazole from donor/acceptor carbenoid 35	190

LIST OF TABLES

Table 1.1: Kinetic Parameters for Intermolecular C-H Insertion.....	19
Table 1.2: Representative RPKA Experiments.....	26
Table 2.1: High TON for Rh ₂ (<i>S</i> -biTISP) ₄	43
Table 2.2 Solvent-Free High TON Dirhodium(II) Catalyzed Cyclopropanation.....	44
Table 2.3: Catalyst activity and high and low catalyst loading.....	53
Table 2.4: Calculated enthalpy ΔH_{rxn} for each injection of the diazo compound.....	71
Table 2.5: Raw Data exported from ReactIR™.....	101
Table 3.1 RPKA Conditions.....	120
Table 3.2: Results from Screening of Dirhodium(II) Catalysts.....	127
Table 3.3 Substrate screening for MK-1-235.....	131
Table 4.1: Panek's optimization of dirhodium donor/acceptor carbenoid Si-H insertion.....	145
Table 4.2: Temperature influence on reaction exotherm.....	148
Table 4.3: Influence of solvent over the relative rate of the reaction.....	159
Table 4.4: Relative Rates for common substrates for C-H functionalization.....	161
Table 4.5: Relative Rate of Si-H insertion with heterocycle additives.....	164

Table 5.1: Observed Rates for Diazo Compound 31	181
Table 5.2: Observed Rates for Diazo Compound 32	182
Table 5.3: Differences in reaction time for diazo compound 33	183

List of Abbreviations

KIE	Kinetic Isotope Effect
DOSP	4-dodecyl phenylsulfonylprolinate
TBSP	4-(tert-butyl)phenylsulfonylprolinate
TISP	2,4,6-tri-isopropylphenylsulfonylprolinate
ee	Enantiomeric excess
EWG	Electron withdrawing group
de	Diastereomeric excess
BNP	Binaphthylphosphonate
TFA	Trifluoroacetate
TPA	Triphenylacetate
DCM	Dichloromethane
NMR	Nuclear Magnetic Resonance
TLC	Thin Layer Chromatography
FTIR	Fourier-transform Infrared
ρ	Hammett reaction constant
σ	Substituent parameter
EDG	Electron donating group
EtOAc	Ethyl acetate
OOct	Octanoate
DBU	1,8-diazabicyclo[5.4.0]undec-7-ene
<i>p</i>-ABSA	para-acetamidobenzenesulfonyl azide

HPLC	High-performance liquid chromatography
HRMS	High-resolution mass spectrometry
APCI	Atmospheric pressure chemical ionization
TFT	Trifluorotoluene
ESI	Electrospray ionization
TON	Turnover number
TOF	Turnover frequency
OPiv	Pivaloate

CHAPTER 1

Introduction to Dirhodium(II) Carbenoid Chemistry

1.1 Description of Chapter

The topics covered in the introductory chapter will provide a comprehensive survey of the central themes in dirhodium(II) donor/acceptor carbene chemistry. These topics will set the foundation for subsequent chapters. First, a general background on typical dirhodium(II) catalysts utilized to induce carbenoid reactivity will be discussed, followed by a description of the classes of diazo compounds and selectivity exhibited by donor/acceptor carbenoids in C-H functionalization. The next section will examine the mechanistic studies that have been conducted on donor/acceptor dirhodium(II) carbenes. This section includes key competition studies that illustrate the relative reactivity of common carbenoid substrates. Additionally, a description will be given of the KIE and Hammett analysis that has provided support for key mechanistic details for cyclopropanation, C-H insertion and Si-H insertion. Next the isolation of the dirhodium(II) carbene, which was pivotal in confirming the mechanistic pathway, will be covered. From there, the seminal kinetic study conducted on C-H functionalization will be discussed because it is the baseline for comparison of C-H functionalization kinetic studies conducted in Chapter 3.

Two recurring themes in the thesis are coordination to the dirhodium(II) catalyst and catalyst decomposition. Studies that have discussed coordination of small molecules to dirhodium(II) catalysts and the influence it has on the activity of the catalyst will be covered. Additionally, recent evidence for catalyst decomposition will be discussed. This work is important because it has presented a possible mechanism for decomposition and

identification of possible deactivated dirhodium complexes. Finally, the theory behind the key kinetic methodology, reaction progress kinetic analysis or RPKA, will be detailed.

1.2 Classes of Metallocarbenoids

The ubiquitous presence of carbon-hydrogen (C–H) bonds in small molecules makes them attractive targets for functionalization; however, the inert nature of C–H bonds presents a significant challenge to synthetic chemists.¹⁻³ Traditional organic chemistry has focused on chemical reactivity at polarizable functional groups, such as carbonyls and aromatic rings (Figure 1.1), however, exciting advances in catalysis has opened the door to functionalizing C–H bonds.⁴ C–H functionalization, however, has been approached in two different methods. Organometallic chemists have focused on “C–H activation” or the insertion of a transition metal into the C–H bond.⁵⁻⁸ Organic chemists, however, have taken an alternative approach through insertion of a divalent carbon into the C–H bond in the form of a metal carbene.^{3,9,10}

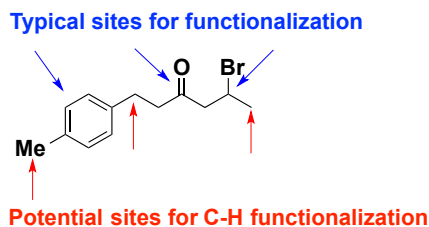


Figure 1.1: Functional group modification compared to C-H functionalization.

The standard method for generating carbenoids is metal induced nitrogen extrusion from diazo compounds.¹¹ As illustrated in Figure 1.2, the central carbon of the metal carbenoid is flanked with either an electron donating (donor) group or an electron-withdrawing (acceptor) group, creating three classes of metal carbenoids.⁹ Acceptor-only metal carbenoids generated from diazoacetates such as ethyl diazoacetate, are noted for their high electrophilicity.¹¹ As a result, carbene dimerization is often a substantial side product in intermolecular carbenoid C–H functionalization reactions with acceptor diazo compounds.¹² Acceptor/acceptor metallocarbenes are equally electrophilic and reactive.¹³ The reactivity exhibited by acceptor and acceptor/acceptor carbenoids typically results in poor chemoselectivity for intermolecular C-H functionalization reactions. Many reactions with traditional acceptor/acceptor and acceptor carbenoids are conducted in an intramolecular fashion to control selectivity.^{11,14,15} While a significant amount of catalyst development has focused on controlling the selectivity of acceptor and acceptor/acceptor carbenoids, a new class of carbenoids, donor/acceptor carbenoids, have demonstrated better chemoselectivity in intermolecular reactions.^{3,9,16,17} Studies in this thesis will focus on the reactivity of donor/acceptor carbenoids.

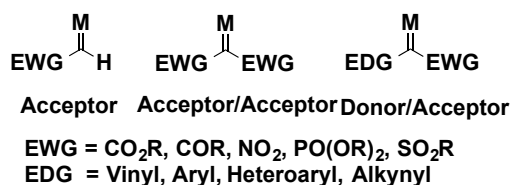


Figure 1.2: Classes of Diazo Compounds.

1.3 Dirhodium (II) Catalysts

A number of transition metal catalysts have been successfully used for the formation transient metal carbenoids from diazo compounds. Dirhodium catalysts, however, have dominated the field of C-H functionalization due to the excellent reactivity and selectivity exhibited by dirhodium(II) donor/acceptor carbenoids (**Figure 1.3**).¹⁸⁻²⁹ The catalytic activity of these complexes is thought to be due to the dirhodium bridge caged within a “lantern” structure.¹³ Nakamura suggested that the second dirhodium atom acts like an electron sink that assists in the C-H functionalization by increasing the electrophilicity of the carbenoid moiety.³⁰ A wide variety of other catalysts decompose diazo compounds but generally they are less reactive than the dirhodium complexes. Amongst the monometallic catalysts that have been utilized in carbenoid chemistry copper bisimines and bisoxazolines have been the most prevalent.^{11,31} In general, dirhodium tetracarboxylate catalysts are kinetically much more active at diazo compound decomposition than copper and dirhodium carboxamidate catalysts.³²

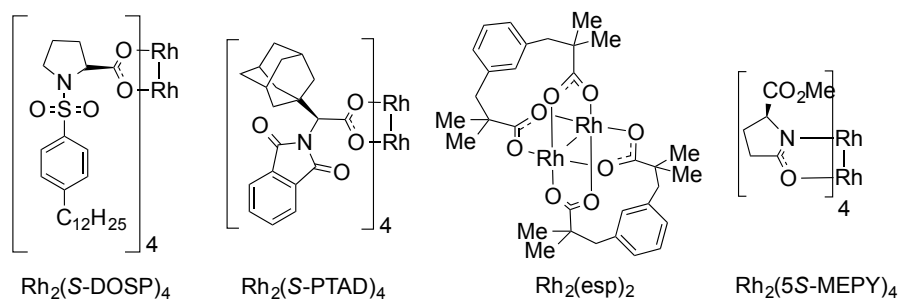


Figure 1.3 Various Dirhodium Catalysts used for C-H Functionalization.

The influence of the dirhodium catalyst structure has been of particular interest in controlling the selectivity of dirhodium carbenoid chemistry. Davies and coworkers have extensively studied the influence the dirhodium(II) tetracarboxylate catalyst structure on the chemoselectivity of dirhodium carbenoid intermolecular cyclopropanation of styrene with donor/acceptor and acceptor carbenoids.^{23,33} In a comprehensive evaluation of achiral and chiral dirhodium tetracarboxylate catalysts, Davies found that the rhodium catalyst structure had minimal influence on the diastereoselectivity of the reaction. Cyclopropanes were synthesized in moderate to high yield and excellent diastereoselectivity.³³ Subsequent studies evaluating relative reactivity suggest that selectivity is not a function of catalyst structure but instead carbene structure.^{23,34}

1.4 Reactivity of Dirhodium(II) Carbenoids

A comparison of the reactivity of the three classes of diazo compounds was made in a study of asymmetric dirhodium(II)-mediated cyclopropanation of styrene (Figure 1.4).³⁴ Based on *in situ* FTIR monitoring of diazo compound decomposition, Davies *et al.* observed that phenyldiazoacetate **1**, a diazo compound containing both donor and acceptor groups are more reactive than the traditional diazo compounds containing only electron-accepting groups. Complete decomposition of phenyldiazoacetate **1** was observed after 3 sec at 0.1 mol% and 60 seconds at 0.01 mol% of the chiral tetracarboxylate catalyst, Rh₂(*S*-DOSP)₄ at 25°C. Significantly slower reaction conversions were observed with acceptor diazoacetate **2** and acceptor/acceptor diazoacetate **3**. The acceptor carbene initially reacts then quickly deactivates, suggesting that catalyst destruction quickly takes place. Very little activity is observed with the acceptor/acceptor carbene under these reaction conditions, even with a catalyst loading of 0.5 mol%.

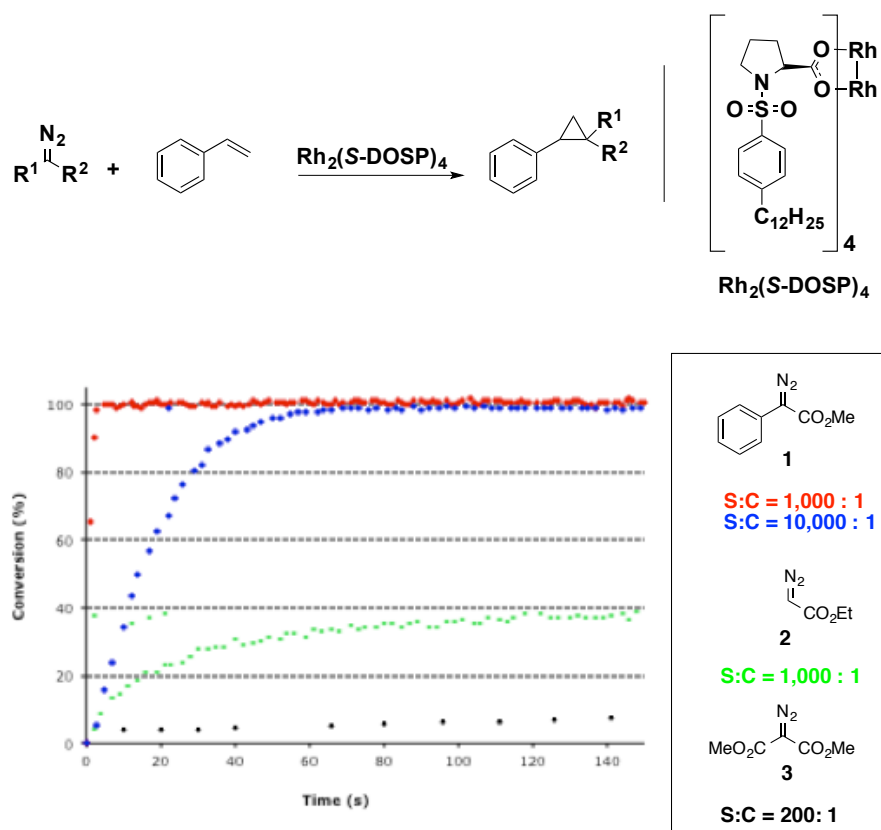
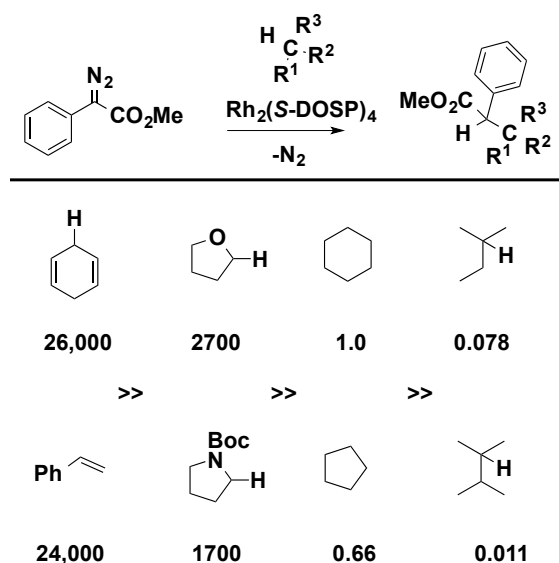


Figure 1.4: Inherent Reactivity of Transient Metal Carbenoids.

Over the past decade a comprehensive picture of the enhanced selectivity of donor/acceptor carbenes has emerged. Relative rate studies have illustrated that dirhodium-bound acceptor carbenes had very little chemoselectivity compared to donor/acceptor carbenoids for cyclopropanation of styrene.²³ Moreover, computational calculations have suggested that the selectivity is a function of a 4.5 kcal/mol potential energy barrier that exists for functionalization with donor/acceptor carbenoids. This barrier was not observed in the computational studies of acceptor carbenes. Together, these results provide evidence that donor/acceptor carbenoids are more stabilized than traditional carbenoids lacking a donor group.

1.5 Site- and Chemo-selectivity of Dirhodium Donor/Acceptor Carbenoids for C-H Functionalization

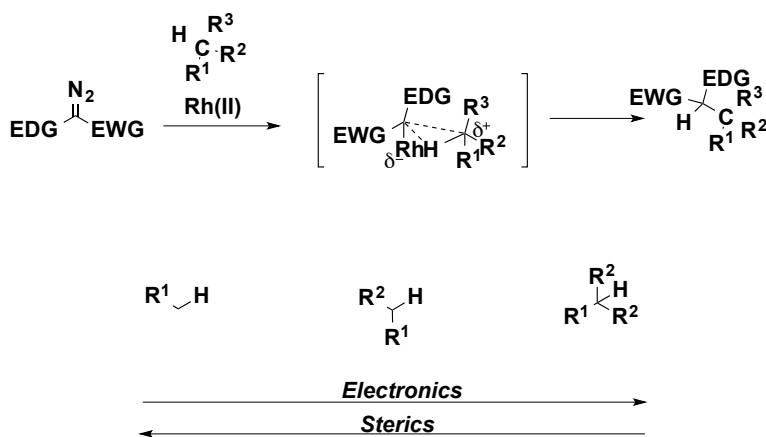
The results in Scheme 1.1 strongly support the overwhelming influence electronics can have over the susceptibility of a C-H bond to undergo functionalization. Superior reactivity was observed with 1,4-cyclohexadiene. The doubly allylic C-H bond is 24,000 times more reactive than the unactivated C – H bonds in cyclopentane and 2,3-dimethylbutane.^{25,34} Additionally, C–H bonds adjacent to heteroatoms typically are more reactive, as is the case for C-H bonds positioned α to N-Boc-pyrrole and furan. These C-H bonds are \sim 3,000 more reactive than the methylene sites on cyclopentane. Electronics, however, are not the only factor which contributes to the reactivity of a C-H bond.



Scheme 1.1: Competition Study of Common Substrates for C-H Functionalization.

Sterics can greatly influence the susceptibility of a bond undergoing C-H functionalization (Scheme 1.2). Secondary C-H bonds are typically preferred due to their

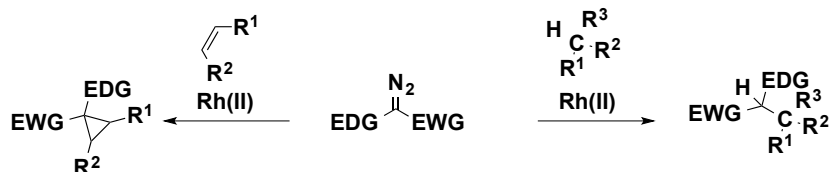
ability to stabilize positive charge build up without too much steric influence.²⁵ Primary C-H bonds can be functionalized if they are electronically activated, such as substrates with primary site α to heteroatoms.³⁵⁻³⁷ Tertiary C-H bonds, which electronically should be more reactive than secondary C-H bonds, can only be activated if they are not too sterically hindered. If the site is too sterically hindered, no C-H functionalization will take place.³⁸



Scheme 1.2: Site Selectivity for Donor/Acceptor Carbenoid C-H Functionalization.

The chemoselectivity exhibited by donor/acceptor dirhodium carbenoids has expanded the utility of C-H functionalization in organic synthesis.^{13,39,40} Reactions that were previously not viable with traditional carbenoids can now be conducted with great

efficiency. Additionally, the advent of chiral ligands for the dirhodium core has rendered donor/acceptor dirhodium carbene reactions highly asymmetric. In particular, cyclopropanation^{24,41-43} and C-H insertion^{4,13,25,44,45}, two of the most widely employed reactions of donor/acceptor dirhodium carbenes, have been utilized as key steps in the synthesis of natural products and pharmaceutically relevant molecules (**Scheme 1.3**)^{40,46-62}. The synthetic value of donor/acceptor dirhodium carbenes has sparked a number of mechanistic studies. In particular, these studies have focused on C-H insertion and cyclopropanation reactions due to the exceptional reactivity of styrene and 1,4-cyclohexadiene.

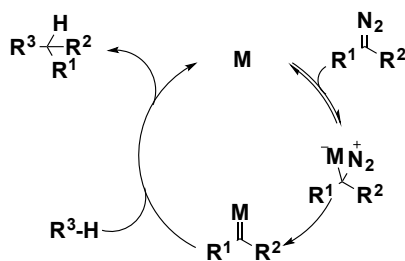


Scheme 1.3: Dirhodium Carbene Cyclopropanation and C-H Insertion.

1.6 Mechanistic Studies of Dirhodium(II) Carbenoid Carbenes

1.6.1 Proposed Mechanism

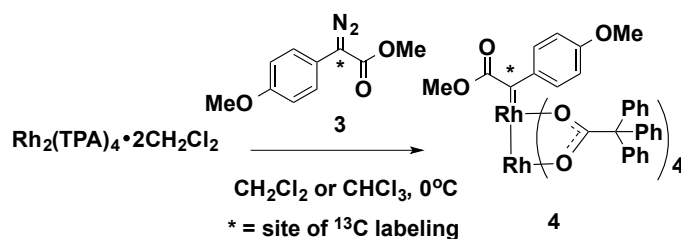
In 1952, Yates proposed the mechanism in **Scheme 1.4** for copper catalyzed diazoketone insertion into N-H, S-H and O-H bonds.⁶³ The Yates model has been generally accepted as the mechanism for metal carbenoid C-H functionalization.^{13,64} The proposed mechanism involves complexation of the negatively charged carbon to the metal, followed by the irreversible loss of nitrogen gas to yield a metal carbenoid. The highly reactive carbenoid can then insert into X-H bonds. In the area of dirhodium carbene C-H functionalization, other less common mechanistic models, including cleavage of the dirhodium dimer, lack empirical evidence.



Scheme 1.4: General Mechanism for Carbenoid Insertion.

1.6.2 Isolation of the Dirhodium(II) Carbene

Structural information about the nature of the transient metal carbenoid has remained elusive for decades. Only recently has the transient metal carbenoid been observed spectroscopically by Berry and Davies.⁶⁵ Scheme 1.5 describes the isolation of the rhodium carbenoid.⁶⁵ Addition of ¹³C labeled diazoacetate **3** to Rh₂(TPA)₄ in CHCl₃ at 0 °C afforded carbenoid **4**, which was stable for up to 20 h. The resultant carbenoid was characterized by UV-Vis, ¹³C NMR, resonance Raman, and MALDI-MS. Spectroscopic characterization of the donor/acceptor carbenoid provides further support for Yates model for metal carbenoid X-H functionalization. This work has been key in providing evidence for the formation of a dirhodium carbenoid in the catalytic cycle.

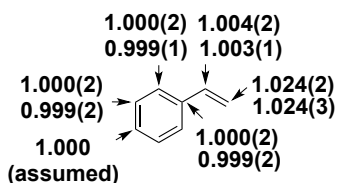


Scheme 1.5: Isolation of Dirhodium(II) Carbene.

1.6.3 KIE Analysis

Computational and Kinetic Isotope Effect (KIE) studies conducted by Davies and Singleton for the cyclopropanation of olefins with unsubstituted vinyl- and aryl diazoacetates probed the mechanism of dirhodium tetracarboxylate catalyzed cyclopropanation.⁶⁶ Computational analysis found that the reaction pathway is concerted asynchronous for the cyclopropanation step. The selectivity exhibited by donor/acceptor carbenoids was found to be due to a 0.5 kcal mol⁻¹ potential energy barrier for the carbenoid trapping that was nonexistent in acceptor carbenoids. KIE experiments for the cyclopropanation of styrene with donor/acceptor diazoacetate **1**, found substantial ¹³C isotope effect (1.024) at the terminal olefinic carbon and much smaller effect and the internal olefinic carbon (1.002). The effect was found to be consistent for both the chiral Rh₂(*S*-DOSP)₄ and the achiral Rh₂(OOct)₄ (Figure 1.5).

Reaction with **1** catalyzed by Rh₂(OOct)₄



Reaction with **1** catalyzed by Rh₂(*S*-DOSP)₄

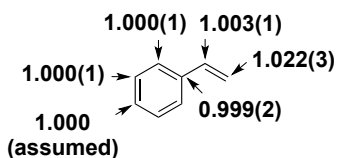


Figure 1.5: ¹³C KIE for Cyclopropanation of Styrene. Standard Deviation in Parenthesis.

¹⁵N kinetic isotope effects (KIE) were reported for the dirhodium(II) carbenoid Si—H insertion into dimethylphenylsilane by Wang. This study was aimed at providing further evidence for the extrusion of nitrogen being rate-limiting rather than diazo compound pre-equilibrium with the dirhodium catalyst. Based on Wang's analysis, the large normal isotope effect observed corresponds to C-N bond fission being rate limiting, which further supports the Yates model for Cu-mediated carbenoid formation.

1.6.4 Hammett Analysis

Hammett evaluation of substituted styrene analogs found that the relative rate of cyclopropanation with methyl phenyldiazoacetate is strongly influenced by the electronic nature of the styrene (Figure 1.6).²³ While the Hammett study suggests a 1.8 kcal/mol energy barrier must exist for donor/acceptor carbenoid trapping, Singleton and Davies had previously calculated a much smaller energy barrier.⁶⁶ As a result, Davies *et al* re-evaluated the initial computational analysis, which underestimated the energy barrier associated with these highly selective reactions. A follow-up study, utilizing much more flexible Rh basis set, was necessary to more accurately describe interactions with rhodium.³⁴

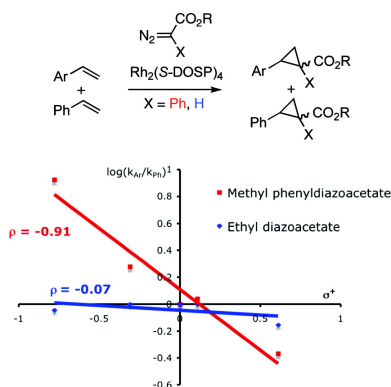


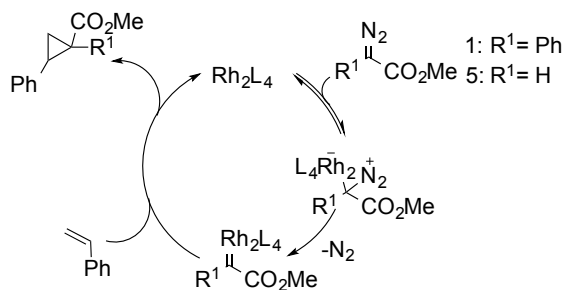
Figure 1.6: Hammett Plot for Cyclopropanation of Styrene Analogs with Diazoacetate^{23,34}

Hammett analysis has also been extended to other dirhodium(II) carbenoid reactions. Wang and coworkers have studied factors that control the rate of dirhodium(II) mediated *p*-substituted aryldiazoacetate decomposition for Si-H insertion into triethylsilane. Kinetic data, compiled in a Hammett study, revealed that the rate of the diazo compound decomposition consumption obeyed first order kinetics. In general, diazo compounds with electron-donating substituents decomposed faster than those with electron withdrawing substituents due to the stabilization or de-stabilization of the Rh(II) carbene intermediate. It is proposed that an electron-withdrawing group stabilizes the diazo compound but destabilizes the Rh(II) carbene intermediate; an electron-donating group operates in the opposite manner.

Furthermore, Wang's study assessed the effects of the dirhodium(II) catalyst. Electron poor dirhodium(II) catalyst, $\text{Rh}_2(\text{O}_2\text{CCF}_3)_4$ demonstrated a much faster reaction rate than $\text{Rh}_2(\text{OAc})_4$ and $\text{Rh}_2(\text{acam})_4$, whereas much slower rates were observed with $\text{Rh}_2(\text{acam})_4$. The larger magnitude of the reaction rate constant for $\text{Rh}_2(\text{O}_2\text{CCF}_3)_4$ suggests more positive charge build-up in the Rh(II) carbene intermediate, supporting the argument that electron withdrawing ligands have very little back-bonding. The Hammett studies conducted by Wang were the first to obtain quantitative data on diazoacetate and ligand electronic effects on rhodium carbene formation.

1.6.5 Computational Analysis

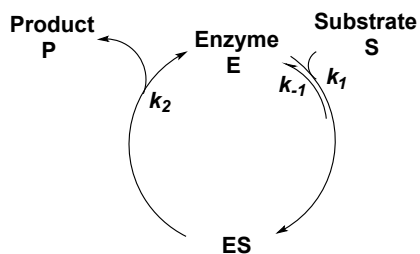
Theoretical calculations have been crucial in providing evidence for proposed mechanistic pathways and origins of donor/acceptor dirhodium carbenoid selectivity. Relative energy calculations for cyclopropanation of styrene propose that a 4.5 kcal/mol potential energy barrier for carbenoid trapping is responsible for the selectivity of donor/acceptor carbenoid **1** (Scheme 1.6).³⁴ Such a barrier is not observed in the cyclopropanation reaction with acceptor carbenoids. Furthermore, calculations propose that nitrogen extrusion is rate-limiting, based on a calculated large potential energy barrier (>11 kcal/mol). Parallel results are observed in the C-H insertion into the activated C-H bond of 1,4 cyclohexadiene. A potential energy barrier of 6.5 kcal/mol is calculated for carbenoid trapping and 11.0 kcal/mol for nitrogen extrusion. In comparison, theoretical calculations suggest that carbenoid trapping (17.0 kcal/mol) is rate-limiting for insertion into the unactivated C-H bonds of cyclohexane.



Scheme 1.6: Mechanism for Cyclopropanation of Styrene with Diazoacetate **1** and **2**.

1.6.6 Michealis-Menten Kinetics

Kinetic studies on dirhodium(II) carbenes have been limited to Hammett analysis and relative rate data; few studies have attempted to associate kinetic parameters or fit data to kinetic models. Aimed at identifying the saturation kinetic parameters for dirhodium(II) carbene reactions, Pirrung and coworkers studied dirhodium(II)-mediated intra- and intermolecular C-H insertion reactions.⁶⁴ Saturation kinetics are typically associated with enzymatic systems and are defined as reactions that undergo a pre-equilibrium step prior to formation of the enzyme-substrate complex (Scheme 1.7). Reactions that follow saturation kinetics are typically defined by the Michaelis-Menten equation. 1.1.^{64,67} A recent goal in the field of organic catalysis has been to identify small molecule catalysts that exhibit similar behavior.⁶⁸⁻⁷⁸

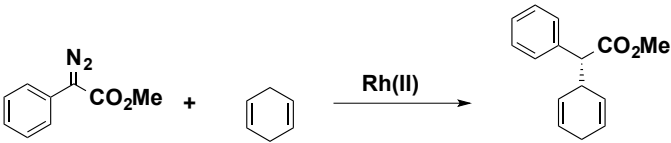


Scheme 1.7: Generic Enzymatic Catalytic Cycle

$$v = \frac{v_{max} \times [substrate]}{K_{MM} + [substrate]} \quad (1.1)$$

In the context of intermolecular reactivity, Pirrung explored C-H insertion into 1,4-cyclohexadiene in the presence of donor/acceptor dirhodium carbenoid **1** under saturation kinetics conditions. The observed kinetic parameters for two achiral dirhodium catalysts and Davies's chiral $\text{Rh}_2(\text{S-DOSP})_4$ can be found in Table 1.1. Pirrung observed that the catalytic efficiency ($k_{\text{cat}}/K_{\text{M}}$) for the chiral catalyst, entry 1, is slower than the achiral catalysts (entry 2 and 3). He asserts that the slower rate may be attributed to the D_2 chiral catalyst having less approach vectors than the achiral catalysts (4 vs 8).

Table 1.1: Kinetic Parameters for Intermolecular C-H Insertion



Entry	Catalyst	K_{M} (mM)	k_{cat} (s^{-1})	$k_{\text{cat}}/K_{\text{M}}$ ($\text{M}^{-1}\text{s}^{-1}$)
1	$\text{Rh}_2(\text{S-DOSP})_4$	24.7	1.58	6.40×10
2	$\text{Rh}_2(\text{Piv})_4$	9.07	1.29	1.42×10^2
3	$\text{Rh}_2(\text{Oct})_4$	9.08	1.27	1.39×10^2

1.7 Coordination to the Dirhodium Core and Catalyst Decomposition

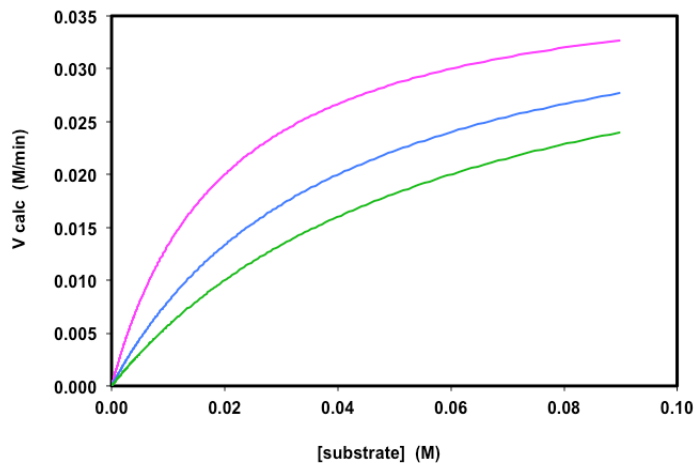
The ability for dirhodium(II) complexes to undergo dynamic interactions at its axial position(s) has been of particular interest to the chemical community. Early observations by Drago and coworkers illustrated that aromatic rings and Lewis bases can strongly bind to the axial positions of the dirhodium(II) complex.^{79,80} Based on Drago's observations, the rate of association of a "base" to the first axial site is generally 10^2 times greater than the rate of association to the second axial site. It is proposed that the drastic rate differences are due to back-bonding from the rhodium(II) to the axial position. Additionally, such interactions prevent simultaneous carbenoid formation. The axially coordinated dirhodium(II) species are typically in equilibrium with free dirhodium(II) species. Furthermore, it has been demonstrated that dirhodium(II) complexes can coordinate to simple olefins as well as undergo enantiomer recognition with amides.⁸¹⁻⁸⁴ Collectively, These studies demonstrate that the dirhodium(II) complex is capable of interacting in a variety of modes outside of typical carbenoid reactivity.

Mechanisms for decomposition of the dirhodium(II) catalysts has been elusive for decades and only recently has some evidence been presented by Du Bois and coworkers.^{85,86} Mechanistic studies on dirhodium(II) mediated C-H amination have discovered that oxidation of the catalyst to a mixed-valent species is possible. UV-Vis and mass spectrometry analysis have recently identified a mixed-valent Rh(II)/Rh(III) tetracarboxylate dimer in the reaction pathway. While the exact mechanism for catalyst oxidation is unknown, this deactivated species is active albeit much less robust than the Rh(II)/Rh(II) species.

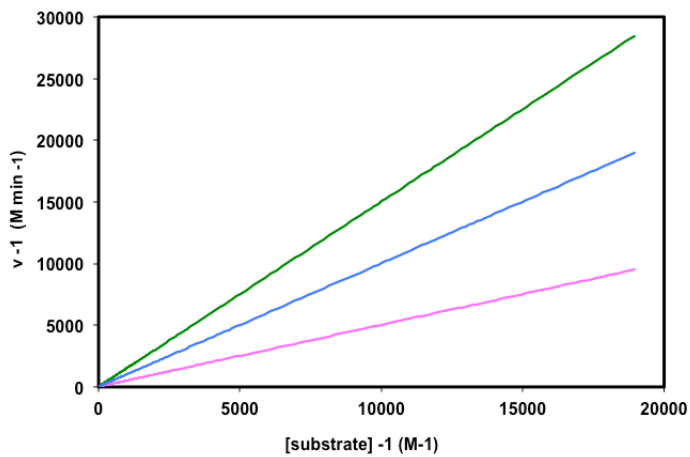
1.8 Technique: Reaction Progress Kinetic Analysis

The work within this dissertation will focus on kinetic studies for dirhodium(II) carbenoid reactions. As such, a description of the key kinetic technique, reaction progress kinetic analysis (RPKA) is necessary. Kinetic studies are useful for developing a better understanding of the mechanism of a specific reaction. This can be done by identifying concentration dependencies and determining the rate and/or equilibrium constants for elementary steps in the reaction. Kinetic information can be established from a number of techniques and methods, this work, however, will utilize (RPKA) as one method for identifying concentration dependencies and catalyst robustness.

Typical catalytic reactions are described by the Michaelis-Menten equation.⁸⁷ The Lineweaver-Burk equation linearizes the classic Michaelis-Menten equation (Figure 1.7).⁸⁸ The development of the Lineweaver-Burk equation 70 years ago was a significant advance in kinetic analysis; however, it can be experimentally tedious to develop Lineweaver-Burk plots.



$$v = \frac{v_{max} [Substrate]}{K_{MM} + [Substrate]}$$



$$\frac{1}{v} = \frac{1}{v_{max}} + \frac{K_{MM}}{v_{max}} \frac{1}{[substrate]}$$

Figure 1.7: Traditional Kinetic Plots (a) Michaelis-Menten Plot, (b) Lineweaver-Burke Plot

Developed by the Blackmond group, RPKA is a method for obtaining a comprehensive picture of complex catalytic behavior.⁶⁷ Classical kinetic methods require numerous experiments and typically only evaluate the “initial” portion of the reaction course. As many of these methods rely on Lineweaver-Burk evaluation, several individual experiments are necessary for each plot. Therefore, the number of kinetic experiments can grow exponentially for complex catalytic experiments. RPKA alternatively, explores mechanistic details *via* continuous monitoring of an entire reaction course. With continuous monitoring, kinetic information can be gained from not only the initial concentration of the reactant(s), but every concentration until the reaction end. Therefore, one RPKA experiment can be equivalent to hundreds of individual “initial rate” experiments.^{67,89}

In a minimal number of experiments, evaluation of the entire reaction progress can quickly deconvolute the influence of the catalyst, substrate(s), and product. These experiments additionally study the stability of the catalyst. The key to RPKA is utilizing an *in situ* method for monitoring a reaction.⁶⁷ The two possible types include an integral and a differential method. Integral methods utilize analytical tools, such as real time FTIR, which rely on a measurable parameter and species concentrations. With such methods the species concentration is proportional to the integral of the reaction rate. For example, real-time FTIR monitors changes in the vibrational stretches of a molecule over time. In turn, the absorbance of vibrational stretches is related to the concentration by Equation 1.2; Beer’s law. The concentration can then be differentiated over time to yield the reaction rate over time (Equation 1.3).

$$A = \epsilon bc \quad (1.2)$$

$$Rate = \frac{dc}{dt} \quad (1.3)$$

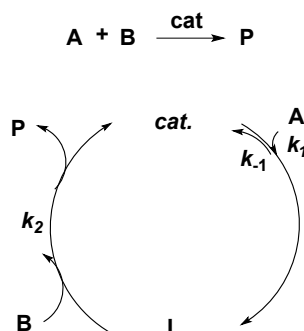
A = absorbance, c = concentration, ϵ = extinction coefficient

Differential methods directly monitor the rate of a reaction. One such example is calorimetry, where the instantaneous heat flow is measured over time. In turn, heat flow, q , is related to reaction rate by the thermodynamic heat of a reaction or enthalpy, ΔH (Equation 1.4)⁶⁷

$$q = \Delta H \times volume \times rate \quad (1.4)$$

q = heat flow, ΔH = thermodynamic heat of a reaction

The arbitrary reaction in Scheme 1.8 will act as an example for defining RPKA experiments as well as how rate equations are formed. Here, **A** and **B** are reactants, **d** is the catalyst, and **I** is an intermediate formed between the catalyst **d** and substrate **A**. We will assume that **A** is the limiting reagent and the substrate that is monitored by our differential or integral analytical tool. Catalytic reaction cycles, such as Scheme 1.13, are described by rate the Michalis-Menten equation (Equation 1.5).



Scheme 1.8: Arbitrary catalytic reaction

$$v = \frac{v_{max}[A]}{K_{MM}+[A]} \quad (1.5)$$

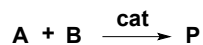
$$v_{max} = k_2[B][d]_{total}, K_{MM} = \frac{k_{-1} + k_2[B]}{k_1}$$

As stated in Equation 1.5, v_{max} , or the maximum rate of the reaction, and K_M , or the Michalis-Menten constant, are dependent upon **[B]**. Therefore, it would be necessary to conduct several experiments at different **[B]** in order to define rate constants k_1 , k_{-1} , and k_2 . Since RPKA experiments covers the entire reaction progress, several hundred concentrations of **[A]** or **[B]** are evaluated in a single experiment.⁶⁷

RPKA of catalytic reactions require two types of experiments: same excess and different excess. Excess, or e , is defined as the concentration difference between two reactants **A** and **B** by Equation 1.6.^{67,90}

$$[A] - [B] = e \quad (1.6)$$

Experiments are considered “same excess” when they have the same value of e , but different initial **[A]** and **[B]**; Table 1.2: entries 1 and 5 illustrate this concept. The goal of “same excess” experiments is to probe catalyst stability. A catalyst that does not undergo activation or deactivation should exhibit the same reaction rate when the **[A]** in experiment two is equivalent to the initial **[A]** in experiment one (*see* Table 1.2 entry 1 and 5, Equation 1.6).

Table 1.1: Representative RPKA Experiments

Entry	[A] ₀ (M)	[B] ₀ (M)	[cat] (M)	[P] ₀ (M)	e (M)	Reaction Type
1	0.09	0.09	0.009	--	0	standard
2	0.09	0.18	0.009	--	0.09	[B] Dependency
3	0.18	0.09	0.009	--	0.09	[A] Dependency
4	0.09	0.09	0.018	--	0	[d] Dependency
5	0.18	0.18	0.009	--	0	Same Excess
6	0.009	0.009	0.009	0.009	0	[P] Dependency

For experiment 1 and 5 of Table 1.1: $e^1 = e^2$ therefore,

$$\text{rate}^1 = \text{rate}^2 \text{ when } [A]_o^1 = [A]_t^2 \quad (1.6)$$

The “same excess” experiment is graphed in Figure 1.8 as [A] vs rate (v) to demonstrate that the reactions have the same rate. Overlap between the two rate plots is observed when no catalyst deactivation or activation is present. In cases when the “same excess” plots do not overlap additional experiments are necessary to probe the source of deactivation or activation. Often a source of catalyst deactivation is substrate or product inhibition. This can be probed by product doping (Table 1.2, entry 6) and “different excess” experiments (Table 1.2, entries 1,2,3,4).

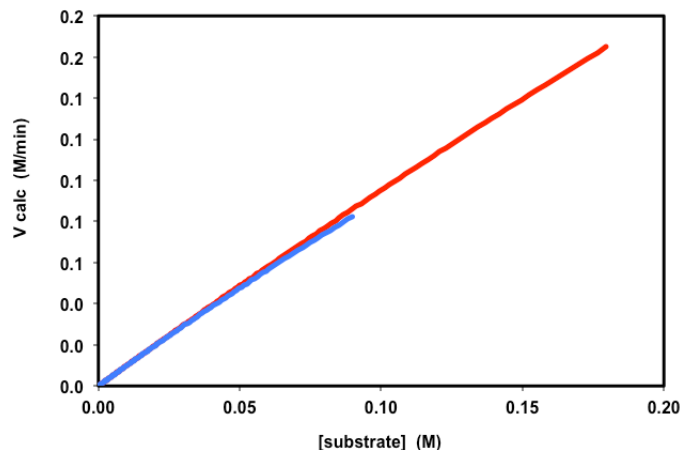


Figure 1.8: Same Excess Plot

Based on the definition of “same excess,” “different excess” is described as two or more experiments with different values of e (Table 1: entries 1 and 3) and **[A]** or **[B]**. Different excess experiments probe concentration dependencies of each reactant and the catalyst. Figure 1.9 is an example of two experiments under “different excess” conditions, where **[A]** has been changed to probe its dependency. A much faster rate is observed at higher concentrations of **[A]** (purple curve) suggesting the reaction has a positive order in **[A]**.

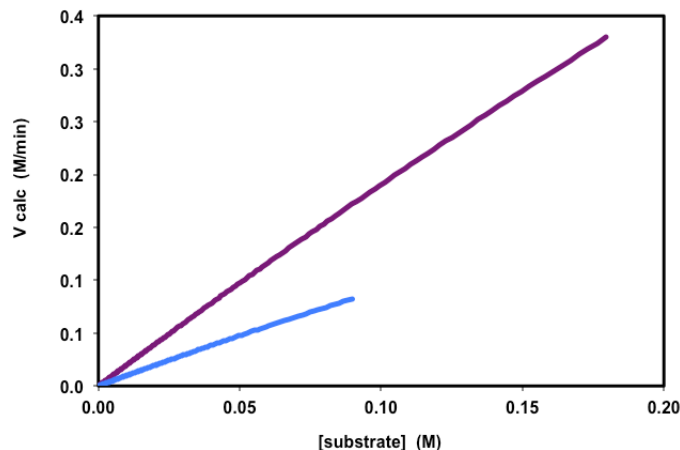


Figure 1.9: Different Excess Plot

Conducting “different” excess experiments allows for the determination of reactant order and reaction rate laws. Rate laws are written in power-law form, where the k is the rate constant, A and B are reactants, and the exponents x and y are the order of each reactant (Equation 1.7).^{67,90,91}

$$rate = k[A]^x[B]^y \quad (1.7)$$

The concentrations for A or B in Equation 1.7 can be substituted into Equation 1.6, where “excess” was defined, to give Equation 9.

$$[A] - [B] = e \quad (1.6)$$

Therefore,

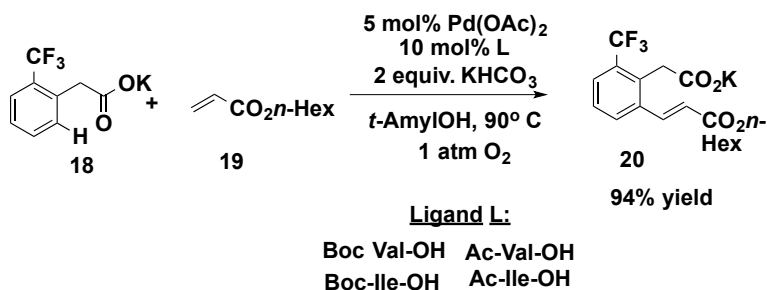
$$[A] = [B] + e \quad (1.8)$$

$$rate = k([B] + e)^x[B]^y \quad (1.9)$$

We see in this very simple rate equation that the term “excess” helps deal with two or more changing concentrations. Therefore, there is no need to conduct experiments where one reactant is held under pseudo-zero order conditions. Because we have defined

the “excess” term, monitoring the concentration change of one substrate allows for kinetic analysis of reactions with more than one substrate. Additionally, Equation 1.9 illustrates that reactant order can be determined by conducting two experiments at “different” excess.

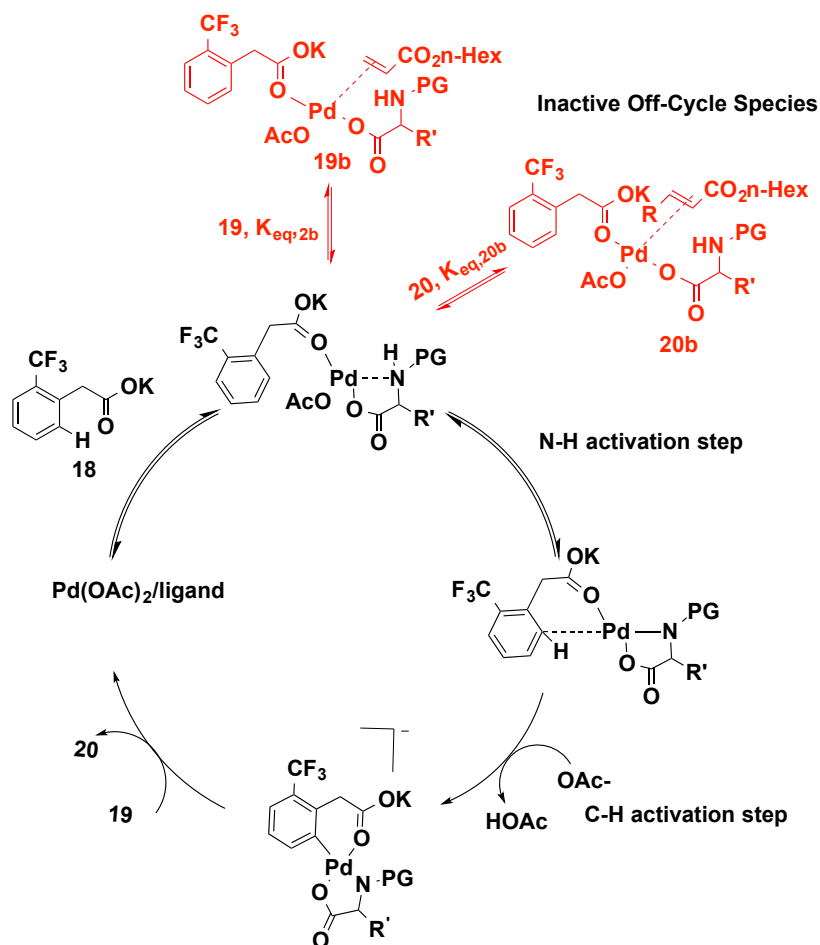
Blackmond *et al* have extensively used this methodology to study several proline⁹²⁻¹⁰⁵ and palladium^{89,106-110} catalyzed reactions. Most recently, Blackmond and Yu have studied Pd(II) catalyzed C-H functionalization⁹⁰. The Yu group has illustrated that the Pd(II) catalyzed olefination in the presence of mono-N-protected amino acid ligands (Scheme 1.9) is widely applicable, however, the mechanistic details of this reaction were unknown. It was proposed that an understanding of the reaction kinetics would potentially aid future catalyst and reaction design.



Scheme 1.9: Yu's C-H Olefination

Utilizing “same excess” and “different excess” protocol Blackmond and Yu were able to unveil key mechanistic details.⁹⁰ “Different excess” experiments revealed that the olefin substrate was in equilibrium with the free Pd(II) catalyst to form off-cycle species **19b**. Additionally, the reaction was zero order in the phenylacetic acid **18** and oxygen, leaving the catalyst as the only reaction driving force. Same excess experiments revealed

that catalyst deactivation was present. The source of the deactivation was found to be unproductive coordination of the product to the Pd(II) catalyst to give **20b**. NMR studies further revealed that the amino acid ligand was crucial in preventing the Pd(II) catalyst from forming less reactive palladium species. With this insight, the Yu group was able to develop a more precise reaction mechanism for the olefination process Scheme 1.10.



Scheme 1.10: Mechanism for Yu's Pd(II) Olefination

RPKA is a useful technique for understanding mechanistic details in catalytic reactions. It is our goal to use RPKA, along with other kinetic techniques, to gain insight into dirhodium(II) carbenoid reactions. Dirhodium carbenoid reactions are highly selective, however, understanding unknown modes of catalyst deactivation can aid the design of new catalysts and reaction protocols.

1.9 Description of Thesis

The first part of this dissertation will discuss the factors that contribute to catalyst deactivation for the cyclopropanation of styrene. Exceptional asymmetric induction is routinely observed up to 10,000 TON of the chiral dirhodium(II) catalyst, $\text{Rh}_2(\text{S-DOSP})_4$, however, under high turnover conditions ($\text{TON} > 10,000$) the enantioselectivity quickly diminishes. Possible causes of this effect are explored *via* kinetic studies. Specifically, catalyst robustness and deactivation are extensively explored to identify modes of catalyst deactivation and suggest reaction conditions that can avoid catalyst deactivation/decomposition. Influence of the catalyst structure on the kinetic activity and electronic of the diazo compound are also explored.

Selective insertion into C – H bonds by donor/acceptor dirhodium(II) carbenes has been shown to be widely applicable to a number of small molecules, however, difficulty often resides in conducting high turnovers of the dirhodium(II) catalyst with both activated and unactivated C – H bonds. Kinetic studies have focused on two common substrates, 1,4 cyclohexadiene and cyclohexane, due to their excellent activity up to 100 TON with $\text{Rh}_2(\text{S-DOSP})_4$, but dismal activity at lower catalyst concentrations. These studies have identified probable causes of catalyst deactivation as well as structural attributes of the dirhodium(II) catalyst that favor high turnover frequency.

Dirhodium(II) donor/acceptor carbenoid insertion into Si-H bonds has been illustrated to be highly asymmetric at high catalyst loadings (≥ 1.0 mol%) and low reaction temperatures (-78 °C). The robust nature of the reaction has made it an ideal system for studying common C-H functionalization substrates and poisons that may bind to the dirhodium(II) core. However, the significant exotherm observed during *in situ*

reaction monitoring complicates kinetic studies. Interesting evidence for catalyst coordination upholding the integrity of the catalyst is also presented.

An overarching goal of C-H functionalization is its application to complex molecule synthesis. In an effort to illustrate the exceptional selectivity of donor/acceptor dirhodium carbenoids, progress toward the core of phorbol have been made by previous graduate student Dr. Pablo Guzman. Using a bis-diazo compound, Dr. Guzman attempts to selectively decompose each diazo compound component. This section of the dissertation will discuss kinetic studies on model substrates that were integral in the design and development of the bis-diazo compound.

- (1) Dangel, B. D.; Godula, K.; Youn, S. W.; Sezen, B.; Sames, D. *J. Am. Chem. Soc.* **2002**, *124*, 11856.
- (2) Johnson, J. A.; Ning, L.; Sames, D. *J. Am. Chem. Soc.* **2002**, *124*, 6900.
- (3) Davies, H. M. L.; Morton, D. *Chem. Soc. Rev.* **2011**, *40*, 1857.
- (4) Davies, H. M. L.; Manning, J. R. *Nature* **2008**, *451*, 417.
- (5) Arndtsen, B. A.; Bergman, R. G.; Mobley, T. A.; Peterson, T. H. *Acc. Chem. Res.* **1995**, *28*, 154.
- (6) Waltz, K. M.; Hartwig, J. F. *Science* **1997**, *277*, 211.
- (7) Saaby, S.; Bayon, P.; Aburel, P. S.; Jorgensen, K. A. *J. Org. Chem.* **2002**, *67*, 4352.
- (8) Bergman, R. G. *Nature* **2007**, *446*, 391.
- (9) Davies, H. M. L.; Beckwith, R. E. J. *Chem. Rev.* **2003**, *103*, 2861.
- (10) Davies, H. M. L. *Angew. Chem. Int. Ed.* **2006**, *45*, 6422.
- (11) Doyle, M. P.; McKervey, M.; Ye, T.; Nature Publishing Group: 1998.
- (12) Hansen, J. H.; Parr, B. T.; Pelphrey, P.; Jin, Q. H.; Autschbach, J.; Davies, H. M. L. *Angew. Chem. Int. Ed.* **2011**, *50*, 2544.
- (13) Davies, H. M. L.; Beckwith, R. E. J. *Chem. Rev.* **2003**, *103*, 2861.
- (14) Ye, T.; McKervey, M. A. *Chem. Rev.* **1994**, *94*, 1091.
- (15) Doyle, M. P.; Forbes, D. C. *Chem. Rev.* **1998**, *98*, 911.
- (16) Davies, H. M. L.; Antoulinakis, E. G. *J. Organomet. Chem.* **2001**, *617-618*, 47.
- (17) Davies, H. M. L. *J. Mol. Catal. A-Chem.* **2002**, *189*, 125.
- (18) Davies, H. M. L.; Huby, N. J. S. *Tetrahedron Lett.* **1992**, *33*, 6935.

- (19) Davies, H. M. L.; Hansen, T. *J. Am. Chem. Soc.* **1997**, *119*, 9075.
- (20) Davies, H. M. L.; Stafford, D. G.; Doan, B. D.; Houser, J. H. *J. Am. Chem. Soc.* **1998**, *120*, 3326.
- (21) Davies, H. M. L.; Stafford, D. G.; Hansen, T.; Churchill, M. R.; Keil, K. *M. Tetrahedron Lett.* **2000**, *41*, 2035.
- (22) Davies, H. M. L.; Stafford, D. G.; Hansen, T. *Org. Lett.* **2000**, *2*, 417.
- (23) Davies, H. M. L.; Panaro, S. A. *Tetrahedron* **2000**, *56*, 4871.
- (24) Davies, H. M. L.; Nagashima, T.; Klino, J. L. *Org. Lett.* **2000**, *2*, 823.
- (25) Davies, H. M. L.; Hansen, T.; Churchill, M. R. *J. Am. Chem. Soc.* **2000**, *122*, 3063.
- (26) Davies, H. M. L.; Antoulinakis, E. G. *Org. Lett.* **2000**, *2*, 4153.
- (27) Davies, H. M. L.; Ren, P. D.; Jin, Q. H. *Org. Lett.* **2001**, *3*, 3587.
- (28) Nadeau, E.; Ventura, D. L.; Brekan, J. A.; Davies, H. M. L. *J. Org. Chem.* **2010**, *75*, 1927.
- (29) Chepiga, K. M.; Qin, C. M.; Alford, J. S.; Chennamadhavuni, S.; Gregg, T. M.; Olson, J. P.; Davies, H. M. L. *Tetrahedron* **2013**, *69*, 5765.
- (30) Nakamura, E.; Yoshikai, N.; Yamanaka, M. *J. Am. Chem. Soc.* **2002**, *124*, 7181.
- (31) Maas, G. *Top. Curr. Chem.* **1987**, *137*, 75.
- (32) Davies, H. M. L. *Eur. J. Org. Chem.* **1999**, 2459.
- (33) Davies, H. M. L.; Rusiniak, L. *Tetrahedron Lett.* **1998**, *39*, 8811.
- (34) Hansen, J.; Autschbach, J.; Davies, H. M. L. *J. Org. Chem.* **2009**, *74*, 6555.

- (35) Davies, H. M. L.; Venkataramani, C. *Angew. Chem. Int. Ed.* **2002**, *41*, 2197.
- (36) Davies, H. M. L.; Venkataramani, C.; Hansen, T.; Hopper, D. W. *J. Am. Chem. Soc.* **2003**, *125*, 6462.
- (37) Davies, H. M. L.; Ni, A. W. *Chem. Commun.* **2006**, 3110.
- (38) Nadeau, E.; Li, Z. J.; Morton, D.; Davies, H. M. L. *Synlett* **2009**, 151.
- (39) Davies, H. M. L.; Antoulinakis, E. G. *J. Organomet. Chem.* **2001**, *617*, 47.
- (40) Davies, H. M. L.; Loe, O. *Synthesis* **2004**, 2595.
- (41) Davies, H. M. L.; Bruzinski, P. R.; Fall, M. J. *Tetrahedron Lett.* **1996**, *37*, 4133.
- (42) Davies, H. M. L.; Bruzinski, P. R.; Lake, D. H.; Kong, N.; Fall, M. J. *J. Am. Chem. Soc.* **1996**, *118*, 6897.
- (43) Thompson, J. L.; Davies, H. M. L. *J. Am. Chem. Soc.* **2007**, *129*, 6090.
- (44) Bergman, R. G. *Nature* **2007**, *446*, 506.
- (45) Godula, K.; Sames, D. *Science* **2006**, *312*, 67.
- (46) Dai, X.; Long, M. S.; Davies, H. M. L. *J. Am. Chem. Soc.* **2005**, *230*, 3150.
- (47) Dai, X.; Wan, Z. L.; Kerr, R. G.; Davies, H. M. L. *J. Org. Chem.* **2007**, *72*, 1895.
- (48) Davies, H. M. L.; Dai, X. *Strat. Tactics Org. Sy.* **2008**, *7*, 383.
- (49) Davies, H. M. L.; Dai, X. *Tetrahedron* **2006**, *62*, 10477.
- (50) Davies, H. M. L.; Dal, X.; Long, M. S. *J. Am. Chem. Soc.* **2006**, *128*, 2485.

- (51) Davies, H. M. L.; Doan, B. D. *J. Org. Chem.* **1998**, *63*, 657.
- (52) Davies, H. M. L.; Lian, Y. J. *Acc. Chem. Res.* **2012**, *45*, 923.
- (53) Davies, H. M. L.; Loe, O. *J. Am. Chem. Soc.* **2004**, *228*, 128.
- (54) Davies, H. M. L.; Loe, O.; Stafford, D. G. *Org. Lett.* **2005**, *7*, 5561.
- (55) Davies, H. M. L.; Sorensen, E. J. *Chem. Soc. Rev.* **2009**, *38*, 2981.
- (56) Davies, H. M. L.; Walji, A. M. *Angew. Chem. Int. Ed.* **2005**, *44*, 1733.
- (57) Lian, Y. J.; Miller, L. C.; Born, S.; Sarpong, R.; Davies, H. M. L. *J. Am. Chem. Soc.* **2010**, *132*, 12422.
- (58) Manning, J. R.; Davies, H. M. L. *Tetrahedron* **2008**, *64*, 6901.
- (59) Ren, P. D.; Twonsend, R. J.; Davies, H. M. L. *J. Am. Chem. Soc.* **2000**, *220*, 52.
- (60) Schwartz, B. D.; Denton, J. R.; Bernhardt, P. V.; Davies, H. M. L.; Williams, C. M. *Synthesis* **2009**, 2840.
- (61) Schwartz, B. D.; Denton, J. R.; Davies, H. M. L.; Williams, C. M. *Aust. J. Chem.* **2009**, *62*, 980.
- (62) Schwartz, B. D.; Denton, J. R.; Lian, Y. J.; Davies, H. M. L.; Williams, C. M. *J. Am. Chem. Soc.* **2009**, *131*, 8329.
- (63) Yates, P. *J. Am. Chem. Soc.* **1952**, *74*, 5376.
- (64) Pirrung, M. C.; Liu, H.; Morehead, A. T. *J. Am. Chem. Soc.* **2002**, *124*, 1014.
- (65) Kornecki, K. P.; Briones, J. F.; Boyarskikh, V.; Fullilove, F.; Autschbach, J.; Schrote, K. E.; Lancaster, K. M.; Davies, H. M. L.; Berry, J. F. *Science* **2013**, *342*, 351.

- (66) Nowlan, D. T.; Gregg, T. M.; Davies, H. M. L.; Singleton, D. A. *J. Am. Chem. Soc.* **2003**, *125*, 15902.
- (67) Blackmond, D. G. *Angew. Chem. Int. Ed.* **2005**, *44*, 4302.
- (68) Hui, B. C.; James, B. R. *Can. J. Chem.* **1974**, *52*, 3760.
- (69) Su, C. C.; Reed, J. W.; Gould, E. S. *Inorg. Chem.* **1973**, *12*, 337.
- (70) Arakawa, H.; Moro, n.; Ozaki, A. *Bull. Chem. Soc. Jpn.* **1974**, *47*, 2958.
- (71) James, B. R.; Wang, D. K. W., *Chem. Commun.* **1977**, 550.
- (72) James, B. R.; Wang, D. K. W. *Can. J. Chem.* **1980**, *58*, 245.
- (73) Shinkai, S.; Ishikawa, Y.; Shinkai, H.; Tsuno, T.; Makishima, H.; Ueda, K.; Manabe, O. *J. Am. Chem. Soc.* **1984**, *106*, 1801.
- (74) Menger, F. M.; Tsuno, T. *J. Am. Chem. Soc.* **1989**, *111*, 4903.
- (75) Hanabusa, K.; Ye, X.; Koyama, T.; Kurose, A.; Shirai, H.; Hojo, N. *J. Mol. Catal.* **1990**, *60*, 127.
- (76) Joshi, A. M.; MacFarlane, K. S.; James, B. R. *J. Organomet. Chem.* **1995**, *488*, 161.
- (77) Corey, E. J.; Noe, M. C. *J. Am. Chem. Soc.* **1996**, *118*, 319.
- (78) Otto, S.; Bertocin, F.; Engberts, J. B. F. N. *J. Am. Chem. Soc.* **1996**, *118*, 7702.
- (79) Drago, R. S.; Tanner, S. P.; Richman, R. M.; Long, J. R. *J. Am. Chem. Soc.* **1979**, *101*, 2897.
- (80) Drago, R. S.; Long, J. R.; Cosmano, R. *Inorg. Chem.* **1981**, *20*, 2920.
- (81) Doyle, M. P.; Colman, M. R.; Chinn, M. S. *Inorg. Chem.* **1984**, *23*, 3684.
- (82) Doyle, M. P.; Wang, L. C.; Loh, K. L. *Tetrahedron Lett.* **1984**, *25*, 4087.

- (83) Doyle, M. P.; Mahapatro, S. N.; Caughey, A. C.; Chinn, M. S.; Colman, M. R.; Harn, N. K.; Redwine, A. E. *Inorg. Chem.* **1987**, *26*, 3070.
- (84) Xu, X. C.; Doyle, M. P. *Inorg. Chem.* **2011**, *50*, 7610.
- (85) Perry, R. H.; Cahill, T. J.; Roizen, J. L.; Du Bois, J.; Zare, R. N. *P. Natl. Acad. Sci. USA* **2012**, *109*, 18295.
- (86) Zalatan, D. N.; Du Bois, J. *J. Am. Chem. Soc.* **2009**, *131*, 7558.
- (87) Michaelis, L.; Menten, M. L. *Biochem. Z.* **1913**, *49*, 333.
- (88) Lineweaver, H.; Burk, D. *J. Am. Chem. Soc.* **1934**, *56*, 658.
- (89) Mathew, J. S.; Klussmann, M.; Iwamura, H.; Valera, F.; Futran, A.; Emanuelsson, E. A. C.; Blackmond, D. G. *J. Org. Chem.* **2006**, *71*, 4711.
- (90) Baxter, R. D.; Sale, D.; Engle, K. M.; Yu, J. Q.; Blackmond, D. G. *J. Am. Chem. Soc.* **2012**, *134*, 4600.
- (91) Baxter, R. D.; Blackmond, D. G. *Tetrahedron* **2013**, *69*, 5604.
- (92) Iwamura, H.; Mathew, S. P.; Blackmond, D. G. *J. Am. Chem. Soc.* **2004**, *126*, 11770.
- (93) Iwamura, H.; Wells, D. H.; Mathew, S. P.; Klussmann, M.; Armstrong, A.; Blackmond, D. G. *J. Am. Chem. Soc.* **2004**, *126*, 16312.
- (94) Mathew, S. P.; Iwamura, H.; Blackmond, D. G. *Angew. Chem. Int. Ed.* **2004**, *43*, 3317.
- (95) Klussmann, M.; Iwamura, H.; Mathew, S. P.; Wells, D. H.; Pandya, U.; Armstrong, A.; Blackmond, D. G. *Nature* **2006**, *441*, 621.
- (96) Klussmann, M.; Mathew, S. R.; Iwamura, H.; Wells, D. H.; Armstrong, A.; Blackmond, D. G. *Angew. Chem. Int. Ed.* **2006**, *45*, 7989.

- (97) Mathew, S. P.; Klusmann, M.; Iwamura, H.; Wells, D. H.; Armstrong, A.; Blackmond, D. G. *Chem. Comm.* **2006**, 4291.
- (98) Blackmond, D. G.; Armstrong, A.; Coombe, V.; Wells, A. *Angew. Chem. Int. Ed.* **2007**, *46*, 3798.
- (99) Zotova, N.; Franzke, A.; Armstrong, A.; Blackmond, D. G. *J. Am. Chem. Soc.* **2007**, *129*, 15100.
- (100) Zotova, N.; Broadbelt, L. J.; Armstrong, A.; Blackmond, D. G. *Bioorg. Med. Chem. Lett.* **2009**, *19*, 3934.
- (101) Zotova, N.; Moran, A.; Armstrong, A.; Blackmond, D. G. *Adv. Synth. Catal.* **2009**, *351*, 2765.
- (102) Zotova, N.; Valera, F.; Blackmond, D. G. *Chem. Indust.* **2009**, *123*, 445.
- (103) Blackmond, D. G.; Moran, A.; Hughes, M.; Armstrong, A. *J. Am. Chem. Soc.* **2010**, *132*, 7598.
- (104) Hein, J. E.; Bures, J.; Lam, Y. H.; Hughes, M.; Houk, K. N.; Armstrong, A.; Blackmond, D. G. *Org. Lett.* **2011**, *13*, 5644.
- (105) Bures, J.; Armstrong, A.; Blackmond, D. G. *J. Am. Chem. Soc.* **2012**, *134*, 6741.
- (106) Blackmond, D. G.; McMillan, C. R.; Ramdeehul, S.; Schorm, A.; Brown, J. M. *J. Am. Chem. Soc.* **2001**, *123*, 10103.
- (107) Rosner, T.; Le Bars, J.; Pfaltz, A.; Blackmond, D. G. *J. Am. Chem. Soc.* **2001**, *123*, 1848.
- (108) Strieter, E. R.; Blackmond, D. G.; Buchwald, S. L. *J. Am. Chem. Soc.* **2003**, *125*, 13978.

(109) Blackmond, D. G.; Schultz, T.; Mathew, J. S.; Loew, C.; Rosner, T.; Pfaltz, A. *Synlett* **2006**, 3135.

(110) Ferretti, A. C.; Mathew, J. S.; Brennan, C.; Blackmond, D. G. *Chem. Indust.* **2009**, 123, 223.

CHAPTER 2

Kinetic Studies on the Donor/Acceptor Dirhodium(II) Carbene

Cyclopropanation of Styrene

2.1 Background

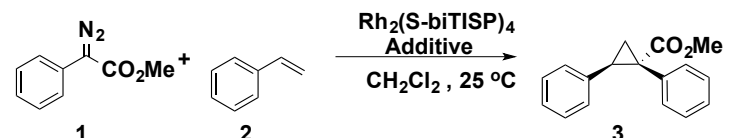
A wide range of synthetically useful transformations can be conducted using dirhodium(II) carbenoid intermediates.¹ Some of the most notable transformations are inter- and intra-molecular C-H functionalization by means of carbenoid-induced C-H insertion and cyclopropanation. Additionally, the advent of a range of chiral dirhodium tetracarboxylate catalysts has rendered many of the synthetically useful carbenoid transformations highly enantioselective.¹⁻¹⁰ A drawback of dirhodium(II) catalysis, however, is the high cost of rhodium.

A long-term challenge in the carbenoid field is the development of practical and sustainable methods for conducting these reactions. Considerable effort has been spent on developing first row transition metal catalysts to replace the dirhodium(II) catalysts.¹¹⁻¹³ Even though there have been some spectacular advances, in general many of the other metal catalysts do not have the catalytic efficiency or display the breadth of carbenoid reactivity that is possible under dirhodium(II) catalysis. Consequently, major efforts have been directed towards enhancing the sustainability of dirhodium(II) catalysts. Therefore, a variety of strategies have been developed to immobilize the catalysts.¹⁴⁻²⁸ The work of graduate student Miss Kathryn Chepiga has focused on immobilization strategies. Studies in this chapter will explore an alternative option, which is to conduct the dirhodium(II)-catalyzed reaction with extremely low catalyst loading.^{29,30}

2.1.1 Dirhodium Catalysts High TON

One method of increasing the practicality of dirhodium(II) catalysts is to conduct the reactions with extremely low catalyst loading. In a study by Davies and coworkers, turnover numbers (TONs) >100,000 were shown to be feasible for the bridging dirhodium(II) catalyst $\text{Rh}_2(\text{S-BiTISP})_2$.²⁹ The additives, methyl benzoate and molecular sieves, were necessary to achieve high TON and enantioselectivity (Table 2.1). In the absence of additives, the level of enantioselectivity and yield dropped precipitously when attempting high-turnover reactions (Table 2.1: entries 1-4). It was proposed that the methyl benzoate additive stabilizes the dirhodium(II) carbenoid complex by coordination to the metal or carbenoid moiety.

Table 2.1: High TON for $\text{Rh}_2(\text{S-biTISP})_4$.



The reaction scheme shows the conversion of diazo ester **1** (methyl diazoacetate) and alkene **2** (styrene) to epoxide **3** (1,2-epoxy-1-phenylethane-1-carboxylate methyl ester). The reaction conditions are $\text{Rh}_2(\text{S-biTISP})_4$, Additive, CH_2Cl_2 , 25 °C.

Entry	Substrate/Catalyst Ratio	Additive ^b	Yield (%)	ee(%)	Time/ h
1	1000	A	72	89	1
2	10 000	A	80	89	6
3	100 000	A	--	--	>144 ^a
4	100 000	B	--	--	>144 ^a
5	100 000	C	82	65	42
6	100 000	D	85	83	28

^a Reaction did not go to completion. ^b A: no additives. B: methyl benzoate (1 equiv.). C: 4 A molecular sieves. D: methyl benzoate (1 equiv.) and 4 A molecular sieves.

Recently, Davies has demonstrated that solvent-free dirhodium(II) catalyzed reactions of donor/acceptor carbenoids can result in TONs of >1,000,000.³⁰ The electrophilic *p*-methoxyphenyl dirhodium carbenoid, **1b**, demonstrated 1,800,000 turnovers in the presence of Rh₂(*S*-PTAD)₄ (Table 2.2: entry 5). These studies reveal that the turnover number was influenced by the choice of catalyst and donor/acceptor carbenoid precursor (Table 2.2). Moreover, under these high turnover conditions a significant drop in the enantioselectivity was observed.

Table 2.2 Solvent-Free High TON Dirhodium(II) Catalyzed Cyclopropanation

$$\text{R}-\text{C}(\text{N}_2)=\text{CO}_2\text{Me} + \text{Styrene} \xrightarrow[\text{Temperature}]{\text{Rh(II)}} \text{Cyclopropane}$$

1a, R = Ph
1b, R = *p*-(MeO)Ph
2
3a, R = Ph
3b, R = *p*-(MeO)Ph

Entry	R	Catalyst	Catalyst loading (mol%)	Time/h	Yield (%)	ee (%)	TON	TOF/h ⁻¹
1	Ph	Rh ₂ (<i>S</i> -DOSP) ₄	0.0003	120	93	58	3.0 × 10 ⁵	2.5 × 10 ³
2 ^a	Ph	Rh ₂ (<i>S</i> -PTAD) ₄	0.00005	96	96	13	1.5 × 10 ⁶	1.5 × 10 ⁴
3	<i>p</i> -(MeO)Ph	Rh ₂ (<i>S</i> -DOSP) ₄	0.0001	144	90	69	8.5 × 10 ⁵	5.9 × 10 ³
4 ^a	<i>p</i> -(MeO)Ph	Rh ₂ (<i>S</i> -PTAD) ₄	0.00005	72	92	51	1.8 × 10 ⁶	2.5 × 10 ⁴

^a Opposite enantiomer formed

The standard reaction conditions for cyclopropanation of styrene with aryldiazoacetates **1a** and **1b** require 0.5-1.0 mol% of dirhodium(II) catalyst to achieve high asymmetric induction. At 25 °C, 88% ee is routinely observed with 1.0 mol% Rh₂(*S*-DOSP)₄ for **1a** and 90% ee in the presence of **1b**. Under the high turnover conditions, the enantioselectivity drops to 58% ee with 0.0003 mol% of Rh₂(*S*-DOSP)₄ for **1a** (Table 2.2, entry 1) and 69% ee for **1b** with 0.0001 mol% of catalyst (Table 2.2, entry 3). Similar trends were observed with Rh₂(*S*-PTAD)₄. Standard conditions require

0.5 mol% of catalyst and result in 21% ee and 96% ee for **1a** and **1b**, respectively. As illustrated in the table, high turnover conditions result in 13% ee and 51% ee. The cause for such a significant change in enantioselectivity is not well understood, however, this work does demonstrate the excellent ability of the dirhodium catalyst to conduct high TON reactions.

2.2 Results

In order to develop general and robust conditions for high turnover carbenoid reactions a much more detailed understanding of factors that contribute to reaction rate and catalyst stability is necessary. Mechanistic studies to date have demonstrated the electrophilic nature and structure of dirhodium(II) carbene can significantly affect selectivity. To our knowledge, no study has identified the contribution catalyst deactivation plays in achieving high enantioselectivity and turnover numbers (TON). Through kinetic techniques and reaction progress kinetic analysis (RPKA) we have established rate laws, probed catalyst deactivation and demonstrated methods for achieving TON's up to 4 million for the dirhodium(II)-catalyzed asymmetric cyclopropanation of styrene.

Reaction Progress Kinetic Analysis or RPKA is used to understand concentration dependencies as well as modes of catalyst deactivation/activation.³¹ Observations made via RPKA, may have been overlooked in prior computational and experimental analysis.³² In this study real-time FTIR (Mettler Toledo ReactIRTM 45M) and reaction calorimetry (Ominical Insight CPR 220 Calorimeter) have been used to monitor the reaction progress. Real-time FTIR allows the tracking of infra-red stretch(es) over time to yield a concentration versus time relationship. This information can then be integrated to

provide reaction rate data. Decomposition of the unique diazoacetate stretch at 2100 cm^{-1} was monitored for all FTIR kinetic studies (Figure 2.1).

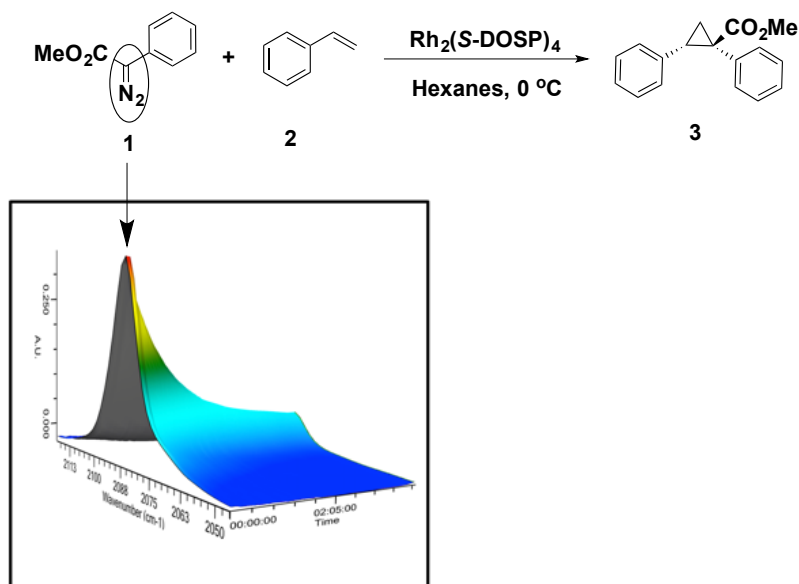
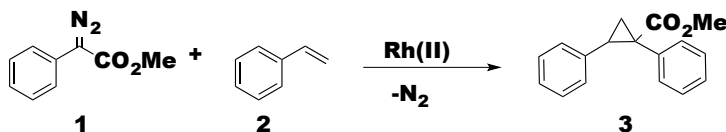


Figure 2.1: Three-dimensional FTIR spectrum of diazo compound **1** recorded with a Mettler Toledo ReactIRTM 45M. The 3D plot illustrates **the wavenumber (cm^{-1} , x-axis) versus peak height (A.U, y-axis) versus time (h:m:s, z-axis) for the reaction of **1** (0.3 M) and **2** (3.0 M) catalyzed by $\text{Rh}_2(\text{S-DOSP})_4$ (0.005 mol%) in hexanes at $0\text{ }^\circ\text{C}$.**

The dirhodium(II) catalyzed cyclopropanation of styrene by phenyldiazoacetate **1** was studied to understand factors that influence the ability of dirhodium(II) catalysts to achieve high turnover numbers (Scheme 2.1). TONs greater than 1.0 million have been recorded using $\text{Rh}_2(\text{S-DOSP})_4$ as catalyst for cyclopropanation with aryldiazoacetates.³⁰ While this standard reaction has been studied extensively computationally,^{33,34} we envisioned that a kinetic study could give insight to catalyst activation or deactivation. Ultimately, connecting the kinetic experiments to product distribution and

enantioselectivity would provide a basis for developing even better high TON processes and could lead to the design of novel catalysts.



Scheme 2.1: Dirhodium(II) catalyzed cyclopropanation of **2** with donor/acceptor diazo compound **1**.

2.2.1 Dirhodium(II) Catalyst Screening

Prior to conducting a full kinetic analysis, several dirhodium(II) catalysts were screened to probe the influence of catalyst structure on the reactivity of the dirhodium(II) carbenoid (Figure 2.2). The reactions were conducted at a low catalyst loading to specifically test the robust nature of the catalyst under high TON conditions. Previous studies have focused on final yield, enantioselectivity and diastereoselectivity as a determinant of whether catalyst structure has influence on carbenoid reactivity.³⁵ However, final product distributions do not assess the catalysts behavior throughout the reaction. Ultimately, monitoring the reaction progress and understanding reaction rates, would evaluate the kinetic activity of the dirhodium(II) catalysts over time.

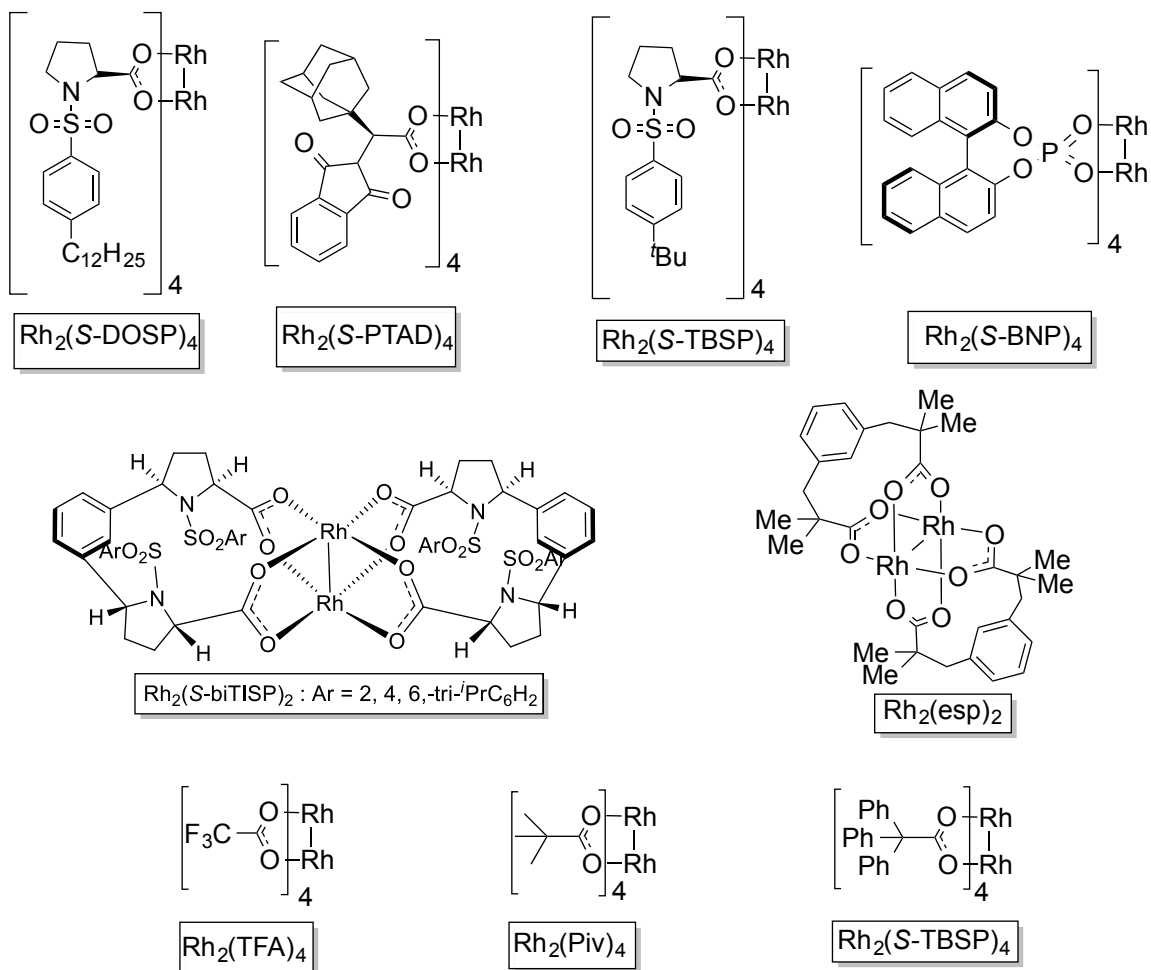


Figure 2.2: Dirhodium(II) catalysts screened in the cyclopropanation of styrene. A variation of chiral, achiral and bridging and non-bridging catalysts were screened. All of the catalysts have shown exceptional catalytic activity at catalyst loadings ≥ 1.0 mol%. Evaluating the catalysts under high turnover conditions (0.005 mol%/20,000 TON) can give insight into structural factors that contribute to high catalytic activity.

Dirhodium(II) carbene cyclopropanation is an exceptionally robust reaction. Work from previous graduate student in the Davies lab, Dr. Jorn Hansen, has illustrated that the reaction was extremely robust at room temperature, with complete decomposition of the diazo compound under catalyst loading of 0.01 mol% achieved in seconds.³⁴ In order to extract kinetic data from this reaction, reaction conditions would need to be identified, in which the reaction did not give off a significant exotherm and could be monitored over several minutes. Optimization of conditions found that 10 equiv. of styrene and 0.005 mol% of catalyst at 0 °C in hexanes was optimum for kinetic studies. Figure 2.3 is an example of a diazo compound decomposition for cyclopropanation of styrene with $\text{Rh}_2(\text{S-DOSP})_4$.

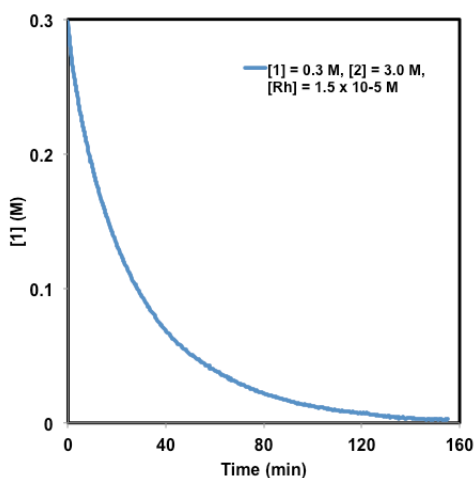


Figure 2.3: Plot generated from ReactIRTM data depicting time(min) versus concentration of **1** for reaction of **2** (3.0 M) catalyzed by $\text{Rh}_2(\text{S-DOSP})_4$ (0.005 mol%) in hexanes at 0 °C.

The concentration vs time data is more useful when plotted in the RPKA format for easy comparison of experiments. Upon fitting the concentration vs time plot with a high order polynomial and integration of the curve, a rate vs concentration plot was constructed (Figure 2.4). In this plot, we see a nearly linear rate decrease for the reaction progress (right to left). Deviation from the theoretically linear plot denotes changes in the catalyst's activity over the course of the reaction.

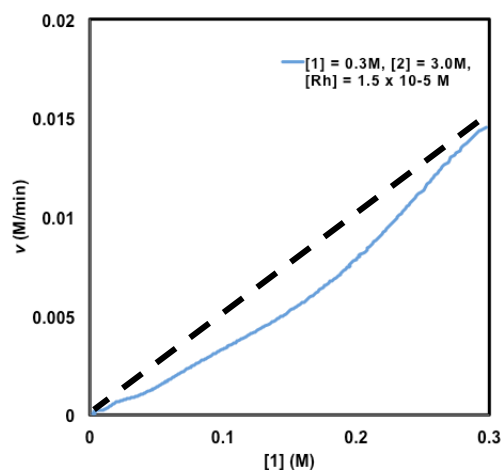


Figure 2.4: Plot of the reaction rate (v (M/min)) versus concentration of **1** for reaction of **2** (3.0 M) catalyzed by $\text{Rh}_2(\text{S-DOSP})_4$ (0.005 mol%) in hexanes at 0 °C. The plot is read from right to left. As the concentration of the diazo compound decreases the rate of the reaction decreases and full conversion to the cyclopropane is observed.

Chiral dirhodium(II) catalysts have shown incredible activity in the cyclopropanation of styrene under the typical catalyst loadings of 1.0 mol%.¹⁰ An interest of this work was to understand how the catalyst behaved at low catalyst loadings/high turnover number conditions. By evaluating the kinetic activity, factors that contribute to catalyst stability could be assessed. The kinetic activity of the chiral catalysts was highly variable as illustrated in Figure 2.5. The tetracarboxylate catalysts $\text{Rh}_2(\text{S-PTAD})_4$ (red curve) and $\text{Rh}_2(\text{S-TBSP})_4$ (purple curve) demonstrated faster reaction rates than $\text{Rh}_2(\text{S-DOSP})_4$ (light blue). Specifically, the reaction with $\text{Rh}_2(\text{S-PTAD})_4$ hits a rate maximum then linearly decreases in rate after initial decomposition of the diazo compound. $\text{Rh}_2(\text{S-TBSP})_4$ has a relatively fast initial rate which quickly deactivates over the course of the reaction. Very little kinetic activity is observed for $\text{Rh}_2(\text{S-biTISP})_4$ and $\text{Rh}_2(\text{S-BNP})_4$.

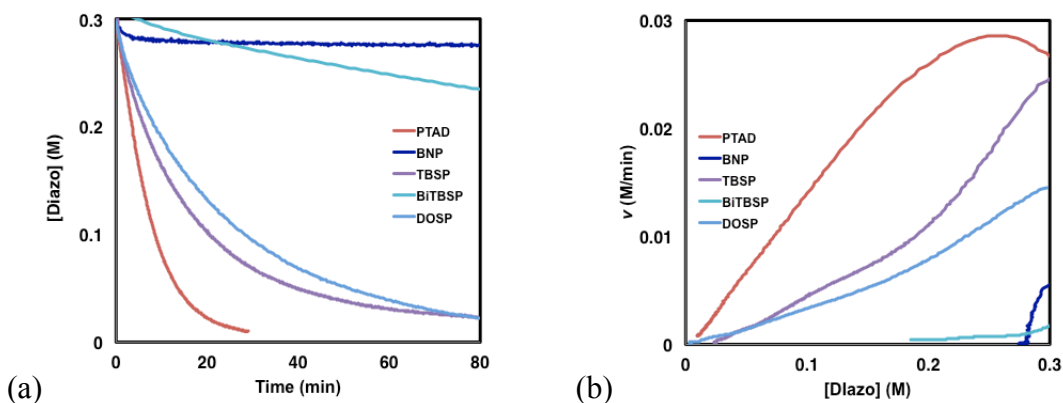


Figure 2.5: Kinetic activity of chiral dirhodium(II) catalysts screening in reaction of **1** (0.3 M) with **2** (3.0 M) at 0.005 mol% of Rh(II) catalyst in hexanes at 0 °C. (A) Concentration of **1** versus time (min) plot. (B) Rate of the reaction versus concentration of **1**. $\text{Rh}_2(\text{S-PTAD})_4$ (red), $\text{Rh}_2(\text{S-DOSP})_4$ (light blue) and $\text{Rh}_2(\text{S-TBSP})_4$ (purple) display exceptional reactivity. Very little activity is observed for $\text{Rh}_2(\text{S-BNP})_4$ (dark blue) and $\text{Rh}_2(\text{biTISP})_4$ (teal). The stark differences among the curves illustrate that the catalysts have very different kinetic activity under high turnover conditions, despite the exceptional asymmetric induction that is observed for all the catalysts at 0.5-1.0 mol% catalyst loading.

In most cases, the levels of enantioselectivity under the high turnover conditions were significantly lower than standard conditions. For example, 43% ee was recorded for the high TON $\text{Rh}_2(\text{S-DOSP})_4$ catalyzed reaction versus 88% ee for a reaction conducted with 1 mol % catalyst loading, 30% ee and 24% ee were observed for $\text{Rh}_2(\text{S-PTAD})_4$ and $\text{Rh}_2(\text{S-TBSP})_4$ respectively. The enantioselectivity observed with the Lewis acidic catalyst $\text{Rh}_2(\text{S-BNP})_4$ (dark blue) was 12% ee, while the bridging dirhodium catalyst $\text{Rh}_2(\text{S-biTISP})_4$ was 18% ee. Table 2.3 demonstrates a comparison between the standard conditions and high TON conditions. Only in the case of $\text{Rh}_2(\text{S-PTAD})_4$ is a higher enantioselectivity observed.

Table 2.3: Catalyst activity and high and low catalyst loading

Entry	Catalyst	Catalyst Loading (mol%)	Solvent	Temp (°C)	% ee	ref.
1	$\text{Rh}_2(\text{S-DOSP})_4$	1.0	Hexanes	25	88	10
2	$\text{Rh}_2(\text{S-DOSP})_4$	0.005	Hexanes	0	43	
3	$\text{Rh}_2(\text{S-PTAD})_4$	1.0	Toluene	25	21	10
4	$\text{Rh}_2(\text{S-PTAD})_4$	0.005	Hexanes.	0	30	
5	$\text{Rh}_2(\text{S-TBSP})_4$	1.0	Pentane	25	86	35
6	$\text{Rh}_2(\text{S-TBSP})_4$	0.005	Hexanes	0	24	
7	$\text{Rh}_2(\text{S-biTISP})_4$	1.0	Hexanes	25	84	29
8	$\text{Rh}_2(\text{S-biTISP})_4$	0.005	Hexanes.	0	18	
9	$\text{Rh}_2(\text{S-BNP})_4$	1.0	Toluene	25	43	10
10	$\text{Rh}_2(\text{S-BNP})_4$	0.005	Hexanes	0	12	

Achiral dirhodium(II) catalysts are typically known to be efficient for the cyclopropanation of styrene at catalyst loadings ≥ 1 mol%, however, this work was interested in how the achiral catalysts compared to chiral catalysts at low catalyst loadings. Figure 2.6 describes achiral dirhodium(II) catalysts screened for the cyclopropanation of styrene. Very little kinetic activity was observed in with achiral catalysts $\text{Rh}_2(\text{TPA})_4$ (black) and $\text{Rh}_2(\text{OPiv})_4$ (orange) supporting empirical data that chiral catalysts have greater activity in donor/acceptor carbenoid chemistry. The achiral bridging catalyst $\text{Rh}_2(\text{esp})_2$ (purple) illustrated steady decomposition over the course of the reaction. Significant deactivation of the catalyst was not observed. The electron poor catalyst $\text{Rh}_2(\text{TFA})_4$ (green) started with very high catalytic activity and quickly deactivated, as a result, the reaction did not go to completion.

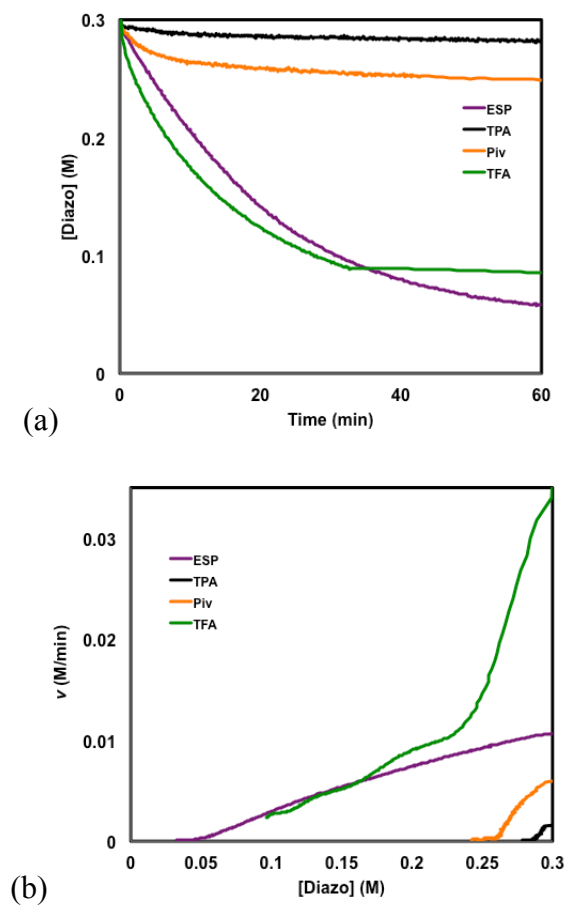


Figure 1.6: Kinetic activity of achiral dirhodium(II) catalysts in the reaction of **1** (0.3 M) and **2** (3.0 M) with 0.005 mol% of Rh(II) catalyst in hexanes at 0 °C. (A) Concentration of **1** (M) versus time (min) is plotted. (B) Rate plot describing the relationship between the reaction rate (v (M/min)) versus concentration of the diazo compound. Together the plots illustrate the exceptional reactivity observed with $\text{Rh}_2(\text{esp})_2$ (purple). $\text{Rh}_2(\text{TFA})_4$ (green) has a very high initial reaction rate and quickly deactivates. Very little kinetic activity is observed for $\text{Rh}_2(\text{TPA})_4$ (black) and $\text{Rh}_2(\text{OPiv})_4$ (orange).

2.2.2 RPKA Studies

Screening dirhodium catalysts provides a quantitative and qualitative view of the activity of the catalyst over the course of the reaction; the screening, however, does not explain the key reaction driving-forces as well as factors that may contribute to catalyst deactivation. Further kinetic analysis of the cyclopropanation of styrene were explored under $\text{Rh}_2(\text{S-DOSP})_4$ catalysis to gain insight into mechanistic details that may have been previously overlooked. “Different” and “same” excess experiments were conducted to generate information about the concentration dependencies. Different excess experiments would access the dependency of **2**, the diazoacetate **1**, and the catalyst. The robustness of the catalyst would be explored in same excess experiments. We speculated that other kinetic experiments would be necessary if catalyst deactivation was observed in the same excess experiments.

The concentration dependency of the catalyst was of particular interest because exceptional enantioselectivities are observed at turnover numbers $<10,000$, however under high turnover number conditions the enantioselectivity quickly drops off. Therefore, one of the first factors assessed was the concentration of catalyst. The blue curve in Figure 2.7 represents the standard conditions with 0.3 M diazo compound, 3.0 M styrene and 0.005 mol% catalyst. The orange curve represents 0.3 M diazo compound, 3.0 M styrene and 0.025 mol% catalyst. Increasing the concentration of the catalyst resulted in a faster reaction rate (orange curve, Figure 2.7). The cyclopropane was formed $>98\%$ conversion and 82% ee. This compared to the 43% ee and $>98\%$ conversion for the standard reaction at 0.005 mol%. The orange curve is also very linear suggesting that there was very little catalyst deactivation over the course of the reaction. The result suggests that there is a positive order dependence of the catalyst. The next factor tested was the concentration dependency on the diazo compound.

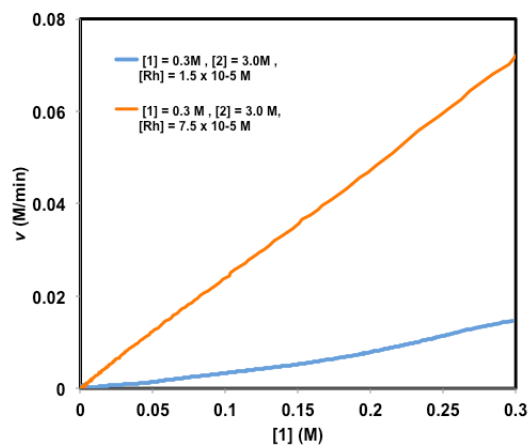


Figure 2.7: Reaction rate v (M/min) versus concentration of **1** for the reaction of **2** with $\text{Rh}_2(\text{S-DOSP})_4$ in hexanes at 0°C . The concentration of $[\text{Rh}]$ is varied. Orange curve illustrates $7.5 \times 10^{-5} \text{ M}$ $\text{Rh}_2(\text{S-DOSP})_4$, Blue curve represents $1.5 \times 10^{-5} \text{ M}$ of $\text{Rh}_2(\text{S-DOSP})_4$.

Assessing the reaction rate concentration dependency on diazo compound was integral in understanding the reaction driving-forces. Therefore, the next set of experiments varied the concentration of the diazo compound **1** from 0.3 M to 0.6 M, while holding all other substrate concentrations constant. Figure 2.8 illustrates the differences between the standard reaction conditions (blue curve) and conditions where the concentration of **1** has been doubled. Increasing the concentration of the diazo compound resulted in >96% conversion and 51% ee of the cyclopropane product. Additionally, and a much faster rate is observed at the higher concentration of **1**. The positive correlation suggests that the reaction is positive order in diazo compound, supporting computational data stating that the extrusion of N₂ is the rate-determining step. The concentration of the styrene was kept at a constant 3.0 M to ensure that cyclopropanation, not diazo compound dimerization was the major reaction.

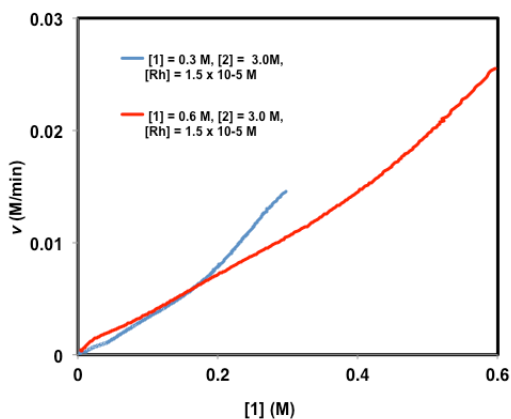


Figure 2.8: Reaction rate v (M/min) versus time (min) for the reaction of **1** with **2** (3.0 M) with Rh₂(S-DOSP)₄ (0.005 mol%) in hexanes at 0 °C. The concentration of **1** is varied. The red curve, [1] = 0.6 M, and blue curve [1] = 0.3 M.

The coordination of olefin moieties and Lewis basic sites is known for dirhodium(II) complexes.³⁶⁻³⁸ Consequently, an evaluation of olefin coordination on the reaction rate was examined. The effect of styrene was probed by decreasing [2] from 3.0 M to 1.5 M, while [1] and [Rh] were kept constant at 0.3 M and 1.5×10^{-5} , respectively (Figure 2.9, purple curve). Under these conditions, the cyclopropane was formed in >96% conversion and 66% ee. When the rate data were plotted against the standard reaction curve (blue), a 2x increase in the reaction rate was noted, signifying that olefin coordination influences the rate of carbenoid formation. Moreover, the purple rate curve depicts a nearly linear activity until 0.12 M of [1], where deactivation is observed.

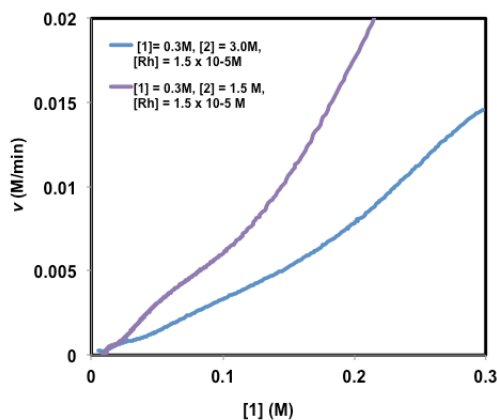


Figure 2.9: Reaction rate v (M/min) versus concentration of 1 for the reaction of **1** (0.3 M) with **2** catalyzed by $\text{Rh}_2(\text{S-DOSP})_4$ (0.005 mol%). The dependence on **2** was varied.. Purple curve, [2] = 1.5 M styrene and blue curve, [2] = 3.0 M.

Studies to this point focused on determining concentration dependences of reaction substrates; however, we employed the “same excess” protocol to assess if there were other sources of catalyst activation or deactivation (Figure 2.10). For the same excess experiment, $e = 2.7$ M. The standard reaction was conducted with 0.3 M diazo compound, 3.0 M styrene (blue curve), 1.5×10^{-5} M catalyst, and resulted in the formation of the cyclopropane in 43% ee. The second experiment utilized 0.6 M diazo compound, 3.3 M styrene, 1.5×10^{-5} M catalyst, and resulted in the formation of the cyclopropane in 42% ee (red curve). The reaction under the standard conditions (blue curve) starts at a much faster rate than the second experiment (red curve). The concentration difference between the styrene and diazo compound is identical in the two experiments, therefore the reactions have the same excess value. In same excess experiments, similar reaction rates should be observed when the reactions meet at a common concentration, if no deactivation of the catalyst is present. In our case identical reaction rates should be present at 0.3 M diazo compound, however, a much slower rate is observed for the red curve, suggesting that there is significant catalyst deactivation.

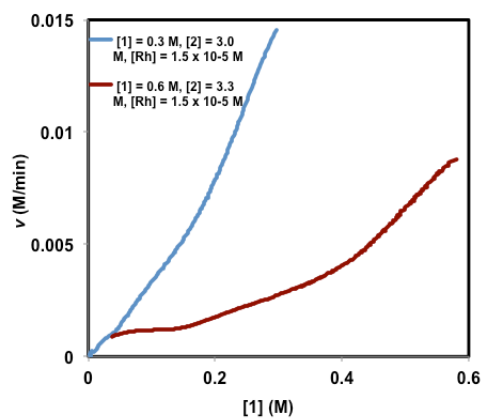


Figure 2.10: Reaction rate v (M/min) versus concentration **1** in reaction with **2** catalyzed by $\text{Rh}_2(\text{S-DOSP})_4$ (0.005 mol%) in hexanes at 0 °C. Red curve illustrates 0.6 M diazo compound, 3.3 M styrene and blue curve represents 0.3 M diazo compound, 3.0 M styrene . Excess or $e = 2.7$ M.

Product inhibition is common in metal-catalyzed reactions and coordination to the metal center, often through olefinic, aromatic, and Lewis basic sites, could potentially minimize the number of turnover numbers a catalyst can undergo. Therefore, the final RPKA experiment conducted, tested for product inhibition (Figure 2.11). Interested in how this type of deactivation could potentially influence catalyst turnover and the enantioinduction of the reaction, the reaction mixture was doped with 0.3 M (1 equiv.) of 95% ee cyclopropane product prior to addition of the catalyst. The diazo, styrene and catalyst were kept under the standard conditions (0.3 M, 3.0 M, and 1.5×10^{-5} M, respectively). The cyclopropane was formed in >85% conversion and 40% ee, however, the rate of formation was significantly slower.

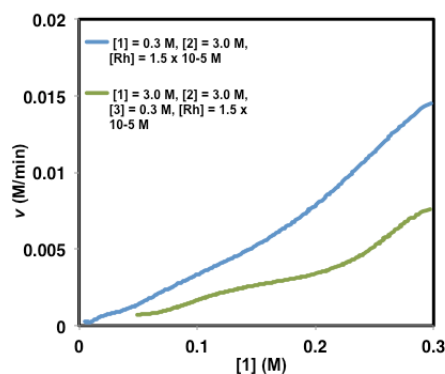
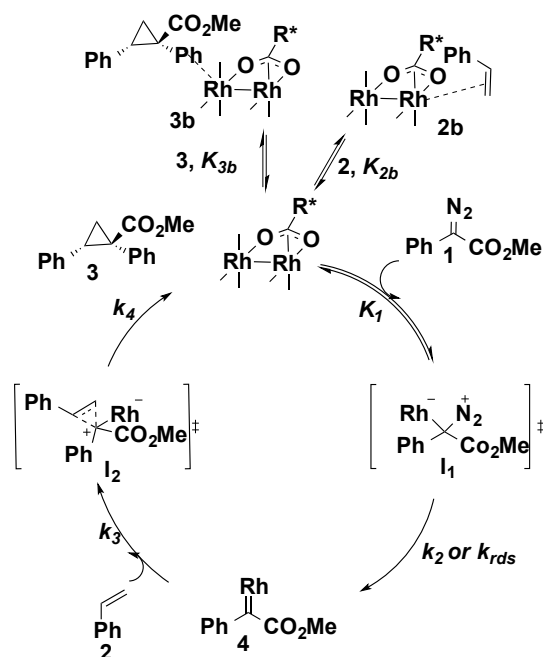


Figure 2.11: Reaction rate v (M/min) versus concentration of **1** (0.3 M) in reaction with **2** (3.0 M) catalyzed by $\text{Rh}_2(\text{S-DOSP})_4$ in hexanes at 0 °C. The green curve is doped with 1 equiv. of **3** (0.3M). Blue curve represents no addition of **3**.

2.2.3 Mechanism and Rate Law

The RPKA has allowed us to establish a modified mechanism for cyclopropanation of styrene (Scheme 2.2). The new catalytic cycle for dirhodium carbenoid cyclopropanation includes two key equilibrium processes. 1) The equilibrium between the unbound catalyst and the styrene bound catalyst and 2) the equilibrium between the unbound catalyst and the product bound catalyst. These additional processes are considered “off-cycle” catalyst reservoirs. “Off-cycle” reservoirs are responsible for catalyst activation/deactivation and lower the total concentration of catalyst participating in “on-cycle” steps.

Once the catalyst is free from one of the equilibrium processes it is available to complex with the diazo compound. This is followed by nitrogen extrusion, resulting in the formation of the dirhodium carbenoid, **4**. The dirhodium carbenoid reacts with the styrene trap in a [1+2] fashion to afford the cyclopropane product, **3**. The catalyst is then free to bind to the cyclopropane product, **3b**, or styrene, **2b**, and re-enter the catalytic cycle.



Scheme 2.2: Mechanism for cyclopropanation of styrene.

A rate law can be derived based on the catalytic cycle described above. In order to develop a rate law all on cycle steps and off cycle steps must be defined. On-cycle steps are steps that permit reaction progression and off-cycle steps are steps that contribute to catalyst deactivation/activation and reaction retardation.

Figure 2.12 depicts the on-cycle and off-cycle elementary steps for the cyclopropanation of styrene by $\text{Rh}_2(\text{S-DOSP})_4$. On-cycle steps include: reversible dirhodium complexation with diazo compound to generate intermediate I_1 (K_1), extrusion of nitrogen to give the dirhodium(II) carbene **4** (k_{rds}), complexation of the **4** with styrene (I_2 , k_3), and finally formation of the product, **3**, and regeneration of the free dirhodium(II) species (k_4). Off-cycle steps are coordination of the dirhodium catalyst to styrene to form **2b** (K_{2b}) and coordination of the dirhodium catalyst to the product to form species **3b**, (K_{3b}).

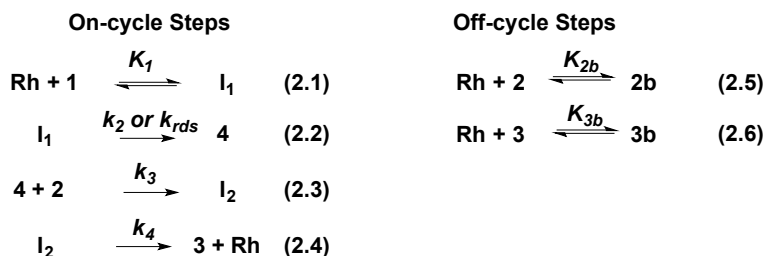


Figure 2.12: On-cycle and Off-cycle elementary steps for the cyclopropanation of **2** (3.0 M) with **1** (0.3 M) catalyzed by Rh₂(S-DOSP)₄ (0.005 mol%) in hexanes at 0 °C.

The generic rate law 2.7 is written where r is rate, k_{rds} is the rate constant for the rate-determining step and **I**₁ is the fleeting intermediate formed prior to the rate-determining step. Only elementary steps prior to the rate-determining step are important because these steps account for the overall rate of the reaction. The concentration of intermediates formed after the rate determining step are fleeting, therefore, their overall contributions are negligible.

$$r = k_{rds}[\text{I}_1] \quad (2.7)$$

Steady-state approximation is used for all on-cycle and off-cycle steps to define the concentration of fleeting intermediate **I**₁. In order to explicitly show elementary steps that define **I**₁, K_1 is written as k_1/k_{-1} (Equation 2.8, 2.9).

$$\frac{d[\text{I}_1]}{dt} = k_1[\text{Rh}][1] - k_{-1}[\text{I}_1] - k_{rds}[\text{I}_1] = 0 \quad (2.8)$$

$$= k_1[\text{Rh}][1] - (k_{-1} - k_{rds})[\text{I}_1] \quad (2.9)$$

The equation is then rearranged to solve for $[I_1]$ (Equation 2.10). Since k_1 , k_{-1} , and k_{rds} are constants, a is used as substitution for $k_1/(k_{-1} + k_{rds})$ (Equation 2.11).

$$[I_1] = \frac{k_1[Rh][1]}{k_{-1} + k_{rds}} \quad (2.10)$$

$$[I_1] = a[Rh][1] \quad (2.11)$$

Next, the catalyst mass balance is determined. $[Rh]_T$ denotes the total concentration of dirhodium(II) and includes the two off-cycle reservoirs of the catalyst (**2b** and **3b**) as well as I_1 (Equation 2.12). $[I_1]$, $[2b]$, $[3b]$ are then defined (Equation 2.13) and solve for $[Rh]$ (Equation 2.15).

$$[Rh]_T = [Rh] + [I_1] + [2b] + [3b] \quad (2.13)$$

$$[Rh]_T = [Rh] + a[Rh][1] + K_{2b}[Rh][2] + K_{3b}[Rh][3] \quad (2.14)$$

$$[Rh]_T = [Rh](1 + a[1] + K_{2b}[2] + K_{3b}[3]) \quad (2.14)$$

$$[Rh] = \frac{[Rh]_T}{(1 + a[1] + K_{2b}[2] + K_{3b}[3])} \quad (2.15)$$

The $[I_1]$ is fully defined in Equation 2.16

$$[I_1] = \frac{a[1][Rh]_T}{(1 + a[1] + K_{2b}[2] + K_{3b}[3])} \quad (2.16)$$

Once [I] is fully defined, it is substituted into the generic rate equation (2.8). The complete rate law (Equation 2.17) is a mathematical description of the reaction. It illustrates the key attributes that contribute to the overall rate of the reaction, including sources of catalyst deactivation. According to the rate equation we have derived, decreasing the extent of product inhibition and or catalyst coordination to styrene would increase the rate of the reaction and potentially result in higher TONs.

$$r = \frac{k_{rds}a[1][Rh]_T}{(1+a[1]+K_{2b}[2]+K_{3b}[3])} \quad (2.17)$$

The order of each component can be determined by Equation 2.18, which compares the logarithm of the initial rates/concentrations for each of the different excess experiments. Mathematical manipulation results in the simplified rate equation 2.19. Here the individual rate constants are simplified into the term k' .

$$\log \left[\frac{(rate)_a}{(rate)_b} \right] = \log \left[\frac{(S)_a}{(S)_b} \right] \quad (2.18)$$

$$r = k'[1]^{0.8}[2]^{-1}[3]^{-1}[Rh_T] \quad (2.19)$$

The generation of a rate law provides a baseline for understanding how concentration dependencies can influence catalyst turnover. Additionally, the kinetic study directly influences the development of novel methods for increasing sustainability, such as heterogeneous catalysis and flow chemistry. While the research goals of graduate student Ms. Kathryn Chepiga are focused on the development of heterogenous dirhodium(II) catalysts and their implementation into flow chemistry, a portion of this work, has explored how the cyclopropanation enantioselectivity is influenced over the course of a reaction(s) with reaction calorimetry .

2.2.4 Reaction Calorimetry

Reaction calorimetry was conducted in the laboratory of Prof. Donna Blackmond at the Scripps Research Institute, as a method to further study the activation/deactivation of $\text{Rh}_2(\text{S-DOSP})_4$. Reaction calorimetry is differential method for *in situ* reaction monitoring; therefore, the rate of the reaction can be directly derived from the heat gain/loss in the reaction. Moreover, studies by Blackmond and Pflatz have demonstrated that multiple injections of substrate into a mixture of trap, catalyst, and solvent result in a kinetic profile for catalyst.³⁹⁻⁴¹ The evaluation of the heat flow per injection was used to identify catalyst deactivation, activation, and any induction periods that may be present during the reaction progress.⁴¹

The reaction calorimetry monitors the heat flow of a reaction over time. By conducting multiple injections of a substrate (diazo compound) into a solution of catalyst/reactants a kinetic profile of the catalyst is observed. For the context of the study, we were interested in observing how product inhibition influenced the heat flow and enantioselectivity over time. A 1.0 M injection of the diazo compound, **1** was made into a 10° C dichloromethane solution of styrene (15 equiv.) and catalyst (0.007 mol%) (Figure 2.13). The single injection was conducted to verify if the reaction could be monitored in the calorimeter. A max heat flow of 1300 mW was recorded and the cyclopropane was formed in 52% ee, 94% yield. Integration of the area under the curve allowed for the determination of the heat of the reaction (ΔH). The calculated heat (enthalpy) associated with the reaction was calculated to be 54 kcal/mol. The experiment was repeated to ensure consistency. The single injection experiment would act as a baseline for subsequent experiments.

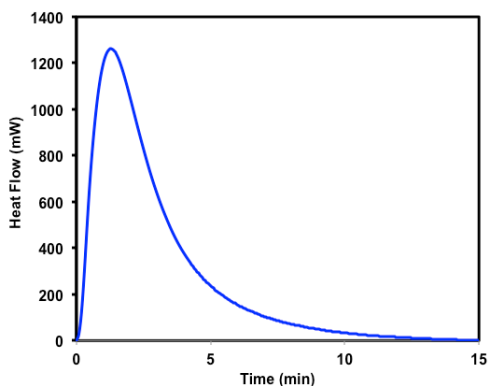


Figure 2.13: Standard heat flow (mW) versus time (min) for reaction of **1** (1.0 M) with **2** (15.0 M) catalyzed by $\text{Rh}_2(\text{S-DOSP})(0.007 \text{ mol}\%)$ in dichloromethane at 10 °C. The reaction rapidly hits a maximum heat flow of 1300 mW, illustrating the extremely exothermic nature of the reaction.

Isolation of the catalyst after a reaction is a significant challenge when operating an extremely low catalyst loading; therefore, multiple injection studies afford a kinetic description of the activity of the catalyst in successive reactions. Figure 2.14 displays five 1.0 M injections **1** into a 15.0 M solution of **2** and $\text{Rh}_2(\text{S-DOSP})_4$ (0.007 mol%) in dichloromethane at 10 °C. A decrease in heat flow per injection was observed, indicative of catalyst deactivation. The deactivation increased as the catalyst conducted more turnover numbers, however, this did not prevent the reaction from going to completion as illustrated in the calculated enthalpies for each injection (Table 2.4). Based on results from RPKA studies, we propose that the decrease in heat flow is a result of increased product coordination.

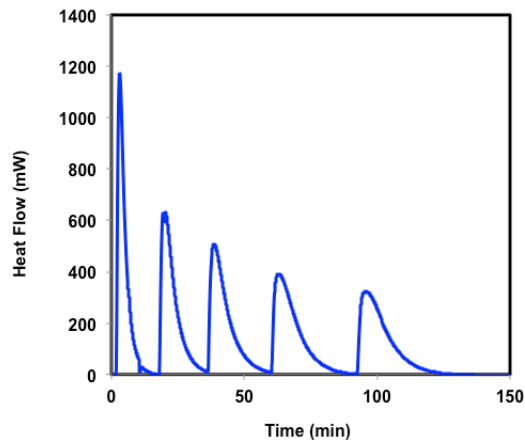


Figure 2.14: Heat flow (mW) versus time (min) for five successive injections of **1** (1.0 M) in the reaction of **2** (15.0 M) catalyzed by $\text{Rh}_2(\text{S-DOSP})_4$ (0.007 mol%) in dichloromethane at 10 °C. A decrease in the heat flow is observed for each injection creating a kinetic profile of the dirhodium(II) catalyst deactivation.

Injection	ΔH_{rxn} (kcal/mol)
1	52.1
2	50.2
3	49.0
4	50.0
5	48.1

Table 2.4: Calculated enthalpy ΔH_{rxn} for each injection of the diazo compound. Less than 5% variance found, demonstrating that the reaction is going to completion per injection.

Encouraged by the results, 10 injections were conducted in an attempt to push the catalyst further (Figure 2.15). Significant decrease in the heat flow was noted after the first and third injection. Injections 4-10, however, resulted a relatively stable heat flow. When samples from the first and last injection were analyzed by HPLC, a significant drop in enantioselectivity was noted. The initial injection was completed in >97% conversion and 54% ee. The last injection resulted in >95% conversion and 13% ee_{inc.} The drop in enantioselectivity and heat flow may suggest that an active, albeit less robust catalytic species forms over the course of the reaction.

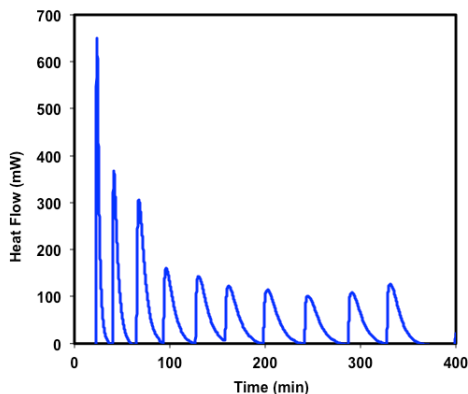


Figure 2.15: Heat flow (mW) versus time (min) for 10 successive injections of **1** (1.0 M) in the reaction of **2** (15.0 M) catalyzed by Rh₂(S-DOSP)₄ (0.0007 mol%) in dichloromethane at 10 °C. Significant decrease in the heat flow is observed for the first three injections. After the initial injections the heat flow remained at a steady point.

A final multiple injection experiment explored how the activity of the catalyst would uphold if five 1.0 M injections were conducted in a 5.0 M (5 equiv.) solution of **2** with 0.007 mol% $\text{Rh}_2(\text{S-DOSP})_4$ (Figure 2.16). Samples (0.05 μL) were taken from each injection to closely monitor changes in the enantioselectivity. With each injection large drops in the heat flow were observed. The enantioselectivity decreased steadily in each run from 45% ee to 12% ee_{inc}. It is postulated that product coordination and catalyst deactivation are responsible for the dramatic decrease in rate and enantioselectivity.

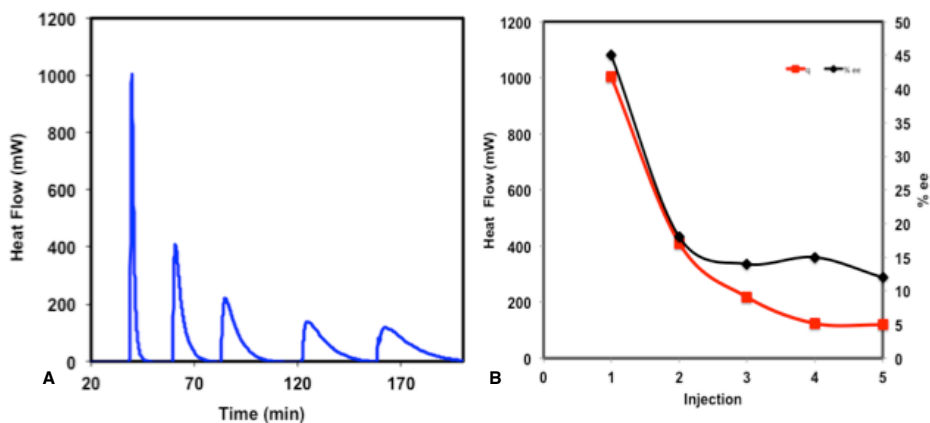


Figure 2.16: (a) Heat flow (mW) versus time (min) for five successive 1.0 M injections of **1** into a 5.0M solution of **2** catalyzed by $\text{Rh}_2(\text{S-DOSP})_4$ (0.007 mol%) in dichloromethane at 10 °C. (b) Heat flow (red, mW) and % ee (black) versus injection number for the reaction depicted in (a).

2.2.5 Addition Experiments

The RPKA and calorimetry results motivated the development of “addition” experiments. The addition experiments would explore how the method of diazo compound addition influences the catalyst turnover and the enantioselectivity of the resulting cyclopropane. Dirhodium(II) carbene reactions are typically conducted by slow addition of the diazo compound to a solution of trap and catalyst. The method decreases the probability of diazo compound side reactivity. RPKA studies, however, have illustrated that quick addition of the catalyst to a mixture of trap and substrate can also result in reactions with similar selectivity to the traditional slow addition method. Nevertheless, key observations from the RPKA and calorimetry experiments propose that styrene and cyclopropane product can significantly deactivate the catalyst. Furthermore, this deactivation has been shown to have a detrimental influence on the enantioselectivity. Therefore, by comparing how the pre-exposure to the styrene trap would affect TON and enantioselectivity, knowledge on how to conduct high TON and high %ee could potentially be obtained.

A baseline was established by slow addition of a 0.5 M (7.5 mmol) solution of diazo compound **1** into a 3.0 M (15.0 mmol) solution of styrene. As demonstrated in Figure 2.17 a diazo compound peak was established over the 1-h addition period. This plot served as a baseline for future addition experiments

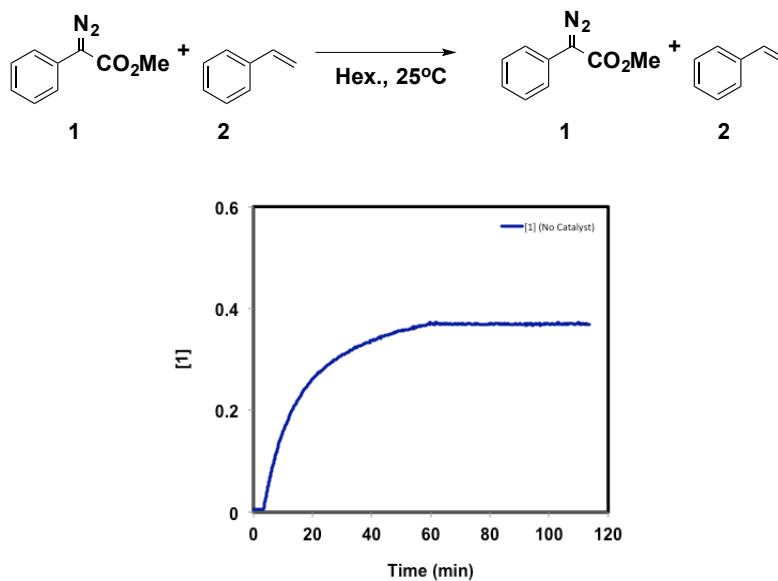


Figure 2.17: Baseline addition plot. Concentration of **1** (M) versus time (min) for the catalyst free addition of **1** (0.5 M) to a solution of **2** (3.0 M) in hexanes at 25 °C.

In the first addition experiment, two equivalents of styrene were premixed with an equivalent of diazo compound and slowly added to a solution of $\text{Rh}_2(\text{S-DOSP})_4$. A diazo compound peak (red) was observed, which leveled off after complete addition of the diazo compound (Figure 2.18). Over the course of the addition, 100 μL samples of the reaction solution were extracted for HPLC analysis. The maximum number of turnovers the catalyst could conduct were 100,000 turnovers, however this method resulted in $\sim 20,000$ turnovers. Additionally, a considerable drop in the enantioselectivity was documented. In the initial sample $t = 30$ sec the enantioselectivity was recorded to be 90% ee (green). Over the course of the reaction, the enantioselectivity steadily dropped to 50% ee in the final sample.

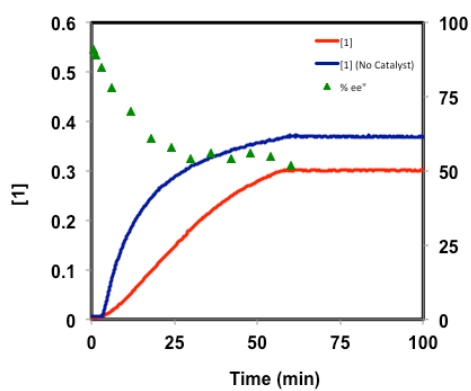
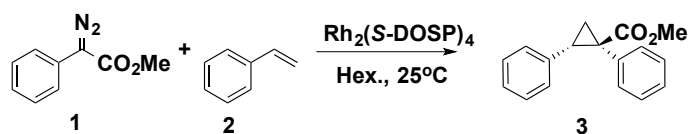


Figure 2.18: Concentration of 1 (M) and % ee of 3 versus time (min) for the slow addition of a 2:1 mixture of 2 and 1 to a solution of $\text{Rh}_2(\text{S-DOSP})_4$ (0.001 mol%) in hexanes at 25 °C. Blue curve is the control run with no catalyst, red is the reaction in the presence of catalyst, and green triangles represent the % ee.

The low TONs observed under the diazo compound and styrene were premixed conditions (Figure 2.17), led to the belief that interaction between olefin and catalyst may be beneficial. To test this theory one equivalent of **1** was added to two equivalents of styrene in solution with the catalyst over a one-hour period (Figure 2.19). The method of addition resulted in higher turnovers of the catalyst (~75,000 TONs). The first 2-3 minutes there was a build-up of the diazo compound. It is possible that some concentration of diazo compound is necessary before the catalyst is capable of conducting higher turnovers. Once the addition was over, diazo compound decomposition was observed over a 1 h period. While the conversion was >75%, the enantioselectivity dropped over the course of the addition from 88% ee to 50% ee. Therefore, while this method was more effective for catalyst turnover, the enantioselectivity remained unstable.

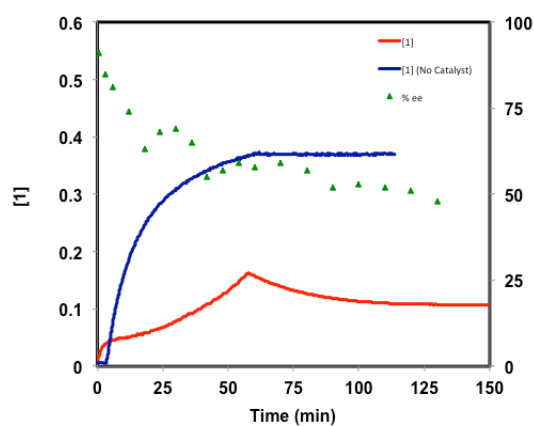
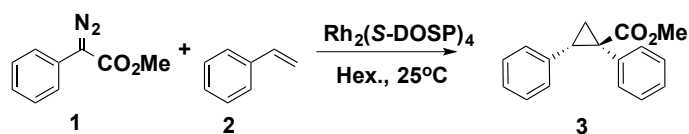


Figure 2.19: Concentration of **1** (M) and % ee of **3** versus time (min) for the slow addition of **1** (0.5 M) into a solution of **2** (3.0 M) and $Rh_2(S-DOSP)_4$ (0.001 mol%) in hexanes at $25^\circ C$. Blue curve is control run with no catalyst, red is the reaction in the presence of catalyst and green triangles represent the % ee.

The addition experiments demonstrated that the enantioselectivity of the reaction changes significantly over the course of the reaction. The change in the enantioselectivity could be a combination of catalyst deactivation and decomposition. As olefin and substrate coordination are significant modes of catalyst inhibition, it was proposed that catalyst deactivation based on unproductive binding to the dirhodium(II) catalyst could possibly be overcome by conducting reactions at higher reaction temperatures. Higher temperatures could potentially shift the “free catalysts” vs olefin/catalyst and/or product/catalyst equilibrium. To test this hypothesis, slow addition of the diazo compound to a solution of catalyst and styrene in refluxing hexanes was conducted.

The experiment conducted in refluxing hexanes resulted in no build up in the diazo compound. The catalyst easily conducted 100,000 turnover numbers (Figure 2.20). More importantly the enantioselectivity remained stable between 76-70% ee. The stable enantioselectivity demonstrates that shifting the equilibrium of the deactivation processes, enables the production of a stable catalytic species.

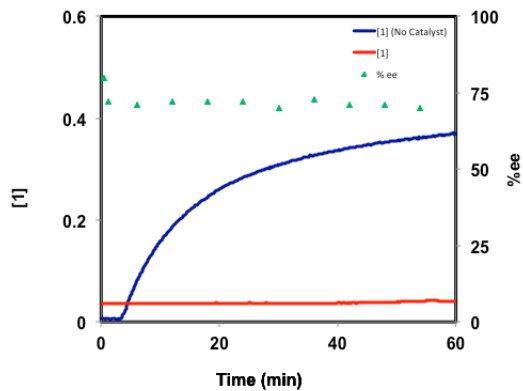
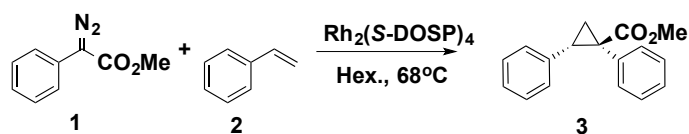
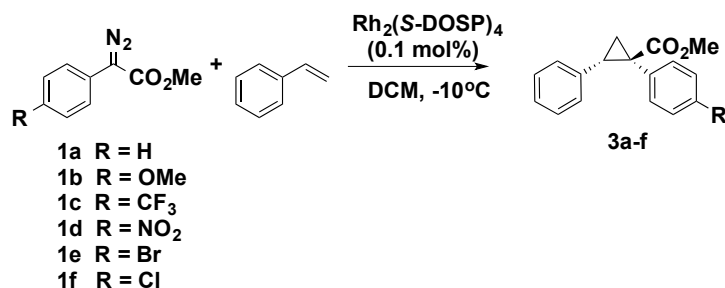


Figure 2.20: Concentration of **1** (M) and % ee of **3** versus time (min) for the slow addition of **1** (0.5 M) into a solution of **2** (3.0 M) and $\text{Rh}_2(\text{S-DOSP})_4$ (0.001 mol%) in hexanes at 68°C . Blue curve is the control run with no catalyst, red is the reaction in the presence of catalyst and green triangles represent the % ee

High turnover experiments by Davies and coworkers demonstrated the ability of $\text{Rh}_2(\text{S-DOSP})_4$ to conduct over 1.0 million turnovers in the cyclopropanation of styrene with donor/acceptor diazo compound **1** under solvent-free conditions.³⁰ Intrigued by the high temperature, 100,000 turnover results, 10 million TON's were attempted. To a refluxing solution of $\text{Rh}_2(\text{S-DOSP})$ (0.00001 mol%) and **2** (1.0 mmol) in 5.0 mL of hexanes, a 1:2 mixture of **1** (52.7 mmol) and **2** (105.2 mmol) in 40 mL of hexanes were added over 20 h. The reaction was then allowed to stir an additional 10 h under reflux. After purification, 41% yield of cyclopropane **3** was formed, representing 4.1 million turnovers of $\text{Rh}_2(\text{S-DOSP})_4$. While this was an exciting result, the enantioselectivity of the reaction was very poor, 8% ee.

2.2.6 Unusual Kinetics for methyl *p*-methoxy-phenyldiazoacetate

Prior to the in depth kinetic studies on cyclopropanation; a screening of aryldiazo compounds were conducted to investigate how the electronic nature of the aryldiazo compound influenced the rate of decomposition. Based on Yates' model and computational studies, electron withdrawing and donating substituents will either stabilize or destabilize the aryldiazoacetate, therefore influencing the rate of diazoacetate decomposition. It is proposed that the rate of decomposition should increase with electron rich aryldiazoacetates and decrease with electron poor aryldiazoacetates. The aryldiazoacetates explored in the study are found in Scheme 2.10. There was some concern that some of the reactions may not go to completion under the high TON conditions, therefore 0.1 mol% of $\text{Rh}_2(\text{S-DOSP})_4$ and 10 equiv. of styrene trap were utilized. To ensure solubility and isothermal conditions reactions were conducted in dichloromethane (DCM) at -10°C .



Scheme 2.3: Rh₂(S-DOSP)₄ (0.10 mol%) catalyzed cyclopropanation of styrene with *p*-substituted aryldiazoacetates in dichloromethane at -10 °C.

A summary of results in Figure 2.21 display the relative rate of reactivity of the diazo compounds under high TON catalyst conditions. The relative rates are based on initial rate measurements from *in situ* FTIR. The results reveal that electron poor diazo compounds decrease the reaction rate, while electron rich aryl diazoacetates increase the initial reaction rate. In general, these results were in accord with thermal aryldiazoacetate decomposition relative rate studies conducted by former graduate student, Dr. Stephanie Ovalles.⁴² Dr. Ovalles observed very slow thermal decomposition rates for compound **1d** in comparison to **1a** and **1b**. In the present case, diazoacetate **1d** demonstrated no reactivity, while 4-trifluoro **1c** and 4-bromo **1e** analogs were very slow at decomposing compared to **1a**. 4-chloro derivative **1f** and 4-methoxy derivative **1b** exhibited faster reaction rates. A caveat to the present results, however, was the difficulty observed in achieving full-decomposition of **1b**.

As the most electron rich aryldiazoacetate, **1b** was expected to react the fastest. The initial rate data demonstrated a very fast decomposition, however, the diazo compound would not fully decompose. After 2 min the reaction completely stopped. The

reaction was allowed to warm to room temperature, however, full decomposition was not observed.

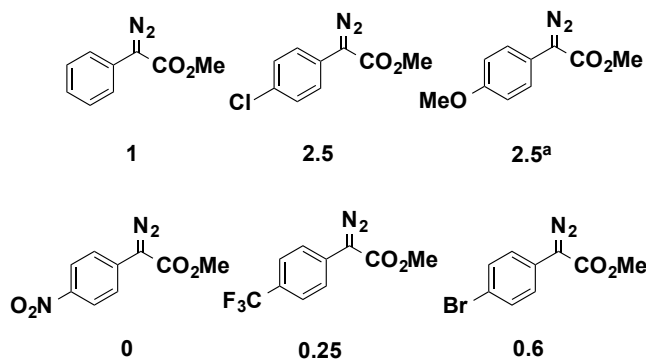


Figure 2.21: Relative rate of reaction for *p*-substituted aryl diazo compounds.

Interested in the behavior of diazoacetate **1b**, olefin concentration dependency was briefly explored. The standard conditions developed for the cyclopropanation kinetics require 10 equiv. of the styrene and 0.005 mol% of catalyst at 0 °C in hexanes. Under the standard conditions a very slow decomposition of **1b** was observed. Figure 2.22 compares the rate of decomposition for **1a** (blue curve) vs **1b** (pink curve) and illustrates that a much slower rate for **1b** as well as much more deactivation of the catalyst over the course of the reaction. It was proposed that if diazo decomposition is rate limiting, a much faster diazo decomposition should take place with an electron rich diazo compound. Therefore, the obtained results were unexpected and led to exploration of the styrene concentration dependency.

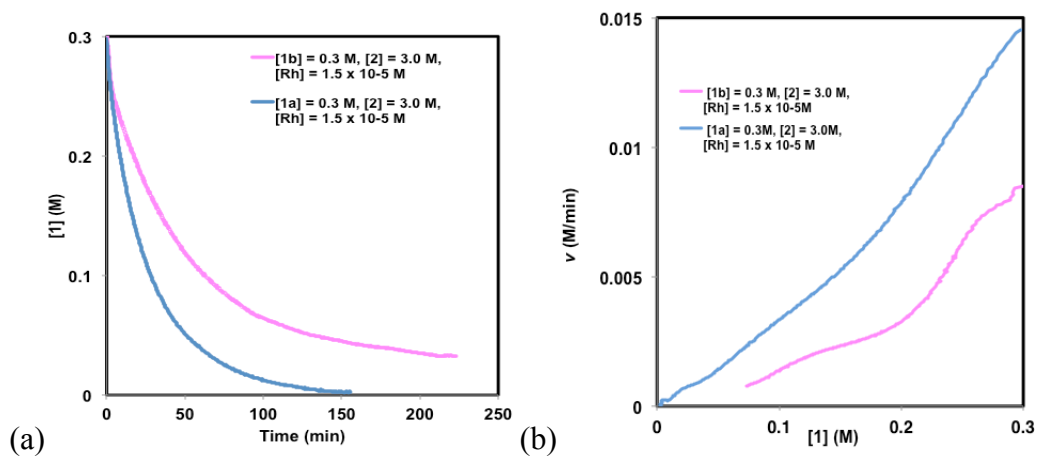


Figure 2.22: Reaction rate comparison for **1a** and **1b** under high TON conditions of 0.3 M (**1a** or **1b**) in reaction with **2** (3.0 M) catalyzed by $\text{Rh}_2(\text{S-DOSP})_4$ (0.005 mol%) in hexanes at 0 °C. (a) Concentration of diazo compound **1a** (blue curve) and **1b** (pink) versus time (min), (b) Reaction rate v (M/min) versus concentration of diazo compound **1a** (blue) and **1b** (pink).

To further probe the kinetic details of the reaction the concentration of the olefin was decreased to 5.0 equiv. Addition of the catalyst resulted in 33% decomposition of the diazo compound (green curve). Further lowering the olefin concentration to 2.0 equiv. resulted in essentially no decomposition (blue curve). Intrigued by the results, the olefin concentration was increased to 20 equiv.. Under these conditions a rapid decomposition of the diazo compound was observed (teal curve). The reaction rate more than tripled with 20 equiv of styrene compared to the initial reaction with 10 equiv. of styrene (Figure 2.23).

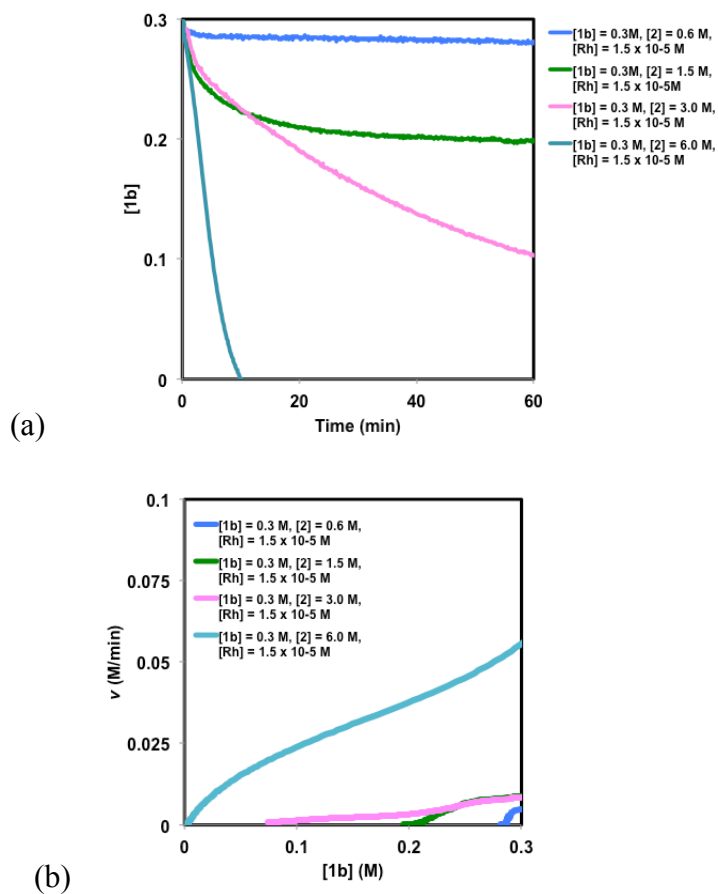


Figure 2.23: Reaction rate comparison for diazo compound **1b** (0.3 M) in reaction with **2** (0.6 M = blue, 1.5 M = green, 3.0 M = pink, 6.0M = teal) catalyzed by $\text{Rh}_2(\text{S-DOSP})_4$ (0.005 mol%) in hexanes at 0 °C. (a) Concentration of diazo compound **1a** versus time (min) at varying olefin concentration (0.6 M – 6.0 M), (b) Reaction rate, v , (M/min) versus concentration of diazo compound **1b** at varying concentrations of **2** (blue) and **1b** (pink).

The olefin dependence observed in the reaction **1b** (0.3 M) with varying concentrations of **2** (0.6 M – 6.0 M) catalyzed by $\text{Rh}_2(\text{S-DOSP})_4$ was unexpected. While a more in depth kinetic analysis is necessary, the results illustrates that high substrate concentration is favored in reactions with **1b**. The result suggests the solvent-free conditions explored by Davies and coworkers were optimum for obtaining high TONs of the dirhodium(II) catalyst.³⁰

2.3 Discussion and Conclusions

The observations attained from the screening of chiral catalysts in the cyclopropanation of styrene provided insight into the differences in the catalytic activity and asymmetric-induction at low catalyst loadings. When placed into context with previous studies, we see that the enantioselectivity is controlled by numerous factors. Recent work by Davies and co-workers, has shown at 1 mol% of catalysts that the enantioselectivity of cyclopropanation conducted by $\text{Rh}_2(\text{R-DOSP})_4$, $\text{Rh}_2(\text{S-PTAD})_4$ and $\text{Rh}_2(\text{S-BNP})_4$ can be attenuated based on the substitution around the aryldiazoacetate carbene precursor.¹⁰

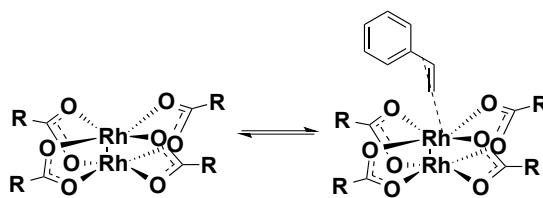
The kinetic work contained in this chapter suggests that many of dirhodium(II) catalysts have diminished activity at low catalysts loadings. For example, $\text{Rh}_2(\text{S-BNP})_4$ is not as active as $\text{Rh}_2(\text{S-PTAD})_4$ and $\text{Rh}_2(\text{S-DOSP})_4$. While the cause for diminished activity of $\text{Rh}_2(\text{S-BNP})_4$ is unknown, the result attests to the excellent activity and stability of $\text{Rh}_2(\text{S-DOSP})_4$ and $\text{Rh}_2(\text{S-PTAD})_4$. Additionally, the bulky chiral catalyst $\text{Rh}_2(\text{S-biTISP})_4$ has very little kinetic activity under the reaction conditions. While $\text{Rh}_2(\text{S-biTISP})_4$ is capable of displaying high enantioselectivity in dirhodium(II) carbenoid reactions, the low kinetic activity under high TON conditions suggests that the bulky

ligands systems cause the catalysts to quickly deactivate.²⁹ Overall, lower enantioselectivities are recorded under high TON conditions (Table 2.3). It is proposed that at low concentrations of Rh(II) catalyst, catalyst decomposition has a significant influence over the activity of the catalyst. These unknown modes of catalyst destruction may potentially lead to lower enantioselectivity.

The activity of the achiral catalysts illustrated that bridging and electron poor catalysts favor higher reactivity. We suspect the high activity of Rh₂(esp)₂ is due to the lack of steric bulk and bridging nature of the catalyst. In general, bridging catalysts are believed to be more kinetically stable and less susceptible to catalyst decomposition, however, the study has shown that the stability of the catalyst is strongly related to the steric bulk of the ligand system.⁴³

The RPKA studies demonstrated that two possible modes of catalyst deactivation exists: coordination of styrene and product to the dirhodium catalyst. It is well established that strong Lewis bases coordinate to the axial sites of dirhodium catalysts; however, few examples of olefins coordinating dirhodium axial sites are known.⁷ Additionally, while several studies have been conducted to establish equilibrium rates (K_{eq}) for olefin and Lewis base coordination, none, to our knowledge, have detailed how axial coordination plays a role in catalyst turnover for metal catalyzed carbenoid reactions. This work shows that such interactions have an influence on the rate of carbenoid reactivity.

The negative reaction rate dependency on the concentration of styrene suggests interaction between the catalyst and styrene (Scheme 2.4). It is possible that the styrene coordinates to one of the axial sites of the catalyst through the olefin or aromatic moiety. The coordinated complex is believed to be in equilibrium with the active catalyst.



Scheme 2.4: Substrate coordination to the dirhodium(II) catalyst. The figure shows olefin coordination, however, aromatic coordination could also be possible.

Additionally, decreasing the interaction between the styrene and the catalyst increases the enantioselectivity. The result suggests that such interactions are detrimental to achieving high asymmetric induction. In subsequent studies, the reaction was conducted with 6.0 M (20 equiv.) of styrene. Under these conditions significantly lower reaction rate was observed ($t_{\text{end}} > 12$ h). The resultant %ee was calculated to be 20 %, illustrating the significant influence the styrene concentration can have on the rate and enantioselectivity.

UV/Vis experiments by Dr. Nicholas Brunelli have confirmed that there are interactions between the dirhodium(II) catalyst and styrene. Titration of the catalyst with small aliquots of styrene, a clear transition dirhodium peaks at 425 and 650 nm was observed (Figure 2.24). Initially the peaks decrease, however, careful tracking reveals that the electronic structure goes through multiple transitions as more styrene is added. Currently, these transitions have been tracked through following the intensity at a single wavelength as a function of the ratio of olefin to the catalyst.

The first transition begins to occur around an olefin to catalyst concentration of approximately 1:1. The transition involves both peaks decreasing with the absorbance around 350 nm increasing. At approximately a ratio of 10:1, this first transition is complete and a second transition begins over the range of 10:1 to 300:1. Throughout

these additions, the peak position for the Rh-Rh bond (650 nm) does not shift. Only after reaching substrate to catalyst ratios of 300:1 does the peak location begin to shift. This transition has been previously associated with the interaction of the olefin with one of the axial sites of the dirhodium catalyst.

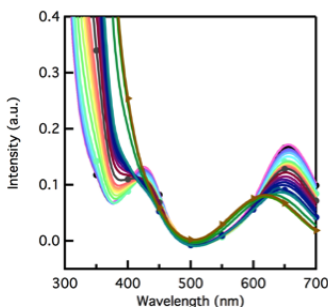
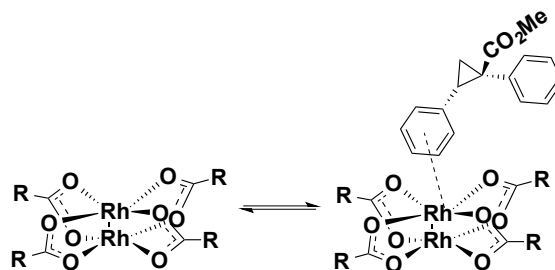


Figure 2.24: UV-Vis titration of the catalyst with styrene, conducted by Dr. Nicholas Brunelli

Through the RPKA product doping experiment we were able to identify product inhibition as a second mode of catalyst deactivation (Scheme 2.5). Equation 2.1 was used to calculate the incremental % ee (or the enantioselectivity of the new cyclopropane formed). It was found that the cyclopropane was generated in 15% ee. In the standard reaction the enantioselectivity was calculated to be 46% ee. It was expected that in the presence of the enantiopure cyclopropane, the new cyclopropane would be formed in 40-50% ee. However, the significant drop in enantioselectivity to 15% illustrates that in the presence of product, catalyst decomposition. One possibility is that the coordinated product displaces a carboxylate ligand(s) and changes the chiral environment of the carbene.

$$ee_{inc} = \left| \frac{(c_2 \times ee_2) - (c_1 \times ee_1)}{(c_2 - c_1)} \right| \quad (2.20)$$



Scheme 2.5: Product coordination to the dirhodium(II) catalyst

Multiple injection calorimetry studies have further demonstrated that the catalyst is altered as the reaction progresses. While the modified catalyst is catalytically active, the enantioselectivity quickly drops off. The identity of the modified catalyst is currently unknown, however, we propose that catalyst decomposition and deactivation possibly play a role in low asymmetric induction. Potential modes of catalyst decomposition include, ligand dissociation and oxidation state changes of the dirhodium core. While it is unclear whether coordination to the catalyst by the substrate and/or product can induce catalyst decomposition, current work in the Davies group is focused on identifying other dirhodium species found along the reaction progress.

The current kinetic study has illustrated that coordination of the styrene trap and cyclopropane product result in lower reaction rates. Based on these results, it is proposed that many of the common substrates for dirhodium(II) carbene chemistry, which olefin and Lewis basic sites, may have a similar influence over the reaction rate. A subsequent study (Chapter 4) expands on this concept. A considerable issue, however, is developing methods that overcome catalyst inhibition. Exploration of different methods of addition for the diazo compound and styrene found that adding the diazo compound to a mixture of catalyst and styrene resulted in higher TON. The result suggests that this type of interaction possibly protects the catalyst from irreversible destruction. Nevertheless, a

drop in enantioselectivity was observed under the addition conditions. Increasing the reaction temperature alleviated this issue. It is postulated that at elevated temperatures the equilibrium processes for coordination to the dirhodium(II) catalyst are shifted. In turn, minimizing the coordination to the catalyst allows for a more stable dirhodium catalyst.

The work in this chapter has attempted to unveil kinetic factors that contribute to the reactivity of dirhodium(II) catalysts at low catalyst loadings. The screening of chiral and achiral catalysts illustrate that the catalysts are overall kinetically different. In depth kinetic analysis with $\text{Rh}_2(\text{S-DOSP})_4$ has identified factors that contribute to catalyst deactivation, most notably olefin and substrate coordination. Reaction calorimetry presented another view of the deactivation by monitoring the activity of the catalyst in successive reactions. Overall the work illustrates that the deactivation is strongly apparent and influences the enantioselectivity of the reaction, however, interactions between the olefin and catalyst are beneficial in conducting high turnovers. Additionally, conducting reactions at higher temperatures results in stable enantioselectivity.

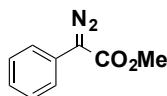
The work, however, has also brought up several questions that still need to be explored. What is the identity of the decomposed or deactivated dirhodium(II) species? Why is the kinetics of the electron rich diazoacetate **1b** different than the standard diazo compound? In general, these questions reveal that there is still much to be learned about the intricate details of the reaction. Future work in the area will be focused on identifying the dirhodium species via mass spectrometry studies, as well as conducting further RPKA experiments on with other aryl diazoacetates.

2.4 Experimental

2.4.1 General Considerations

All experiments were carried out in oven-dried glassware under inert atmosphere. All chemicals were purchased, or found in the Davies Group Diazo Compound Library unless otherwise stated. All solvents used were either distilled or retrieved out of the solvent system and degassed 15 minutes prior to usage. Flash column chromatography was performed on silica gel. ^1H NMR Spectra were recorded at 400 and 600 MHz on a Varian 400, Inova 400, and Inova 600. ^{13}C NMR was recorded at 100 MHz on a Varian and Inova 400.

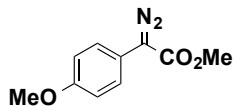
2.4.2 Characterization of Known Diazo Compounds



1a

Methyl phenyldiazoacetate

1,8-diazobicycloundec-7-ene (DBU) (39.9 mmol, 1.0 equiv) was added to a solution of the methyl phenylacetate (36.3 mmol, 1.0 equiv) and *p*-ABSA (43.6 mmol, 1.2 equiv) in 40 mL of acetonitrile and stirred for 16 h at rt. The reaction mixture was quenched with 50 mL of saturated NH_4Cl solution and extracted with Et_2O (3 x 25mL). The combined ether extracts were dried with MgSO_4 and filtered. The residue was concentrated and purified by flash chromatography using 20% Et_2O /hexanes to yield the desired product. Isolated as an orange oil. 5.90 g (92% yield.) ^1H NMR (400 MHz, CDCl_3) δ 7.48 (d, 2H, $J=8.7\text{Hz}$), 7.37 (t, 2H, $J=8.3\text{ Hz}$), 7.17 (t, 1H, $J=7.2\text{ Hz}$), 3.85 (s, 3H). The spectroscopic data are consistent with previously reported data.⁴⁴

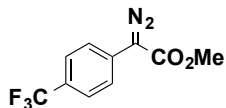


1b

Methyl 4-methoxyphenyldiazoacetate

Acetyl chloride (2.60 mL, 36.1 mmol, 1.2 equiv) was added to a solution of *p*-methoxyphenylacetic acid (5.00 g, 30.1 mmol, 1.0 equiv) in anhydrous methanol (100 mL) and allowed to stir for 2 h. The reaction mixture was quenched with saturated aqueous NaHCO₃ and extracted with diethyl ether (3x 30 mL). The combined ether extracts were dried with MgSO₄ and filtered. The residue was concentrated *in vacuo* to give the desired acetate that was used crude in the next step.

DBU (5.0 mL, 33.1 mmol, 1.1 equiv) was added to a solution of *p*-ABSA (8.67 g, 36.1 mmol, 1.2 equiv) and the crude acetate (5.42 g, 30.1 mmol, 1.0 equiv) in 100 mL of acetonitrile. This was stirred for 12 hr and then quenched with saturated aqueous NH₄Cl solution and extracted with diethyl ether (3x 25 mL). The combined ether extracts were dried with MgSO₄ and filtered. Then the residue was concentrated *in vacuo* and purified by flash chromatography using 10% Et₂O/pentane to give the desired product as an orange solid, 4.65 g (75% yield). ¹H NMR (400 MHz, CDCl₃) δ 7.37 (d, 2H, *J* = 9.2 Hz), 6.92 (d, *J* = 9.2, 2H, Hz), 3.84 (s, 3H), 3.81 (s, 3H). The spectroscopic data are consistent with previously reported data.⁴⁵

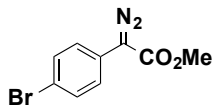


1c

Methyl 4-trifluoromethylphenyldiazoacetate

Acetyl chloride (1.0 mL, 12.7 mmol, 1.2 equiv) was added to a solution of *p*-trifluoromethylphenylacetic acid (2.17 g, 10.6 mmol, 1.0 equiv) in anhydrous methanol (50 mL) and allowed to stir for 2 h. The reaction mixture was quenched with saturated aqueous NaHCO₃ and extracted with diethyl ether (3x 25 mL). Combined ether extracts were dried with MgSO₄ and filtered. The residue was concentrated *in vacuo* to give the desired acetate that was used crude in the next step.

DBU (1.6 mL, 10.3 mmol, 1.1 equiv) was added to a solution of *p*-ABSA (2.69 g, 11.2 mmol, 1.2 equiv) and the crude acetate (2.05 g, 9.4 mmol, 1.0 equiv) in 50 mL of acetonitrile. The reaction mixture was stirred for 12 h, then quenched with saturated aqueous NH₄Cl solution and extracted with diethyl ether (3x 25 mL). The combined ether extracts were dried with MgSO₄ and filtered. The residue was then concentrated *in vacuo* and purified the remaining residue by flash chromatography using 10% Et₂O/pentane to give the desired product as an orange solid, 2.02 g (88% yield). ¹H NMR (400 MHz, CDCl₃) δ 7.62 (m, 4H), 3.89 (s, 3H). The spectroscopic data are consistent with previously reported data.²⁹



1e

Methyl 4-bromo-phenyldiazoacetate

Acetyl chloride (6.9 mL, 96.5 mmol, 1.2 equiv) was added to a solution of 4-bromophenylacetic acid (17.29 g, 80.4 mmol, 1.0 equiv) in 100 mL of methanol. The reaction mixture was allowed to stir for 16 h at rt. The mixture was then quenched with 100 mL saturated NaHCO₃ solution and extracted with Et₂O (3x 25 mL). The combined ether extracts were then dried with MgSO₄ and filtered. The residue was concentrated *in vacuo* to give the desired acetate and used crude in the next step.

DBU (12.4 mL, 39.9 mmol, 1.1 equiv) was added to a solution of the methyl 4-bromophenylacetate (17.03 g, 74.3 mmol, 1.0 equiv) and *p*-ABSA (21.43 g, 81.7 mmol, 1.2 equiv) in 100 mL of acetonitrile and stirred for 12 h at rt. Then the reaction mixture was quenched with saturated NH₄Cl solution and extracted with Et₂O (3x25 mL). The combined ether extracts were then dried with MgSO₄ and filtered. The residue was then concentrated *in vacuo* and purified by flash chromatography using 10% Et₂O/pentane to yield the desired product as an orange solid, 15.9 g (84% yield). ¹H NMR (400 MHz, CDCl₃) δ 7.50 (d, 2H, *J* = 8.5 Hz), 7.37 (d, 2H, *J* = 8.5 Hz), 3.86 (s, 3H). The spectroscopic data are consistent with previously reported data.⁴⁵

2.4.3 General procedure for kinetic measurements on ReactIR™

Experiments were carried out with a Mettler Toledo ReactIR™ 45m instrument equipped with a 9.5mm x 12” AgX 1.5m SiComp probe. Stock solutions of diazo compounds and Rh (II) catalysts in dichloromethane were prepared. To a dry round bottom flask was added a stir bar, trap, dichloromethane and an aliquot of diazo compound solution. The reaction was cooled to 10 °C (*p*-dioxane, CO_{2(s)} bath) or 0 °C (ice/water bath) and allowed to equilibrate for 30 min. The ReactIR™ probe was then inserted and the instrument set up for a continuous scan experiment. The scan was started and, at $t_0 = 20$ sec, an aliquot of the catalyst solution was injected by syringe in one movement with vigorous stirring.

The standard reaction of **1a** (0.3M) with **2** (3.0) catalyzed by Rh₂(*S*-DOSP)₄ (0.005 mol%) in hexanes at 0 °C was run 2x to ensure the validity of the procedure. Additionally, crude ¹HNMR samples were taken to ensure that cyclopropanation was the only catalytic process at work. A representation of the raw peak height of **1a** (M) vs time (hh:mm:ss) for two separate runs is found in Figure 2.25.

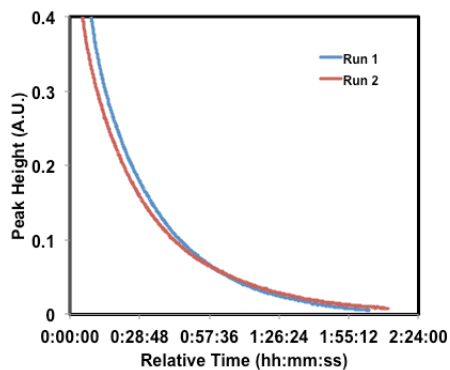
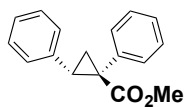


Figure 2.25: Plot of the peak height (A.U.) versus relative time (hh:mm:ss) of **1** for reaction of **2** (3.0 M) catalyzed by $\text{Rh}_2(\text{S-DOSP})_4$ (0.005 mol%) in hexanes at 0 °C. Trial 1 (blue) and trial 2 (red)

2.4.4. Characterization Data of Known Cyclopropanation Products



3

methyl (1*R*,2*S*)-1,2-diphenylcyclopropane-1-carboxylate.

% ee by HPLC: 1% i-PrOH/hexanes, 1.0 mL/min, S,S-Whelk. ^1H NMR (400 MHz, CDCl_3): δ 7.11-7.09 (m, 3H), 7.03-7.00 (m, 5H), 6.76-6.74 (m, 2H), 3.63 (s, 3H), 3.11 (dd, 1H, $J=7.0, 9.5$ Hz), 2.13 (dd, 1H, $J=5.0, 9.5$ Hz), 1.86 (dd, 1H, $J=5.0, 7.0$ Hz). The spectroscopic data are consistent with previously reported data.³⁰

2.4.5 Representative Kinetic Plots, Equations, and Rate Derivation

2.4.6 Calibration Curve for Methyl Phenyldiazoacetate

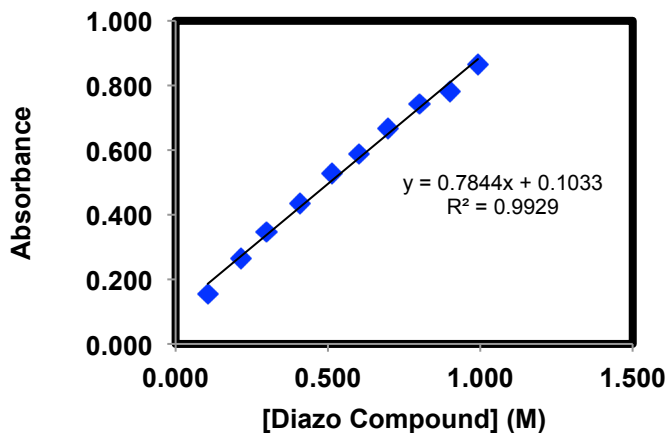


Figure 2.26: Calibration Curve for Methyl Phenyldiazoacetate

Concentration of the diazo compound over the course of the reaction was calculated using Beer's Law formula:

$$A_{\text{corr}} = \epsilon bc \quad (2.21)$$

Where: A_{corr} is the corrected absorbance.

ϵ is extinction coefficient.

b is the cell path length ($b = 1$ in this case)

c is concentration of the analyte.

The percent conversion, η , was estimated from the following formula:

$$\eta = (|A_t - A^\circ| / |A_0 - A^\circ|) * 100\% \quad (2.22)$$

Where: A_t = Absorbance at time t .

A° = Absorbance at full conversion.

A_0 = Initial absorbance before reaction was started.

2.4.7 Determination of reaction rate for RPKA:

Raw data from the ReactIR™ IC IR software can be exported into Excel or Matlab. An example of raw ReactIR™ data is below for the reaction of 1a (0.3 M) with 2 (3.0 M) catalyzed by Rh₂(S-DOSP)₄. The sampling rate was 5 seconds over a 3-hour period. The first 3 minutes of sampling are shown below:

Table 2.5: Raw Data exported from ReactIR™

Relative Time	Peak 1	Relative Time	Peak 1	Relative Time	Peak 1
0:00:07	0.406335	0:01:09	0.407617	0:02:07	0.405947
0:00:13	0.408228	0:01:11	0.407393	0:02:13	0.40805
0:00:14	0.408637	0:01:16	0.407142	0:02:14	0.408512
0:00:20	0.408005	0:01:18	0.407087	0:02:20	0.408308
0:00:21	0.407867	0:01:23	0.408252	0:02:21	0.408263
0:00:27	0.409212	0:01:25	0.408504	0:02:27	0.408556
0:00:28	0.409503	0:01:30	0.408384	0:02:28	0.40862
0:00:34	0.408374	0:01:32	0.408358	0:02:34	0.40835
0:00:35	0.408126	0:01:37	0.407572	0:02:35	0.408291
0:00:41	0.407227	0:01:39	0.407402	0:02:41	0.407499
0:00:42	0.407033	0:01:45	0.407878	0:02:42	0.407329
0:00:48	0.407206	0:01:46	0.407981	0:02:48	0.408112
0:00:49	0.407244	0:01:52	0.40841	0:02:49	0.408284
0:00:55	0.407658	0:01:53	0.408503	0:02:55	0.408207
0:00:57	0.407748	0:01:59	0.409106	0:02:56	0.408191
0:01:02	0.408483	0:02:00	0.409236	0:03:02	0.408231
0:01:04	0.408642	0:02:06	0.406537		

As shown in section 2.4.6, Beer's law can be used to determine the concentration of the diazo compound. A plot of the concentration of diazo compound 1a versus time is then generated. An example of such a plot is shown below in Figure 2.27.

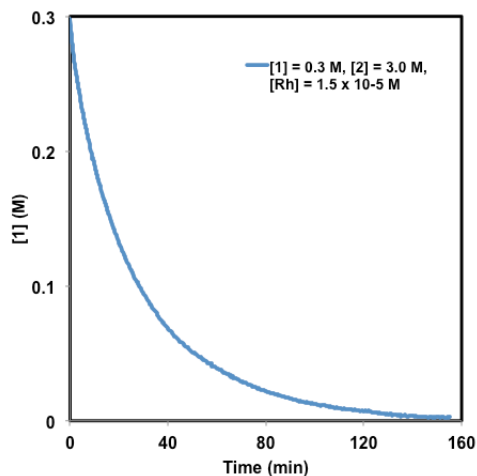


Figure 2.27: Plot generated from ReactIR™ data depicting concentration of **1a** versus time (min) for reaction of **2** (3.0 M) catalyzed by Rh₂(S-DOSP)₄ (0.005 mol%) in hexanes at 0 °C.

The curve generated from the concentration versus time plot is then fit to a higher-order polynomial. For the example above, a 6th order polynomial is fit to the curve to give equation 2.23 with an R² value of 0.99979.

$$y = 3\text{E-}13x^6 - 2\text{E-}10x^5 + 4\text{E-}08x^4 - 4\text{E-}06x^3 + 0.0003x^2 - 0.012x + 0.2865 \quad (2.23)$$

The polynomial function where ‘y’ represents concentration (c) and ‘x’ represents time (t) is then differentiated to obtain the reaction rate at each concentration of the diazo compound (Equation 2.24)

$$\frac{dc}{dt} \quad (2.24)$$

The reaction rate can then be plotted against concentration of the diazo compound to obtain plots such as 2.28, which are read from right to left in order to observe how the rate of the reaction changes as the diazo compound decomposes.

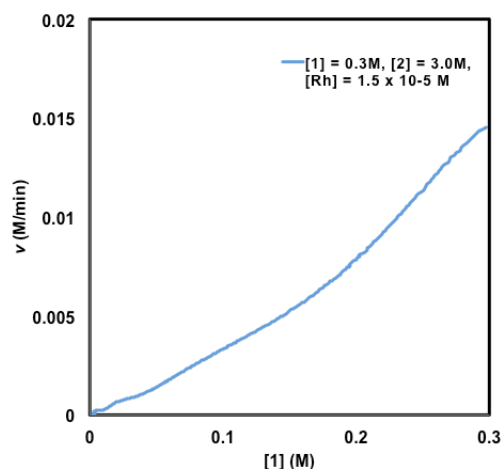


Figure 2.28: Plot of the reaction rate (v (M/min)) versus concentration of **1** for reaction of **2** (3.0 M) catalyzed by $\text{Rh}_2(\text{S-DOSP})_4$ (0.005 mol%) in hexanes at 0 °C.

2.4.8 Multiple Injection Kinetic Experiments

General procedure for multiple injection kinetic measurements on differential scanning calorimeter:

Experiments were carried out with an Ominical Insight CPR 220 Calorimeter. The calorimeter continuously monitors the enthalpy balance around the vessel. 5.35 M stock solutions of methyl phenyldiazoacetate and 0.00075 M $\text{Rh}_2(\text{S-DOSP})_4$ in dry dichloromethane were prepared. To a dry 8 mL septa sealed vial was added a stir bar, trap, dichloromethane and 0.1 mL of the 0.00075 M stock solution of $\text{Rh}_2(\text{S-DOSP})_4$ to give a total volume of 5 mL. The reaction was placed in calorimeter compartment and equilibrated at 10 °C (chiller). After 30 min when the calorimeter signal reacted a constant value. 1 mL syringes with 0.1 mL of the 5.36 M solution of methyl phenyldiazoacetate were equilibrated in the calorimeter injection ports at 10 °C for 30 min. A rubber seal was placed on the end of the syringe to prevent evaporation. The diazo

compound was then added to the reaction mixture in one movement with vigorous stirring at 675 rpm. When the calorimeter signal returned to the baseline, injection of the diazo compound was repeated. 0.05 mL samples of the reaction were taken after each run for HPLC analysis.

The heat flow measured by the calorimeter, takes into account the heat transfer of the reaction and the heat transfer of the instrument. To correct for the time constant heat transfer of the instrument a “tau-correction” was conducted after each run. Without this correction, the peak height and shape of the heat flow curves would not reflect the heat transfer of the reaction. At the end of the experiment, when the calorimetric signal had returned to a constant value, a calibration procedure was started: the τ correction switch was moved to the “on” position; when the calorimetric signal had reached a new constant value, the switch was moved to the “off” position; when the signal had returned to the previous constant value, the data was saved and the calorimeter turned off. The software provided by Omnical (Winsight – version 2.1) was used to perform the τ correction calibration and calculate the value of τ . The corrected calorimetric curve was then exported to an Excel spreadsheet

Heat flow (q), rate (v), fraction conversion (f), and [substrate] were calculated from the following formulas:

Heat flow (q) of a reaction is related to the rate and enthalpy of the reaction by:

$$q = \Delta H_{\text{rxn}} \times (\text{reaction volume}) \times \text{rate} \quad (2.25)$$

Fraction conversion and concentration are determined by the following equations

$$\text{Fraction conversion} = f = f_{\text{final}} \times \frac{\int_0^t q(t) dt}{\int_0^{t_{\text{final}}} q(t) dt} \quad (2.26)$$

$$[\text{substrate}] = [\text{substrate}]_0 \times (1 - f) \quad (2.27)$$

Incremental enantioselectivity was calculated by the following formula:

$$e.e.(inc) = \frac{[(c_2 \times e.e._2) - (c_1 \times e.e._1)]}{c_2 - c_1} \quad (2.28)$$

Where: *e.e.* is enantioselectivity and *c* is the concentration of product.

Representative multiple injection tau corrected data plot for cyclopropanation of styrene with aryl dirhodium carbenoid (raw data) can be found in Figure 2.29.

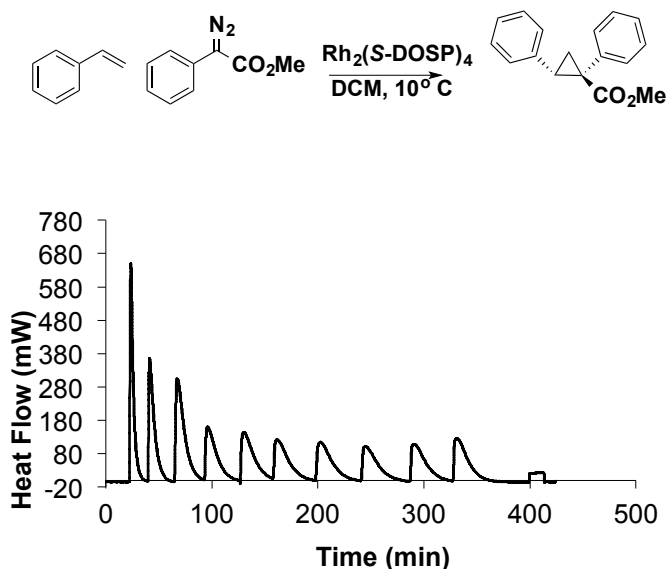


Figure 2.29: Tau corrected plot for multiple injection experiment (raw data). Heat flow (mW) versus time (min) for 10 successive injections of **1** (1.0 M) in the reaction of **2** (15.0 M) catalyzed by $Rh_2(S-DOSP)_4$ (0.0007 mol%) in dichloromethane at 10 °C.

2.4.9 Addition Experiments

Control Experiment:

To a 20 mL volumetric flask, 7.5 mmol (1.0 equiv.) of diazo compound **1a** was added and diluted in dry hexanes. To a separate 5.0 mL volumetric flask, 15 mmol (2 equiv.) of **2** was added and dissolved in dry hexanes. The solution of **2** was then added to a 50 mL 2-neck flask, fit with ReactIR™ probe and stir bar. The ReactIR™ software was initiated (5 second scanning for 3 hours) and a baseline was established over 4 minutes. Once a steady signal was obtained, the solution of **1a** was added dropwise to the solution of **2** via syringe pump over a 1-hr period. After addition, the software was allowed to run for an additional hour to establish a steady maximum signal of **1a**. The data was then imported into an excel spreadsheet and processed.

Addition Experiment A:

In a 20 mL volumetric flask, 7.5 mmol (1.0 equiv.) of diazo compound **1a** was mixed with 15 mmol (2.0 equiv.) of **2** and dissolved in hexanes. To a 50 mL 2-neck flask fit with ReactIR™ probe and stir bar, 5.0 mL of dry hexanes are added. 0.1 mL of a 0.00075 M stock solution of $\text{Rh}_2(\text{S-DOSP})_4$ was added to the 50 mL 2-neck flask. The ReactIR™ software was initiated (5 second scanning for 3 hours) and a baseline is established over 5 minutes. Next, the diazo-styrene solution was added to the catalyst solution over a one-hour period via syringe pump. During the addition, 100 μL reaction samples were taken for HPLC analysis. The samples were taken at $t = 30$ seconds, 90 seconds, 3 min, 6 min, 12 min, 18 min, 24 min, 30 min, 36 min, 42 min, 48 min, 54 min, and 60 min, After the initial 60 min addition, samples were taken in 10 min intervals until decomposition of the

diazo compound was no longer observed. The data was then imported into Excel and processed.

Addition Experiment B:

In a 20 mL volumetric flask, 7.5 mmol (1 equiv.) of diazo compound 1a was dissolved in hexanes. In a separate 5.0 mL volumetric flask, 15 mmol (2.0 equiv.) of **2** was added and dissolved in hexanes. The solution of **2** was added to a 50 mL 2-neck flask fit with ReactIRTM probe and stir bar. Next, 0.1 mL of a 0.00075 M stock solution of Rh₂(S-DOSP)₄ was added to the solution of **2**. The ReactIRTM software was initiated (5 second scanning for 3 hours) and a baseline was established over 4 minutes. Next, the diazo compound solution was added to the catalyst solution over a one-hour period via syringe pump. During the addition 100 μL reaction samples were taken for HPLC analysis. The samples were taken at t= 30 seconds, 90 seconds, 3 min, 6 min, 12 min, 18 min, 24 min, 30 min, 36 min, 42 min, 48 min, 54 min, and 60 min, After the initial 60 min addition, samples were taken in 10 min intervals until decomposition of the diazo compound was no longer observed. The data was then imported into Excel and processed.

- (1) Davies, H. M. L.; Morton, D. *Chem. Soc. Rev.* **2011**, *40*, 1857.
- (2) Nadeau, E.; Li, Z. J.; Morton, D.; Davies, H. M. L. *Synlett* **2009**, 151.
- (3) Nadeau, E.; Ventura, D. L.; Brekan, J. A.; Davies, H. M. L. *J. Org. Chem.* **2010**, *75*, 1927.
- (4) Li, Z. J.; Davies, H. M. L. *J. Am. Chem. Soc.* **2010**, *132*, 396.
- (5) Briones, J. F.; Hansen, J.; Hardcastle, K. I.; Autschbach, J.; Davies, H. M. L. *J. Am. Chem. Soc.* **2010**, *132*, 17211.
- (6) Lian, Y. J.; Davies, H. M. L. *J. Am. Chem. Soc.* **2011**, *133*, 11940.
- (7) Li, Z. J.; Parr, B. T.; Davies, H. M. L. *J. Am. Chem. Soc.* **2012**, *134*, 10942.
- (8) Wang, H. B.; Guptill, D. M.; Varela-Alvarez, A.; Musaeov, D. G.; Davies, H. M. L. *Chem. Sci.* **2013**, *4*, 2844.
- (9) Qin, C. M.; Davies, H. M. L. *Org. Lett.* **2013**, *15*, 310.
- (10) Chepiga, K. M.; Qin, C. M.; Alford, J. S.; Chennamadhavuni, S.; Gregg, T. M.; Olson, J. P.; Davies, H. M. L. *Tetrahedron* **2013**, *69*, 5765.
- (11) Doyle, M. P.; McKervey, M. A.; Ye, T. *Modern Catalytic Methods for Organic Synthesis with Diazo Compounds: From Cyclopropanes to Ylides*; Wiley, 1998.
- (12) Doyle, M. P.; Phillips, I. M. *Tetrahedron Lett.* **2001**, *42*, 3155.
- (13) Muller, P.; Bolea, C. *Helv. Chim. Acta.* **2002**, *85*, 483.
- (14) Doyle, M. P.; Eismont, M. Y.; Bergbreiter, D. E.; Gray, H. N. *J. Org. Chem.* **1992**, *57*, 6103.
- (15) Doyle, M. P.; Timmons, D. J.; Tumonis, J. S.; Gau, H. M.; Blossey, E. C. *Organometallics* **2002**, *21*, 1747.

- (16) Doyle, M. P.; Yan, M.; Gau, H. M.; Blossey, E. C. *Org. Lett.* **2003**, *5*, 561.
- (17) Hultman, H. M.; de Lang, M.; Arends, I. W. C. E.; Hanefeld, U.; Sheldon, R. A.; Maschmeyer, T. *J. Catal.* **2003**, *217*, 275.
- (18) Hultman, H. M.; de Lang, M.; Nowotny, M.; Arends, I. W. C. E.; Hanefeld, U.; Sheldon, R. A.; Maschmeyer, T. *J. Catal.* **2003**, *217*, 264.
- (19) Lloret, J.; Estevan, F.; Bieger, K.; Villanueva, C.; Ubeda, M. A. *Organometallics* **2007**, *26*, 4145.
- (20) Lloret, J.; Stern, M.; Estevan, F.; Sanau, M.; Ubeda, M. A. *Organomet.* **2008**, *27*, 850.
- (21) Nozaki, H.; Takaya, H.; Moriuti, S.; Noyori, R. *Tetrahedron* **1968**, *24*, 3655.
- (22) Oohara, T.; Nambu, H.; Anada, M.; Takeda, K.; Hashimoto, S. *Adv. Synth. Catal.* **2012**, *354*, 2331.
- (23) Takeda, K.; Oohara, T.; Anada, M.; Nambu, H.; Hashimoto, S. *Angew. Chem. Int. Ed.* **2010**, *49*, 6979.
- (24) Takeda, K.; Oohara, T.; Shimada, N.; Nambu, H.; Hashimoto, S. *Chem-Eur. J.* **2011**, *17*, 13992.
- (25) Watanabe, N.; Matsuda, H.; Kuribayashi, H.; Hashimoto, S. *Heterocycles* **1996**, *42*, 537.
- (26) Davies, H. M. L.; Walji, A. M. *Org. Lett.* **2003**, *5*, 479.
- (27) Davies, H. M. L.; Walji, A. M.; Nagashima, T. *J. Am. Chem. Soc.* **2004**, *126*, 4271.
- (28) Davies, H. M. L.; Walji, A. M. *Org. Lett.* **2005**, *7*, 2941.

- (29) Davies, H. M. L.; Venkataramani, C. *Org. Lett.* **2003**, *5*, 1403.
- (30) Pelphrey, P.; Hansen, J.; Davies, H. M. L. *Chem. Sci.* **2010**, *1*, 254.
- (31) Blackmond, D. G. *Angew. Chem. Int. Ed.* **2005**, *44*, 4302.
- (32) Baxter, R. D.; Sale, D.; Engle, K. M.; Yu, J. Q.; Blackmond, D. G. *J. Am. Chem. Soc.* **2012**, *134*, 4600.
- (33) Davies, H. M. L.; Panaro, S. A. *Tetrahedron* **2000**, *56*, 4871.
- (34) Hansen, J.; Autschbach, J.; Davies, H. M. L. *J. Org. Chem.* **2009**, *74*, 6555.
- (35) Davies, H. M. L.; Rusiniak, L. *Tetrahedron Lett.* **1998**, *39*, 8811.
- (36) Doyle, M. P.; Colman, M. R.; Chinn, M. S. *Inorg. Chem.* **1984**, *23*, 3684.
- (37) Doyle, M. P.; Wang, L. C.; Loh, K. L. *Tetrahedron Lett.* **1984**, *25*, 4087.
- (38) Doyle, M. P.; Mahapatro, S. N.; Caughey, A. C.; Chinn, M. S.; Colman, M. R.; Harn, N. K.; Redwine, A. E. *Inorg. Chem.* **1987**, *26*, 3070.
- (39) Blackmond, D. G.; Rosner, T.; Pfaltz, A. *Org. Process. Res. Dev.* **1999**, *3*, 275.
- (40) Blackmond, D. G.; Schultz, T.; Mathew, J. S.; Loew, C.; Rosner, T.; Pfaltz, A. *Synlett* **2006**, 3135.
- (41) Ferretti, A. C.; Mathew, J. S.; Blackmond, D. G. *Ind. Eng. Chem. Res.* **2007**, *46*, 8584.
- (42) Ovalles, S. R.; Hansen, J. H.; Davies, H. M. L. *Org. Lett.* **2011**, *13*, 4284.
- (43) Espino, C. G.; Fiori, K. W.; Kim, M.; Du Bois, J. *J. Am. Chem. Soc.* **2004**, *126*, 15378.

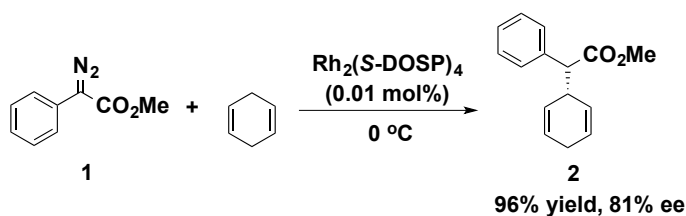
- (44) Baum, J. S.; Shook, D. A.; Davies, H. M. L.; Smith, H. D. *Syn. Commun.* **1987**, *17*, 1709.
- (45) Davies, H. M. L.; Hansen, T.; Churchill, M. R. *J. Am. Chem. Soc.* **2000**, *122*, 3063.

CHAPTER 3

Kinetic Studies on Donor/Acceptor Dirhodium(II) Carbene C-H Functionalization

3.1 Background

The chiral tetraproline dirhodium(II) catalyst, $\text{Rh}_2(\text{S-DOSP})_4$, is capable of conducting extremely high turnover numbers (TONs) in the reactions of donor/acceptor diazoacetates.^{1,2} The excellent activity displayed by the dirhodium(II) catalyst, however, is limited to the cyclopropanation of styrene under solvent-free conditions. Attempts at C-H insertion into 1,4-cyclohexadiene with low catalyst loading was not as successful, resulting in a maximum of 10,000 TONs (Scheme 3.1).² Moreover, attempts at C-H functionalization of unactivated substrates such as cyclohexane, under low catalyst loadings resulted in very little activity of the catalyst and substantial drop in enantioselectivity.³



Scheme 3.1: Solvent-free C-H insertion into 1,4 cyclohexadiene

Theoretical calculations have been conducted to probe the mechanistic pathways for dirhodium(II) donor/acceptor carbenoid C-H insertion into common substrates, such as 1,4-cyclohexadiene and cyclopentane.⁴ Based on these calculations diazo decomposition was proposed to be rate-limiting for C-H insertion into 1,4 cyclohexadiene, while carbenoid insertion is rate-limiting for C-H insertion into cyclopentane. While the computational analysis has contributed to the understanding of the reactivity of donor/acceptor carbenoids, an understanding of what pathways may be

involved in deactivation or decomposition of the catalyst has not yet been achieved. Studies in this chapter will discuss kinetic techniques that have been used to study dirhodium(II) donor/acceptor carbene C-H insertion into 1,4-cyclohexadiene and cyclohexane. The ultimate goal of this work is to enhance the understanding of all the facets involved in the rhodium-catalyzed reactions of diazo compounds so that it will be possible to achieve C-H functionalization routinely with high TON's.

3.2 Results

3.2.1 RPKA for C-H insertion into 1,4-Cyclohexadiene

The first goal of these kinetic studies was to determine the differences between the kinetics of cyclopropanation of styrene and C-H insertion into 1,4-cyclohexadiene. Competition studies have demonstrated that styrene and 1,4-cyclohexadiene are about equally efficient at trapping rhodium carbene intermediates. However, the rhodium catalysts result in much higher TON's in cyclopropanation of styrene compared to C-H insertion of 1,4-cyclohexadiene.⁵ With this in mind, the standard conditions for the cyclopropanation RPKA study (10 equiv. of olefin, 0.005 mol% catalyst, 0 °C in hexanes) were initially explored for C-H insertion into 1,4 cyclohexadiene. To our surprise, no decomposition of the diazoacetate was observed. Optimization of the reaction found that decreasing the olefin concentration to 1.0 equivalent (0.3 M) and increasing the catalyst concentration to 0.01 mol% resulted in >90% conversion to **2** (Figure 3.1).

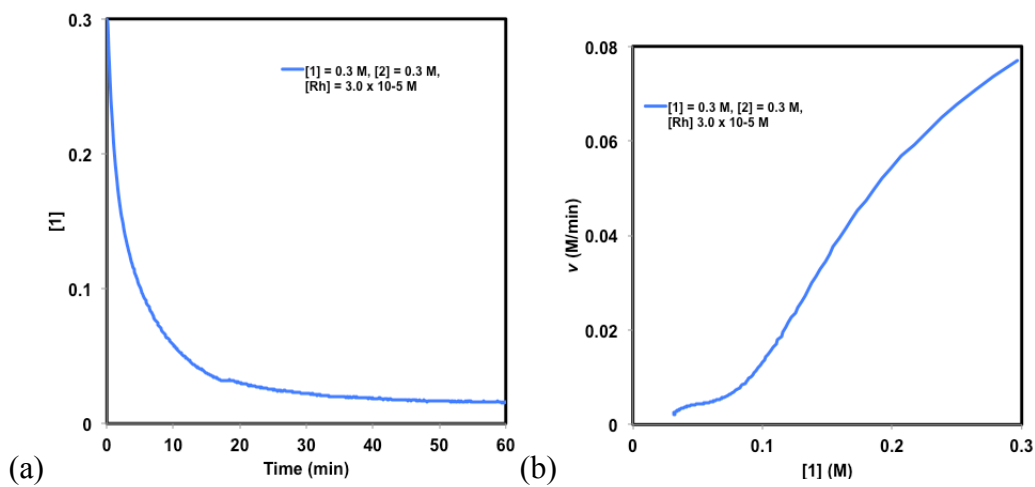


Figure 3.1 Standard kinetic plots for the reaction of **1** (0.3 M) with **2** (0.3 M) catalyzed by $\text{Rh}_2(\text{S-DOSP})_4$ (0.01 mol%) in hexanes at 0 °C. (A) Concentration of **1**(M) versus time (min) plot. (B) Rate of the reaction v (M/min) versus concentration of **1** (M).

Olefin coordination has been shown to have a significant influence on the rate of the diazo decomposition in cyclopropanation of styrene; therefore it was proposed that similar interactions would be observed in the C-H insertion reaction. The concentration of **2** was increased to 0.6 M (2.0 equiv), resulting in a ~30% conversion to the C-H insertion product (Figure 3.2, red curve). The activity of the catalyst decreased significantly as the olefin concentration was increased. Such reactivity corresponds to a strong negative order concentration dependence on the olefin trap. The interaction was so significant that the catalyst died after ~5,000 TON. Consistent with results from the cyclopropanation study and titration studies by Doyle and coworkers,^{6,7} 1,4-cyclohexadiene is proposed to bind strongly to the dirhodium core.

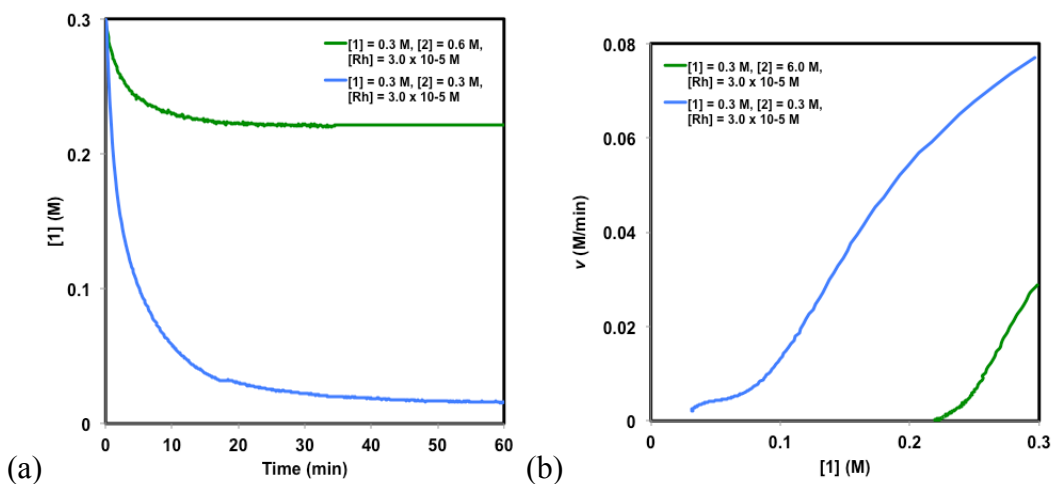


Figure 3.2: Influence of increasing concentration of **2** for the reaction of **1** (0.3 M blue and green) with **2** (0.3 M blue, 0.6M green) catalyzed by Rh₂(S-DOSP)₄ (0.01 mol%) in hexanes at 0 °C. (A) Concentration of **1** (M) versus time (min) plot. (B) Rate of the reaction v (M/min) versus concentration of **1** (M).

The identification of the reaction driving forces is integral in explaining what factors contribute to increasing catalyst turnover. The concentration dependencies of the catalyst and diazo compound were determined in subsequent different excess experiments. Decreasing the catalyst concentration to 1.5×10^{-5} M or 0.005 mol% resulted in a substantially slower reaction rate and 10% conversion to the insertion product (Figure 3.3). The result illustrates that the catalyst quickly deactivates at extremely low concentrations.

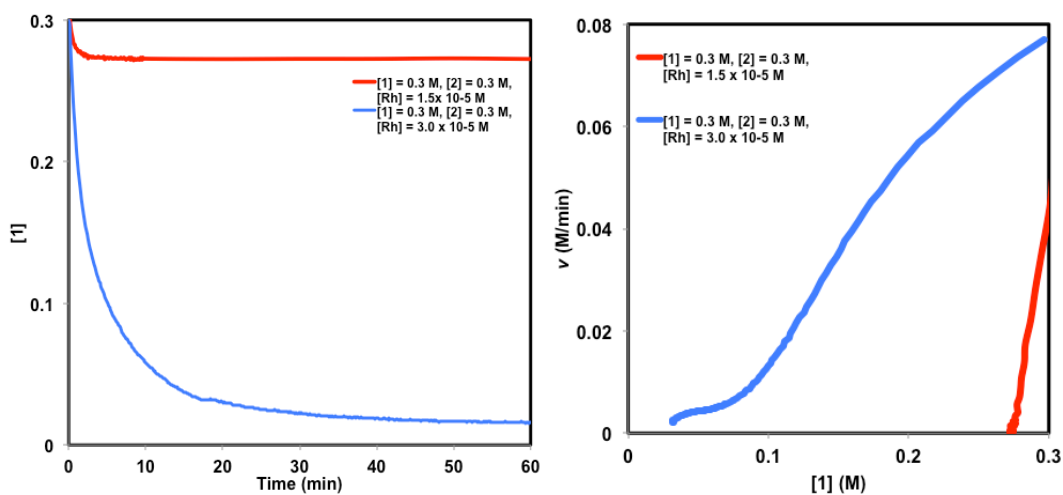


Figure 3.3: Influence of decreasing concentration of $\text{Rh}_2(\text{S-DOSP})_4$ for the reaction of **1** (0.3 M blue and red) with **2** (0.3 M blue, and green) catalyzed by $\text{Rh}_2(\text{S-DOSP})_4$ (0.005 mol% - Red, 0.01 mol% - Blue) in hexanes at 0 °C. (A) Concentration of **1**(M) versus time (min) plot. (B) Rate of the reaction v (M/min) versus concentration of **1** (M).

Theoretical calculations postulate that diazo compound decomposition is rate limiting⁴, therefore, it was expected that the reaction would have a positive order dependence on the diazo compound. Decreasing the diazoacetate concentration from 0.3 M to 0.15 M while keeping the olefin and catalyst concentrations constant, provided a slower reaction rate (Figure 3.4). The result suggests that the reaction has a positive order in diazo compound concentration.

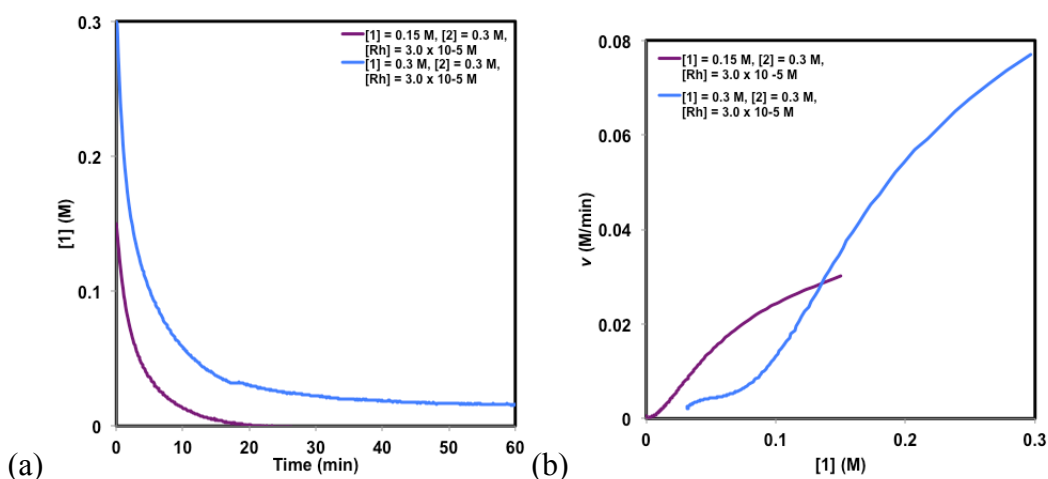


Figure 3.4: Influence of decreasing concentration of **1** for the reaction of **1** (0.3 M blue and 0.15 M purple) with **2** (0.3 M blue, and purple) catalyzed by $\text{Rh}_2(\text{S-DOSP})_4$ (0.01 mol% - blue and purple) in hexanes at 0 °C. (A) Concentration of **1** (M) versus time (min) plot. (B) Rate of the reaction v (M/min) versus concentration of **1** (M).

The next set of experiments probed the activity of the catalyst. The catalyst concentration was kept at a constant 3.0×10^{-5} M while the concentration of **1** and the trap were increased to 0.6 M each. The excess for these experiments are defined as 0 ($0.6 \text{ M} - 0.6 \text{ M} = 0$). If deactivation of the catalyst is not observed, then the rate plots (blue and green) should overlap at 0.3 M diazo compound. However, compared to the standard conditions, the same excess experiment in Figure 3.5 demonstrated significant deactivation of the catalyst. The reaction started at a much slower rate and resulted in $\sim 50\%$ conversion. As olefin coordination was already been identified as a method of catalyst deactivation, we suspected the product would additionally coordinate to the catalyst through the olefin moiety

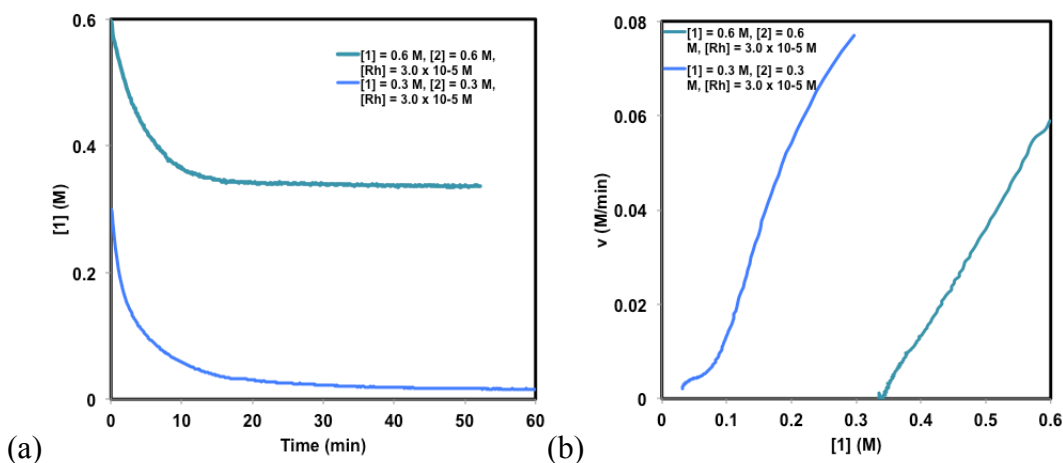


Figure 3.5: Same excess experiment illustrates that there is significant catalyst deactivation for the reaction of **1** (0.3 M blue and 0.6 M teal) with **2** (0.3 M blue, and 0.6 M teal) catalyzed by $\text{Rh}_2(\text{S-DOSP})_4$ (3.0×10^{-5} M - blue and teal) in hexanes at 0°C . (A) Concentration of **1** (M) versus time (min) plot. (B) Rate of the reaction v (M/min) versus concentration of **1** (M).

Based on the significant amount of deactivation observed in the same excess experiment, it was imperative to test if product inhibition was operative. In order to test for product coordination to the dirhodium catalyst, one equivalent (0.3 M, 1.50 mmol) of the insertion product was added to the reaction mixture to probe product inhibition. As a result, 30% conversion and a much slower rate were observed (Figure 3.6). The reaction was nearly 4x slower via the addition of product. Based on the result, it is proposed that product inhibition has a significant influence over the rate of the reaction.

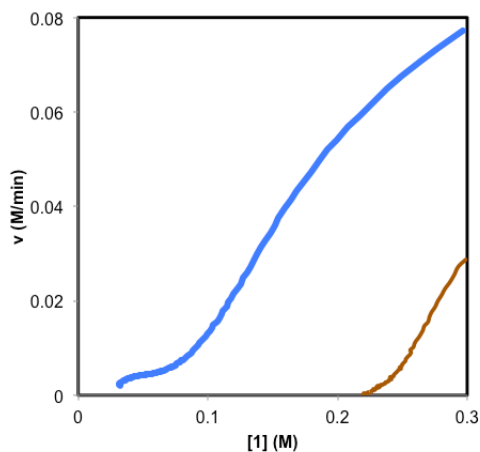


Figure 3.6: Product doping experiment containing **3** (0.3 M for brown curve, 0.0 M for blue) for the reaction of **1** (0.3 M blue and brown) with **2** (0.3 M blue and brown) catalyzed by $\text{Rh}_2(\text{S-DOSP})_4$ (3.0×10^{-5} M - blue and brown) in hexanes at 0 °C.

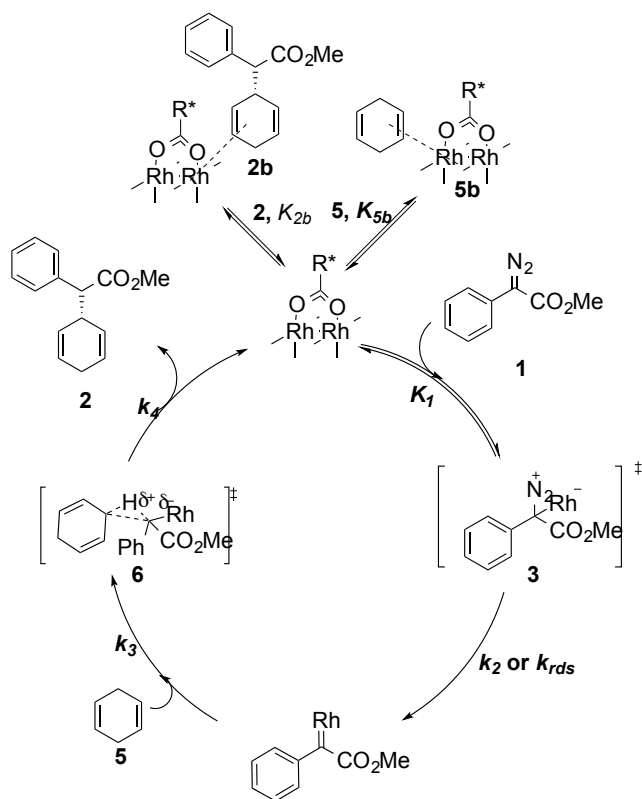
Table 3.1 describes the RPKA conditions that were used for C-H insertion into 1,4-cyclohexadiene. These results demonstrate that the concentration of catalyst and diazo compound are the reaction driving forces, while olefin and product act as inhibitors. These results are parallel to results obtained in the cyclopropanation chemistry.

Table 3.1 RPKA Conditions

$\text{Rh}_2(\text{S-DOSP})_4$
Hexanes, 0° C

Entry	[1] ₀ (M)	[olefin] ₀ (M)	[Rh] (M)	[2] ₀ (M)	e (M)	Reaction Type
1	0.3	0.3	1.5 x 10 ⁻⁵	--	0	standard
2	0.3	0.6	1.5 x 10 ⁻⁵	--	0.3	[olefin] Dependency
3	0.15	0.3	1.5 x 10 ⁻⁵	--	0.15	[A] Dependency
4	0.3	0.3	3.0 x 10 ⁻⁵	--	0	[Rh] Dependency
5	0.6	0.6	1.5 x 10 ⁻⁵	--	0	Same Excess
6	0.3	0.3	1.5 x 10 ⁻⁵	0.3	0	[2] Dependency

The RPKA experiments allow for development of a reaction mechanism as well as rate law. The mechanism includes off-cycle reservoirs of the catalyst, which have been identified as olefin and product inhibition. The remaining on-cycle steps follow the predicted pathway for C-H insertion. Complexation of the diazo compound to the dirhodium(II) catalyst is followed by nitrogen extrusion to yield the rhodium carbene **4**. The carbene then inserts into the C-H bond to give **2** and the unbound the catalyst. The catalyst is in turn susceptible to coordination to **5** and/or **2**. From the elementary steps described herein, we can establish the rate law.



Scheme 3.2: Mechanism for C-H insertion

RPKA experiments established parallel concentration dependencies between the C-H insertion and cyclopropanation chemistry, suggesting that the rate law for C-H insertion into 1,4-cyclohexadiene is similar to the rate law derived for cyclopropanation of styrene in Chapter 2. For this reason, full development of the rate law will not be explicitly discussed (See Chapter 2.2.3). The rate law in Equation 3.1 defines the concentration dependences for the key factors controlling the reaction rate. The order of each substrate is defined by Equation 3.2, to yield the simple rate law in Equation 3.3.

$$r = \frac{k_{rds}a[\mathbf{1}][Rh]_T}{(1+a[\mathbf{1}] + K_{5b}[\mathbf{5}] + K_{2b}[\mathbf{2}])} \quad (3.1)$$

$$\log \left[\frac{(rate)_a}{(rate)_b} \right] = \log \left[\frac{(S)_a}{(S)_b} \right] \quad (3.2)$$

$$r = k'[\mathbf{1}]^{0.5}[\mathbf{5}]^{-1}[\mathbf{2}]^{-1}[Rh_T] \quad (3.3)$$

Kinetic studies on the dirhodium(II) mediated C-H into 1,4-cyclohexadiene by a donor/acceptor carbenoid has unveiled that the catalyst deactivation occurs. The deactivation is identified as persistent olefin substrate and product inhibition. These factors were found to have a significant influence on the enantioselectivity of the reaction. With knowledge of the reaction driving forces as well as evidence from the cyclopropanation study that slow addition of the diazo compound at higher temperatures can achieve full-conversion to the insertion product and stable enantioselectivity, higher TON's were attempted.

3.2.2 High TON for C-H Insertion into 1,4-Cyclohexadiene

The evaluation of the addition method in the cyclopropanation of styrene (Chapter 2.1) demonstrated that catalyst deactivation could be avoided by conducting experiments at higher temperatures. It is postulated that higher temperatures shift the equilibrium of product and olefin coordination. Encouraged by those results, similar conditions were explored for the C-H insertion into 1,4 cyclohexadiene.

Addition of **1** (0.375 M, 7.5 mmol) to a refluxing solution of **5** (3.0 M, 15 mmol) with Rh₂(S-DOSP)₄ (0.001 mol%) in hexanes at 68 °C resulted in 100,000 TONs for the dirhodium catalyst (Figure 3.7). Previous attempts of 100,000 TON at 25 °C were unsuccessful as diazo compound quickly built up, indicating catalyst deactivation.

Samples of the reaction were taken over specific time intervals and analyzed by HPLC to assess the enantioselectivity of the reaction over time. A stable enantioselectivity of 75 %ee was recorded.

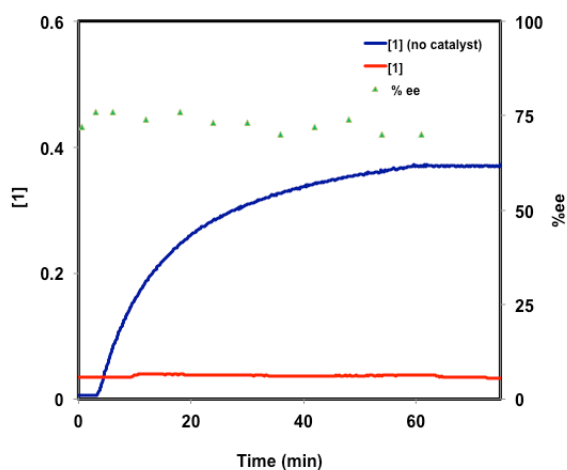
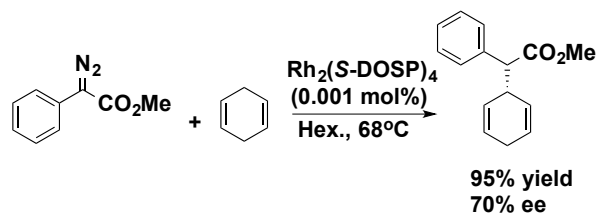


Figure 3.7: Concentration of **1** (M) and % ee of **2** versus time (min) for the slow addition of **1** (0.375M) to a solution of **5** (3.0 M) catalyzed by $\text{Rh}_2(\text{S-DOSP})_4$ (0.001 mol%) in hexanes at 68 °C. Blue curve is the uncatalyzed control experiment, red is the reaction in the presence of $\text{Rh}_2(\text{S-DOSP})_4$ and green triangles represent the % ee.

3.2.3 Reaction Calorimetry

Reaction calorimetry has been shown to be a viable method for identifying the kinetic activity of a catalyst.⁸⁻¹⁰ Further kinetic studies on the $\text{Rh}_5(\text{S-DOSP})_4$ mediated C-H insertion into 1,4 cyclohexadiene were attempted using reaction calorimetry. Multiple injection reaction calorimetry results, however, were inconclusive. Sequential injections of 1.5 mmol diazo compound into a solution of 0.1 mol% catalyst and 1,4-cyclohexadiene in DCM at 10 °C illustrate that catalyst deactivation is present, however, calculated heat (ΔH) per injection indicated that conversion was low (Figure 3.8). Additionally, measurement of the enantioinduction for the C-H insertion products could not be obtained because the product aromatized prior to analysis.

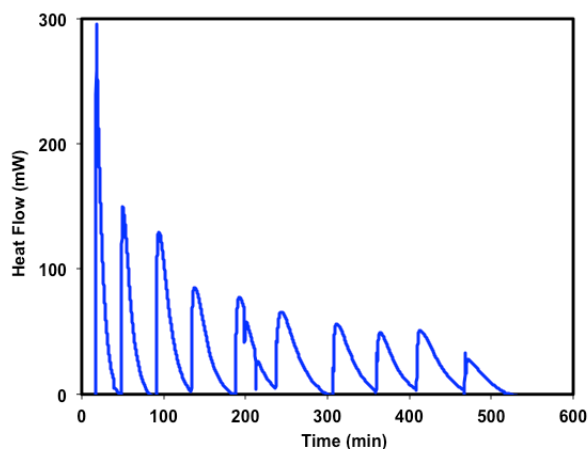


Figure 3.8: Heat flow (mW) versus time (min) for 10 successive injections of **1** (1.0 M) in the reaction of **5** (15.0 M) catalyzed by $\text{Rh}_2(\text{S-DOSP})_4$ (0.0007 mol%) in dichloromethane at 10 °C.

3.2.4 Bridging vs. Non Bridging Catalysts

Dirhodium(II) tetracarboxylate catalysts exhibit remarkable activity in carbenoid and nitrenoid mediated C-H functionalization.^{5,11-22} An overall goal has been to develop more robust catalysts that can undergo high catalyst turnovers, particularly in C-H insertion. The catalysts that are currently used to induce reactivity are believed to have high initial kinetic activity. At low catalyst loadings drops in yield and enantioselectivity are observed, suggesting that the activity of the catalyst may not hold over the course of the reaction. While the cause of this drop in enantioselectivity is unknown, one possibility could be dissociation of one or more carboxylate ligand. To circumvent the possibility of ligand dissociation “tethered” or bridging dirhodium(II) catalysts have been developed.

Du Bois and coworkers have developed a number of chiral and achiral bridging catalysts for nitrenoid mediated C-H functionalization, many which are unpublished. In collaboration with the Du Bois group, bridged and non-bridged dirhodium(II) tetracarboxylate catalysts, were compared to gain insight on ligand features that contribute to catalyst stability in C-H insertion of 1,4 cyclohexadiene (Figure 3.9). Reactions were monitored via ReactIRTM, following the decomposition of the carbenoid precursor (diazo compound) at 2100 cm^{-1} . The temporal reaction profiles were plotted to establishing turnover frequency, which was critical in comparison of the bridging vs. non-bridging catalysts. The enantioselectivity of each reaction was obtained by graduate student Ms. Kathryn Chepiga.

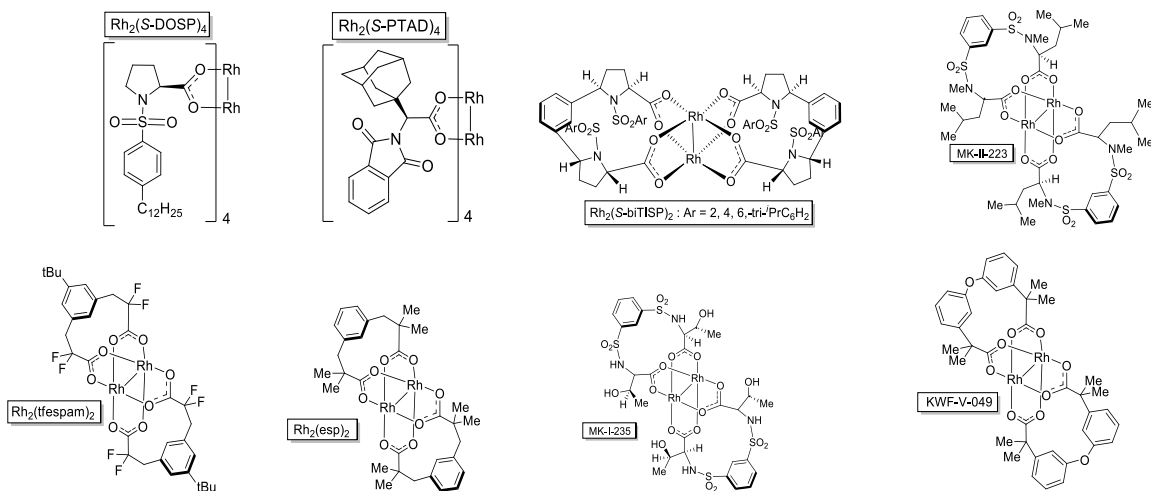
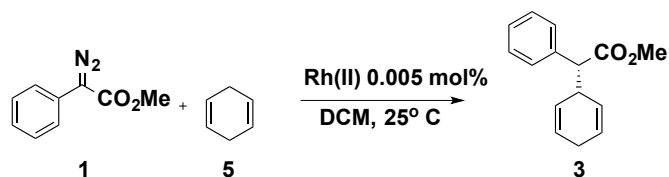


Figure 3.9 Dirhodium(II) catalysts screened

Table 3.2 describe results from TON/TOF screening of chiral and achiral bridging and non-bridging dirhodium(II) catalysts at 0.005 mol% catalyst loading. It was expected that the activity of the catalysts would vary significantly; therefore, experiments were conducted at 25 °C in dichloromethane to ensure full conversion for the reaction of **1** (0.3M) with 1.5 M (5 equiv) of **5**. Exceptional turnover numbers were observed for both Davies and Du Bois' catalysts. In general, Du Bois' bridging catalysts retained kinetic activity throughout the reaction course. Superior TOF's were observed with Rh₂(esp)₂ and MK-1-235 (entries 4 and 5). Davies' Rh₂(S-DOSP)₄, proved to be very kinetically active under these reaction conditions. We attribute the increased activity of Rh₂(S-DOSP)₄ to the temperature of the reaction. At 25 °C, a large exotherm is observed for the Rh₂(S-DOSP)₄ (0.005 mol%) mediated C-H insertion of **5**, therefore, the exceptional kinetic activity observed in this experiment may be due to the temperature jump. In comparison, the bridging catalyst, Rh₂(S-biTISP)₄, exhibited very little activity. It is suspected that the bulky nature of the catalyst prevented high TOF's.

Table 3.2: Results from Screening of Dirhodium(II) Catalysts

Entry	Catalyst	% Conv.	% ee	TON	TOF _{avg} (hr ⁻¹)
1	Rh ₂ (S-DOSP) ₄	90%	27%	18,000	6,000
2	Rh ₂ (S-PTAD) ₄	92%	52%	18,400	767
3	Rh ₂ (S-biTISP) ₄	44%	42%	8,800	367
4	Rh ₂ (esp) ₂	>99%	--	20,000	24,000
5	MK-1-235	>99%	30%	20,000	6,250
6	MK-II-223	90%	6%	18,000	514
7	KWF-V-049	>99%	--	20,000	20,000
8	Rh ₂ (tfesbam) ₂	42%	--	8,400	8,400

Evaluation of the temporal ReactIRTM plots allowed for a visual description of the dirhodium(II) catalysts kinetic activity over the course of the C-H insertion reaction (Figure 3.10). Non-bridging catalyst, Rh₂(S-PTAD)₄ exhibited high kinetic activity initially, however, this activity quickly deteriorated over time. It is postulated that the low TOF after the initial reactivity is associated with catalyst decomposition or product inhibition. In comparison, Du Bois' KWF-V-049 demonstrated high TOF throughout the course of the reaction suggesting that the catalyst is not susceptible to decomposition or deactivation.

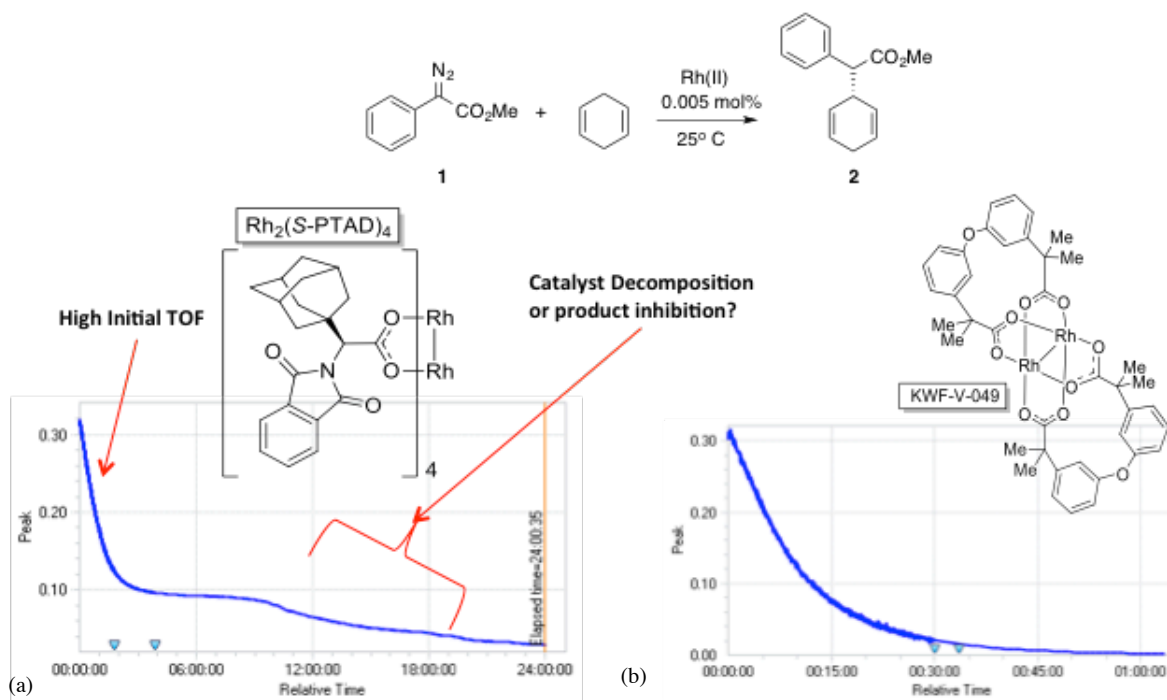


Figure 3.10: Peak height of **1** (A.U.) versus relative time (hh:mm:ss) for the TOF comparison between nonbridged dirhodium(II) catalyst $\text{Rh}_2(\text{S-PTAD})_4$ (0.005 mol%) and bridging catalyst KWF-V-049 (0.005 mol%) for the reaction of **1** (0.3 M) with **5** (1.5 M) in dichloromethane at 25 °C. (a) Kinetic profile of $\text{Rh}_2(\text{S-DOSP})_4$. (b) Kinetic profile of KWF-V-049.

3.2.5 Exploration of MK-1-235

In the C-H insertion of 1,4 cyclohexadiene, MK-1-235 demonstrated moderate enantioselectivity. To date, chiral variants of bridging dirhodium(II) catalysts are limited, therefore, it was important to further explore the scope and limitations of MK-1-235 (Figure 3.11).

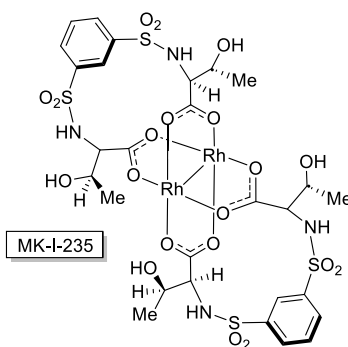


Figure 3.11: Du Bois' catalyst MK-1-235

MK-1-235 exhibited poor solubility in dichloromethane, therefore, follow up studies were conducted in ethyl acetate. The change in the solvent resulted better solubility of MK-1-235, however, lower enantioselectivity and conversion were observed. (Figure 3.12, Table 3.3: entry 1). It is not completely understood why lower yields and enantioselectivity were observed. It is suspected, however, that the lower conversion is due to competitive coordination of trap and solvent to the axial site of the dirhodium(II) catalyst.

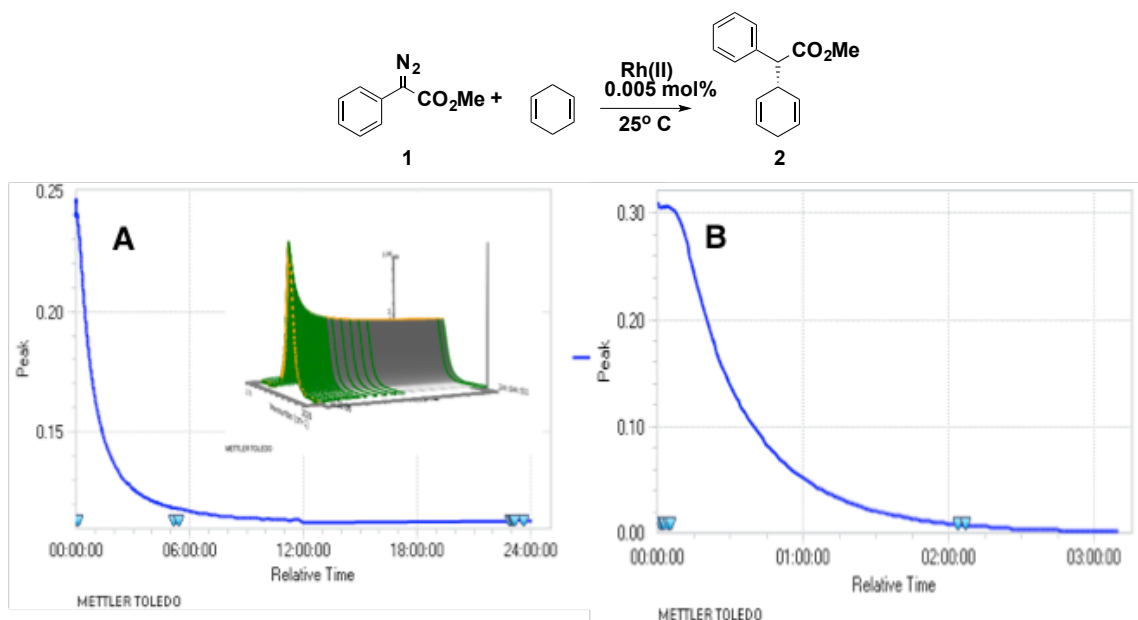
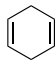
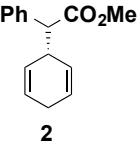
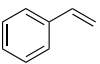
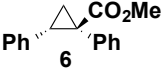
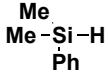
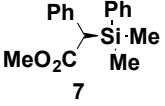
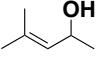
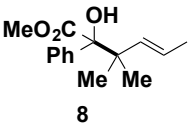
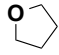
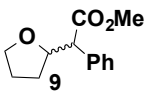


Figure 3.12: Kinetic profile of MK-1-235 (0.005 mol%) for the reaction of **1** (0.3 M) with **5** (1.5 M). (a) Reaction is conducted in ethyl acetate and low conversion is observed. (b) Reaction conducted in dichloromethane, higher conversion.

Interested in the initial results obtained with MK-1-235 other carbenoid reactions were explored (Table 3.3). High conversion was observed for cyclopropanation and Si-H insertion (entries **2** and **3**). The enantioselectivity, however was very low with 2% ee and 20% ee, respectively. Very little activity was observed in the tandem ylide formation/[2,3] sigmatropic rearrangement and C-H insertion into furan (entries 4 and 5). Despite modest results with Si-H insertion, catalyst material was limited and exploration of the catalyst ended.

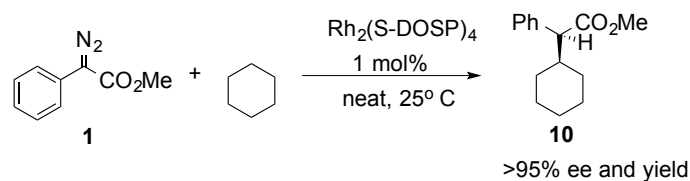
Table 3.3 Substrate screening for MK-1-235

Entry	Substrate	Catalyst Loading	Product	% Conversion	% ee	TON
1		0.005 mol %	 2	55%	26%	11,000
2		0.005 mol %	 6	90%	2%	18,000
3		0.005 mol %	 7	95%	20%	19,000
4		0.05 mol %	 8	16%	--	3,200
5		0.005 mol %	 9	7%	--	1,400

The study illustrated that bridging dirhodium(II) catalysts exhibited higher TOF's than traditional non-bridging catalysts. It is proposed that the increased activity of the catalyst is due to added stability of the tethered ligand. On-going research in the Davies lab is focused on synthesizing other chiral dirhodium (II) bridging catalysts.

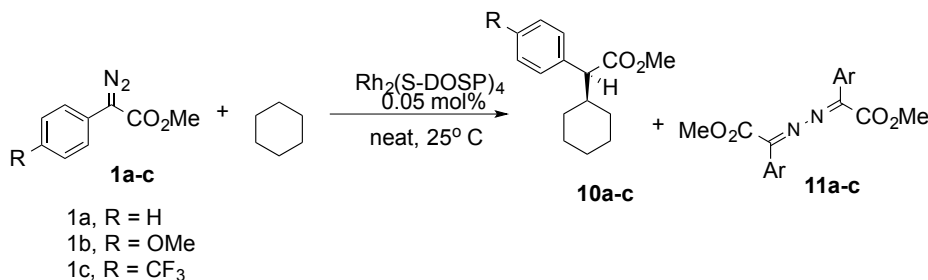
3.2.6 C-H insertion into Cyclohexane

As kinetic parameters were established for C-H insertion into 1,4 cyclohexadiene, an expansion to less reactive systems was explored. In particular, high TON C-H insertion into cyclohexane has been an interest of the Davies lab for some time (Scheme 3.3). Excellent enantioselectivity and conversion to the insertion product can be obtained with 1 mol% of the catalyst. A decrease in the catalyst loading, however, results in significant drop in yield and enantioselectivity.



Scheme 3.3: C-H insertion into cyclohexane.

The basis for the substantial deactivation of the catalyst is not well understood. Theoretical calculations on C-H insertion of cyclopentane postulate that carbene insertion is rate-limiting. Therefore, the reactive carbene may possibly react with the dirhodium(II) complex or ligands to destroy the catalyst structure. The goal of this study was to gain insight into factors that contributed to catalyst decomposition. Cyclohexane lacks any Lewis basic sites or olefin moieties, therefore it was proposed that off-reservoirs of the catalyst may not be persistent and other modes of catalyst deactivation may be observed.

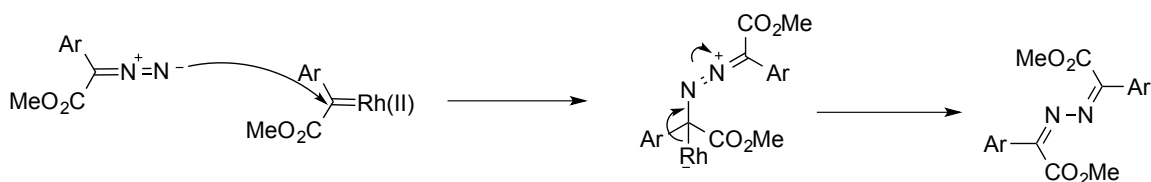


Scheme 3.4: Kinetic results for C-H insertion into cyclohexane.

Attempts at RPKA for C-H insertion into cyclohexane, however were unsuccessful. Addition of the catalyst to a mixture of the diazo compound and cyclohexane at 25 °C, resulted in a 1:7 mixture of the desired product **10a** and azine **11a**.

It is proposed that the azine is formed from reaction of the rhodium carbene with the diazo compound (Scheme 3.5). The ratio of C-H insertion product to azine could be attenuated by changing the electronics of the diazo compound. Increasing the electron density to the aryl moiety resulted in selective formation of the azine. In comparison,

switching to an electron poor aryl diazo compound resulted in 6:1 ratio of **10c**:**11c**. Conducting the reaction at higher temperatures, resulted in mixtures of the desired product and azine. Consequently, high TON conditions for selective C-H insertion product could not be established. The azine formation is an alternative pathway for the dirhodium carbene, therefore, kinetics for the C-H insertion into cyclohexane could not be conducted.



Scheme 3.5: Proposed mechanism for azine formation.

3.3 Discussion and Conclusions

The work in this chapter has provided mechanistic insight into dirhodium(II) donor/acceptor carbenoid C-H insertion. RPKA studies illustrated the effect trap and product inhibition can have over the rate of the reaction. Furthermore, kinetic studies have provided further evidence that bridging dirhodium catalysts are more kinetically active than non-bridging catalysts. Exploration of various carbenoid reactions with MK-1-235 has demonstrated that high conversion can be obtained, however the enantioselectivity is moderate at best. Unfortunately kinetic studies could not be conducted on C-H insertion into cyclohexane due to the persistent formation of azine. Currently alternative methods for understanding mechanistic details of unactivated C-H bonds are underway utilizing mass spectrometry techniques by the Zare and Davies group. Additionally, the synthesis of other chiral bridging dirhodium(II) catalysts is being

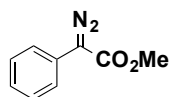
conducted in the Davies group. Future work will focus on better understanding the mechanistic details that were outside of the scope of RPKA.

3.4 Experimental

3.4.1 General Considerations

All reactions were carried out in oven-dried glassware under inert atmosphere. All chemicals were purchased, or found in the Davies Group Diazo Compound Library unless otherwise stated. All solvents used were either distilled or retrieved out of the solvent system and degassed 15 minutes prior to usage. Flash column chromatography was performed on silica gel. ¹H NMR Spectra were recorded at 400 and 600 MHz on a Varian 400, Inova 400, and Inova 600. ¹³C NMR was recorded at 100 MHz on a Varian and Inova 400.

3.4.2 Characterization of Known Diazo Compounds



1

See Chapter 2.4.2 compound **1a**.

3.4.3 General procedure for kinetic measurements on ReactIR™ for C-H Functionalization Reactions

Experiments were carried out with a Mettler Toledo ReactIR™ 45m instrument equipped with a 9.5mm x 12” AgX 1.5m SiComp probe. Stock solutions of diazo compounds and Rh(II) catalysts in the appropriate solvent were prepared. To a dry round bottom flask was added a stir bar, trap, solvent and an aliquot of diazo compound solution. Unless otherwise noted, the reaction was cooled to 10 °C (*p*-dioxane, CO_{2(s)}) bath) or 0 °C (ice/water bath) and allowed to equilibrate for 30 min. The ReactIR™ probe was then inserted and the instrument set up for a continuous scan experiment. The scan

was started and, at $t_0 = 20$ s, an aliquot of the catalyst solution was injected by syringe in one movement with vigorous stirring.

The standard reaction of **1** (0.3M) with **5** (0.3) catalyzed by $\text{Rh}_2(\text{S-DOSP})_4$ (0.005 mol%) in hexanes at 0 °C was run 2x to ensure the validity of the procedure. Additionally, crude ^1H NMR samples were taken to ensure that C-H insertion was the only catalytic process at work. A representation of the raw peak height of **1** (M) vs time (hh:mm:ss) for two separate runs is found in Figure 3.13.

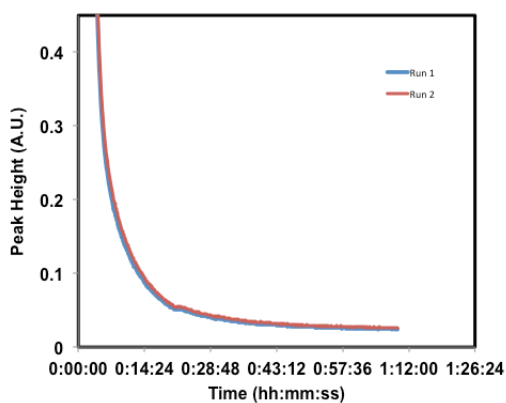
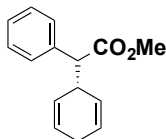


Figure 3.13: Plot of the peak height (A.U.) versus relative time (hh:mm:ss) of **1** for reaction of **2** (3.0 M) catalyzed by $\text{Rh}_2(\text{S-DOSP})_4$ (0.005 mol%) in hexanes at 0 °C. Trial 1 (blue) and trial 2 (red)

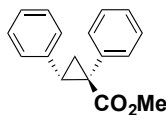
3.4.4 Characterization Data of Known C-H functionalization Products



2

methyl (*S*)-2-(cyclohexa-2,5-dien-1-yl)-2-phenylacetate

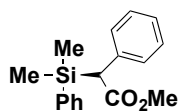
¹H NMR (400 MHz, CDCl₃): δ 7.33-7.29 (m, 4H), 7.28-7.25 (m, 1H), 5.82-5.79 (m, 1H), 5.73-5.66 (m, 2H), 5.28-5.25 (m, 1H), 3.67 (s, 3H), 3.50-3.46 (m, 1H), 3.42 (d, 1H, J = 10.5 Hz), 2.63-2.59 (m, 2H). The spectroscopic data are consistent with previously reported data.²



6

methyl (1*R*,2*S*)-1,2-diphenylcyclopropane-1-carboxylate.

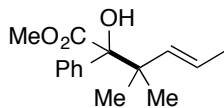
See Chapter 2.4.4 compound 3.



7

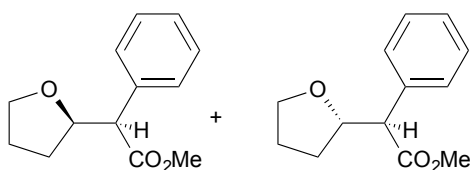
methyl (*R*)-2-(dimethyl(phenyl)silyl)-2-phenylacetate

¹H NMR (400 MHz, CDCl₃) δ 7.32–7.25 (m, 5H), 7.18–7.05 (m, 5H), 3.53 (s, 1H), 3.48 (s, 3H), 0.28 (s, 3H), 0.25 (s, 3H). Spectroscopic data are consistent with previously reported data.²⁵



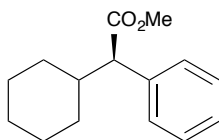
8

^1H NMR (400 MHz, CDCl_3): d 7.73-7.72 (2H, m), 7.33-7.27 (3H, m), 5.22 (1H, s), 3.85 (3H, s), 3.69 (1H, s), 1.71 (3H, s), 1.49 (3H, s), 1.22 (3H, s), 1.17 (3H, s). Spectroscopic data are consistent with previously reported data.²³



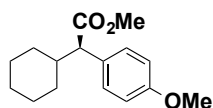
9a/9b

^1H NMR (400 MHz, CDCl_3) (major diastereomer) δ 7.40 - 7.26 (m, 5 H), 4.46 (dt, 1 H, $J = 8.3$, 7.0 Hz), 3.84 - 3.70 (m, 2H), 3.67 (s, 3H), 3.62 (d, 1 H, $J = 8.4$ Hz), 2.11 (m, 1 H), 1.88 (m, 1 H), 1.67 (m, 1 H); ^1H NMR (400 MHz, CDCl_3) (minor diastereomer) δ 7.36 - 7.26 (m, 5 H), 4.52 (dt, 1 H, $J = 9.9$, 7.0 Hz), 3.95 - 3.79 (m, 2 H), 3.69 (s, 3H), 3.52 (d, 1 H, $J = 9.9$ Hz), 1.90 - 1.77 (m, 2 H), 1.68 (m, 1 H), 1.43 (m, 1H); The spectroscopic data are consistent with previously reported data.²⁴



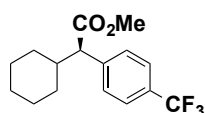
10a

^1H NMR (400 MHz, CDCl_3) δ 7.31- 7.22 (m, 5H), 3.64 (s, 3H), 3.22 (d, $J = 10.6$ Hz, 1H), 2.03-1.97 (m, 1H), 1.74 (m, 2H), 1.81 – 1.55 (m, 4H), 1.33-1.01 (m, 5H), 0.87-0.70 (m, 1H). The spectroscopic data are consistent with previously reported data.³



10b

^1H NMR (400 MHz, CDCl_3) δ 7.23 (d, $J = 8.4$ Hz, 2H), 6.84 (d, $J = 8.4$ Hz, 2H), 3.78 (s, 3H), 3.65 (s, 3H), 3.16 (d, $J = 10.6$ Hz, 1H), 1.93 (m, 1H), 1.78 – 1.55 (m, 4 H), 1.33-0.99 (m, 5H), 0.71 (m, 1H). The spectroscopic data are consistent with previously reported data.³



10c

^1H NMR (400 MHz, CDCl_3) δ 7.56 (d, $J = 8.1$ Hz, 2H), 7.45 (d, $J = 8.1$ Hz, 2H), 3.65 (s, 3H), 3.30 (d, $J = 10.6$ Hz, 1H), 2.01 (m, 1H), 1.74 (m, 2H), 1.81 – 1.55 (m, 4 H), 1.33-1.03 (m, 5H), 0.78 (m, 1H). The spectroscopic data are consistent with previously reported data³

3.4.5 Representative Kinetic Plots, Equations, and Rate Derivation

Calibration Curve for Methyl Phenylldiazoacetate (1)

See Chapter 2.4.6.

3.4.6 Derivation of Rate Law

See Chapter 2.2.3

3.4.7 Determination of reaction rate for RPKA:

See Chapter 2.4.7

3.4.8 Multiple Injection Kinetic Experiments

See Chapter 2.4.8

3.4.9 Addition Experiments

Control Experiment:

To a 20 mL volumetric flask, 7.5 mmol (1.0 equiv.) of diazo compound **1a** was added and diluted in hexanes. To a separate 5.0 mL volumetric flask, 15 mmol (2 equiv.) of **5** was added and dissolved in hexanes. The solution of **5** was then added to a 50 mL 3-neck flask, fit with ReactIRTM probe, stir bar, and reflux condenser. The reaction was brought to reflux and the ReactIRTM software was initiated (5 sec scanning for 3 h). A baseline was established over 4 min. Once a steady signal was obtained, the solution of **1a** was added dropwise to the solution of **5** via syringe pump over a 1-h period. After addition, the software was allowed to run for an additional hour to establish a steady maximum signal of **1**. The data was then imported into an excel spreadsheet and processed.

Addition Experiment:

In a 20 mL volumetric flask, 7.5 mmol (1 equiv.) of diazo compound **1** was dissolved in hexanes. In a separate 5.0 mL volumetric flask, 15 mmol (2.0 equiv.) of **5** was added and dissolved in hexanes. The solution of **5** was added to a 50 mL 3-neck flask fit with ReactIRTM probe, stir bar, and reflux condenser. Next, 0.1 mL of a 0.00075 M stock solution of Rh₂(S-DOSP)₄ was added to the solution of **5**. The reaction was brought to reflux (68 °C) and the ReactIRTM software was initiated (5 sec scanning for 3 h). A baseline was established over 4 min. Next, the diazo compound solution was added to the catalyst solution over a 1-h period via syringe pump. During the addition 100 µL reaction samples were taken for HPLC analysis. The samples were taken at t= 30 seconds, 90 seconds, 3 min, 6 min, 12 min, 18 min, 24 min, 30 min, 36 min, 42 min, 48 min, 54 min, and 60 min, After the initial 60 min addition, samples were taken in 10 min intervals until

decomposition of the diazo compound was no longer observed. The data was then imported into Excel and processed.

- (1) Davies, H. M. L.; Venkataramani, C. *Org. Lett.* **2003**, *5*, 1403.
- (2) Pelphrey, P.; Hansen, J.; Davies, H. M. L. *Chem. Sci.* **2010**, *1*, 254.
- (3) Davies, H. M. L.; Hansen, T.; Churchill, M. R. *J. Am. Chem. Soc.* **2000**, *122*, 3063.
- (4) Hansen, J.; Autschbach, J.; Davies, H. M. L. *J. Org. Chem.* **2009**, *74*, 6555.
- (5) Davies, H. M. L.; Morton, D. *Chem. Soc. Rev.* **2011**, *40*, 1857.
- (6) Doyle, M. P.; Colman, M. R.; Chinn, M. S. *Inorg. Chem.*, **1984**, *23*, 3684.
- (7) Doyle, M. P.; Wang, L. C.; Loh, K. L. *Tetrahedron Lett.* **1984**, *25*, 4087.
- (8) Blackmond, D. G.; Rosner, T.; Pfaltz, A. *Org. Process Res. Dev.* **1999**, *3*, 275.
- (9) Blackmond, D. G.; Schultz, T.; Mathew, J. S.; Loew, C.; Rosner, T.; Pfaltz, A. *Synlett* **2006**, 3135.
- (10) Ferretti, A. C.; Mathew, J. S.; Blackmond, D. G. *Ind. Eng. Chem. Res.* **2007**, *46*, 8584.
- (11) Davies, H. M. L.; Beckwith, R. E. J. *Chem. Rev.* **2003**, *103*, 2861.
- (12) Davies, H. M. L.; Manning, J. R. *Nature*. **2008**, *451*, 417.
- (13) Davies, H. M. L.; Du Bois, J.; Yu, J. Q. *Chem. Soc. Rev.* **2011**, *40*, 1855.
- (14) Hansen, J. H.; Gregg, T. M.; Ovalles, S. R.; Lian, Y. J.; Autschbach, J.; Davies, H. M. L. *J. Am. Chem. Soc.* **2011**, *133*, 5076.
- (15) Doyle, M. P.; McKervey, M. A.; Ye, T. *Modern Catalytic Methods for Organic Synthesis with Diazo Compounds: From Cyclopropanes to Ylides*; Wiley, 1998.

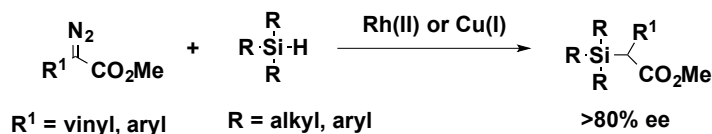
- (16) Espino, C. G.; Du Bois, J. *Angew. Chem. Int. Ed.* **2001**, *40*, 598.
- (17) Hinman, A.; Du Bois, J. *J. Am. Chem. Soc.* **2003**, *125*, 11510.
- (18) Wehn, P. M.; Lee, J. H.; Du Bois, J. *Org. Lett.* **2003**, *5*, 4823.
- (19) Espino, C. G.; Fiori, K. W.; Kim, M.; Du Bois, J. *J. Am. Chem. Soc.* **2004**, *126*, 15378.
- (20) Espino, C. G.; Du Bois, J. *Modern Rhodium-Catalyzed Organic Reactions* **2005**, 379.
- (21) Du Bois, J. *Org. Process Res. Dev.* **2011**, *15*, 758.
- (22) Roizen, J. L.; Harvey, M. E.; Du Bois, J. *Acc. Chem. Res.* **2012**, *45*, 911.
- (23) Li, Z. J.; Parr, B. T.; Davies, H. M. L. *J. Am. Chem. Soc.* **2012**, *134*, 10942.
- (24) Davies, H. M. L.; Hansen, T. *J. Am. Chem. Soc.* **1997**, *119*, 9075.

Chapter 4

Kinetic Studies on Donor/Acceptor Dirhodium(II) Carbene Si-H Insertion

4.1 Background

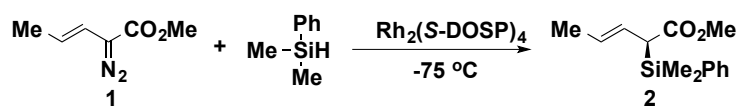
The asymmetric metal-carbene mediated Si-H insertion is a useful method for the synthesis of chiral silanes.¹⁻⁵ Chiral silanes are diverse organic intermediates, most often utilized in the asymmetric allylation and crotylation of aldehydes.⁶⁻¹⁰ Therefore, the development of methods for synthesizing chiral silanes has been a long-standing interest in organic chemistry. In particular, the application of dirhodium(II) and copper(I) aryl and vinyl carbenoids for Si-H insertion has been of interest to Doyle, Davies and Paneck (Scheme 4.1).^{2,3,7} Notably, Davies and co-workers have illustrated the exceptional asymmetric induction that can be obtained utilizing dirhodium(II) donor/acceptor carbenes when Rh₂(S-DOSP)₄ is used as catalyst.³ Paneck has exploited the use of Rh(II) carboxylates and Cu(I) salts for the synthesis of chiral allyl silanes in natural product synthesis.⁶⁻¹¹ A drawback to this chemistry, however, is the requirement for high catalyst loading and low reaction temperatures for high levels of asymmetric induction.



Scheme 4.1: Vinyl and aryl dirhodium(II) and copper(I) carbenoids are commonly utilized in the synthesis of chiral silanes.

Studies on asymmetric Si-H insertion by dirhodium(II) carbenoids have illustrated the sensitivity in achieving high enantio-induction. Based on independent studies by Davies and Panek, the requirement for high asymmetric induction includes low reaction temperature (-75 °C) and high catalyst loading (≥ 1.0 mol%).^{3,7} In one study, Panek and coworkers noted an increase in the enantioselectivity from 88% ee to 96% ee when the catalyst loading was increased from 1.0 mol% to 3.0 mol%.⁷ Additionally, increasing the concentration of silane trap has also been shown to increase enantioselectivity (Table 4.1). We suspect that the subtle changes in conditions having a large influence over the enantioselectivity is due to catalyst decomposition or deactivation. While, several kinetic studies have studied dirhodium(II) Si-H, none have commented on whether the catalyst undergoes decomposition or deactivation.

Table 4.1: Paneks' optimization of dirhodium donor/acceptor carbenoid Si-H insertion. Varying silane concentration and catalyst loading can have a significant influence over the % ee of the reaction.



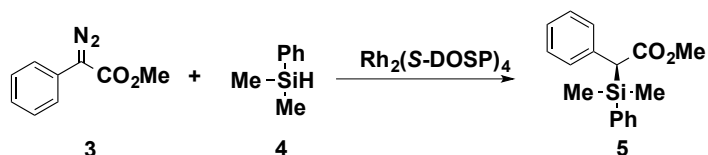
Entry	Catalyst Loading (mol%)	Equiv. of silane	Yield (%)	ee (%)
1	1	1.5	65	48
2	1	5	70	88
3	2	5	68	93
4	3	5	72	96

The kinetic studies on asymmetric Si-H insertion have focused on providing mechanistic evidence for the rate-limiting step.¹²⁻¹⁴ Work by Wang and coworkers focused on the electronic influence of the aryldiazoacetate and dirhodium(II) catalyst. These studies found that the electron donating or withdrawing nature of the aryl moiety and electronics of the catalyst can greatly influence the rate of the reaction.^{12,13} Additionally, ¹⁵N KIE studies have confirmed diazo decomposition as the rate-limiting step for Si-H insertion.¹⁴ In order to gain further mechanistic understanding on the Si-H insertion, RPKA experiments were conducted on the standard Si-H insertion using aryldiazoacetates as the carbene precursors and Rh₂(S-DOSP)₄ as the catalyst

4.2: Project Logic

Understanding catalyst deactivation is critical in assessing factors that contribute to high turnover number and high levels of enantioselectivity. The work conducted in this chapter focuses on kinetic studies to evaluate catalyst deactivation in Si-H insertion as well as the kinetic influence of common organic substrates utilized in C-H functionalization. At the onset of this work, we did not intend to study the enantioselectivity of the reaction because under the ambient temperatures planned for this study the levels of enantioselectivity for the reaction would be very low. Instead we postulated that the studies could give insight to whether catalyst decomposition was taking place. Additionally, while alkyl substituted silanes would have been optimum in the prevention of axial catalyst coordination, the infra-red signals for trimethyl- and triethylsilane overlapped with the diazo compound stretch, preventing the extraction of kinetic data. Consequently, dimethylphenylsilane was used as the trap (Scheme 4.2). We

suspected that minimal coordination of the Si-H trap would be observed; however, different excess experiments probing trap concentration would confirm this expectation.



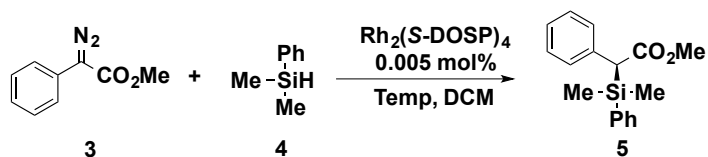
Scheme 4.2: Dirhodium donor/acceptor carbenoid mediated Si-H insertion reaction explored for the kinetic studies in this work.

4.3 Results

4.3.1. Si-H Kinetic Studies

Typical silane insertion reactions require 4-5 equiv. of silane trap; therefore, we initially explored 4 equiv. of silane with 0.005 mol% of catalyst. It was found at 10 °C the reaction was very exothermic, noting at 15 °C temperature rise. Decreasing the temperature to 0 °C and -20 °C still resulted in significant exotherms (10-15 °C) and decrease in catalytic activity. Catalytic activity was completely lost when the reaction was conducted at -75 °C under the high turnover conditions (Table 4.2). Increasing the concentration of the silane had no effect on deterring the exotherm or initial reaction rate. It was concluded that the reaction was close to zero order in silane and due to exotherm released from the reaction, only the initial 5 seconds of the reaction were utilized to extract kinetic data (Figure 4.1). For this reason, we abandoned the RPKA methodology and studied the reaction under the method of initial rates, utilizing the first 5 seconds of the reaction.

Table 4.2: Temperature influence on reaction exotherm for the reaction of **3** (0.3 M) with silane **4** (1.2 M) catalyzed by $\text{Rh}_2(\text{S-DOSP})_4$ in DCM.



Entry	Temp. (°C)	$T_i - T_{\max}$ (°C)
1	10	15
2	0	15
3	-20	10
4	-75	nr

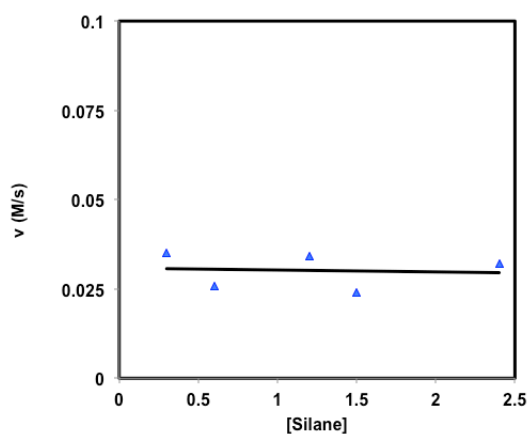


Figure 4.1: The initial rate of the reaction (v (M/s)) for the first 5 sec versus concentration of silane **4** (0.2-2.5 M) for the reaction of **3** (0.6 M) catalyzed by $\text{Rh}_2(\text{S-DOSP})_4$ (0.005 mol%) in dichloromethane at 10 °C. The plot shows that there is very little variance in the rate of the reaction upon increasing the concentration of silane.

The concentration dependencies of the diazo compound and catalyst were briefly explored to identify reaction-driving forces, as well as to determine whether the diazo compound decomposition was the rate-limiting step under these conditions. Varying diazo concentration, we found decreasing the concentration of diazo compound resulted in a slower reaction rate (Figure 4.2). This result is consistent with the results of Wang and co-workers, illustrating the rate dependency on diazo compound concentration. At higher concentrations of diazo compound, however, the rate tapers off, which is often observed in situations where saturation kinetics are at work.

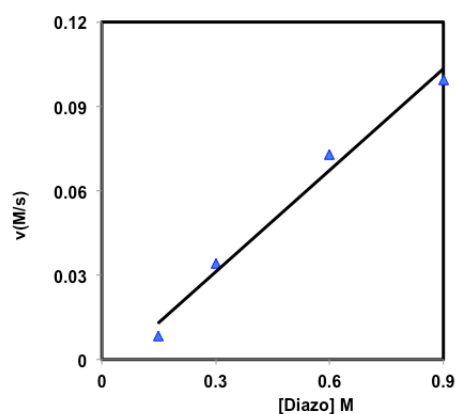


Figure 4.2: The initial rate of the reaction (v (M/s)) for the first 5 sec versus concentration of **3** (0.2-0.9 M) for the reaction of **4** (1.2 M) catalyzed by $\text{Rh}_2(\text{S-DOSP})_4$ (0.005 mol%) in dichloromethane at 10 °C. The initial rate of the reaction is plotted against the concentration of the diazo compound. The rate of the reaction decreases as the concentration of the diazo compound is decreased.

Increasing the concentration of catalyst had a positive influence on the rate of the reactions. Interestingly, while a nearly linear relationship was observed at higher catalyst concentrations, lowering the concentration to 1.0×10^{-5} M resulted in virtually no reaction, signifying catalyst deactivation or decomposition when trying to conduct 100,000 TON (Figure 4.3).

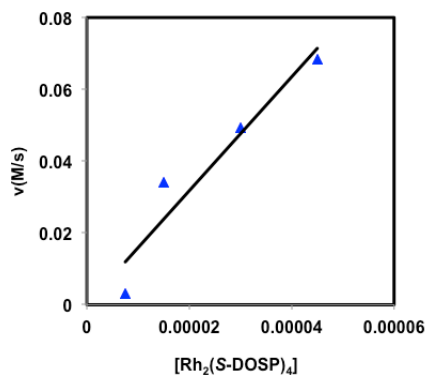


Figure 4.3: The initial rate of the reaction (v (M/s)) for the first 5 sec versus concentration of $\text{Rh}_2(\text{S-DOSP})_4$ (0.00001 - 0.000045 M) for the reaction of **4** (1.2 M) and **3** (0.4 M) in dichloromethane at 10°C . The initial rate of the reaction vs $[\text{Rh}_2(\text{S-DOSP})_4]$. As the concentration of catalyst is decreased the rate of the reaction decreases. At very low concentrations of catalyst (1.5×10^{-5} M) very little activity is observed.

4.3.2 Reaction Calorimetry

The inability to conduct RPKA studies, led us to explore multiple injection calorimetry for visualization of catalyst deactivation. Figure 4.4 illustrates the results of this study conducted on a 5.0 mL scale at 10 °C. In the initial screening, 0.2 mL injections of 1.5 mmol diazo compound were added to a solution of 1.2M dimethylphenylsilane and 0.007 mol% catalyst at 10 °C. The first injection resulted in 700 mW exotherm. Full decomposition of the diazo compound was observed after 20 min. The second injection, however, resulted in an exotherm of 250 mW. Intrigued by the significant decrease in exotherm after the first injection, a third injection was attempted resulting in a heat flow of <10 mw. Upon removal the calorimeter, an orange solution was retrieved signifying that the reaction did not go to completion. Additionally, calculation of the enthalpy (ΔH) per injection (49 kcal, 14 kcal, and 1 kcal respectively), further illustrates the partial conversion to the insertion product. Such a result suggests that the catalyst is significantly destroyed after ~14,000 TON. These results were unexpected, based on the robust nature of the reaction exhibited in kinetic studies. The results, however led to further exploration of multiple injection calorimetry.

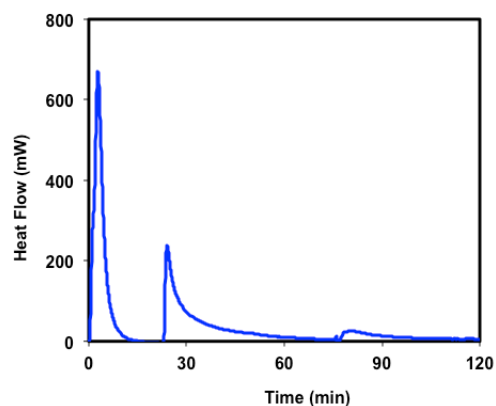
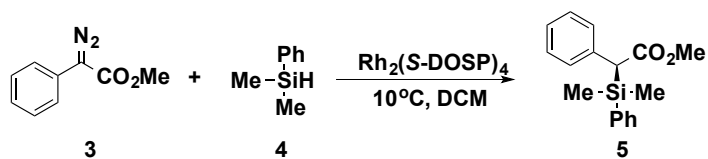


Figure 4.4: Multiple injection calorimetry. The heat flow of the reaction (mW) versus reaction time (min) for the reaction of **4** (1.2 M) with 0.2 mL injections of **3** (7.5 M) catalyzed by $\text{Rh}_2(\text{S-DOSP})_4$ (0.007 mol%) in dichloromethane at 10 °C. Full decomposition of the diazo compound is observed in the first injection. Subsequent injections, however, show little to no activity of the catalyst suggesting significant catalyst deactivation. The source of the deactivation is unknown.

The previous result inspired the exploration of conducting super high TON in one injection to test if the catalyst could uphold kinetic activity without a “rest” period. Here we define a “rest” period as the time between injections. Therefore, we opted to reduce the three injections of 1.5 mmol diazo compound into a single injection of 4.5 mmol. The single injection would have the same total concentration of the three injections previously conducted. To our surprise the full conversion of the diazo compound to the silane insertion product was observed after 12 min with a maximum of 3900 mW heat flow (Figure 4.5). This result suggested that the catalyst could indeed conduct ~42,000 TON, which means that higher TON’s can be achieved in a single batch reaction compared to a series of smaller batch reactions.

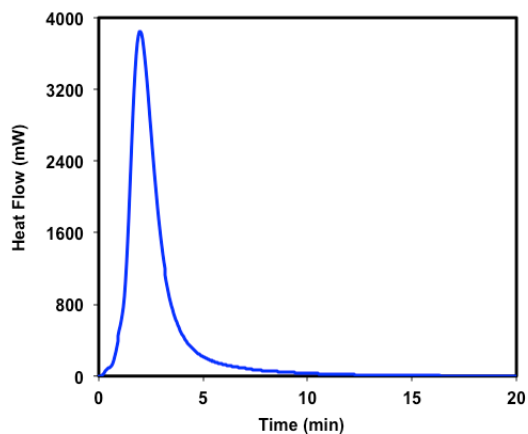
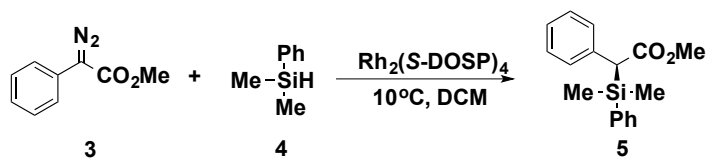


Figure 4.5: The heat flow of the reaction (mW) versus reaction time (min) for the reaction of **4** (1.2 M) with one 0.2 mL injection of **3** (4.5 mmol) catalyzed by $\text{Rh}_2(\text{S-DOSP})_4$ (0.007 mol%) in dichloromethane at 10 °C. 42,000 TONs of the catalyst was completed when the concentration of the diazo compound was increased from 1.5 mmol to 4.5 mmol. The heat released from the reaction reached a max heat of 3900 mW.

Kinetic studies on dirhodium(II) donor/acceptor carbenoid mediated cyclopropanation and C-H insertion illustrated that olefin coordination deactivated the catalyst; however, the interaction seemed to be integral in achieving high TONs of the dirhodium(II) catalyst. To test this hypothesis in the silane studies, addition of a “dummy olefin” to the reaction mixture was probed to determine if higher TON’s could be achieved. A “dummy olefin” was defined as an organic molecule containing double bond(s) where C-H insertion or cyclopropanation were not viable reaction pathways. In this regard, we chose to add one equivalent of trans-stilbene to the reaction mixture. Dirhodium(II) donor/acceptor carbenoids are not capable of cyclopropanating trans olefins due to steric restrictions. therefore, we were confident that any enhanced reactivity observed would be due to interaction between the olefin and the rhodium(II) catalyst and Si-H insertion.

Figure 4.6 describes the results of the multiple injection studies with trans-stilbene as an additive. Addition of diazo compound (1.5 mmol) resulted in an exotherm of 700 mW. Following the first injection, a second injection was conducted, resulting in an exotherm of 500 mW. Third and fourth injections resulted in 200 and 100 mW, respectively. While deactivation of the catalyst was still apparent, the results were a considerable improvement in catalyst efficiency compared to the previous multiple injection studies conducted in the absence of the alkene.

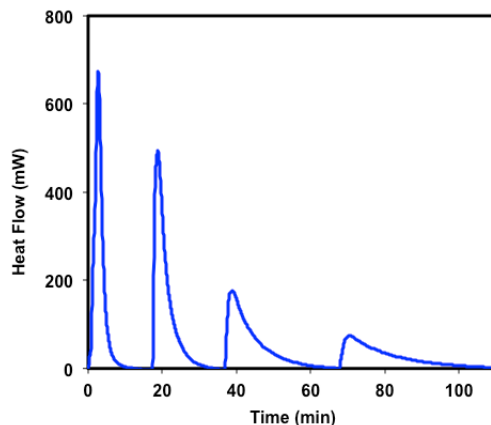
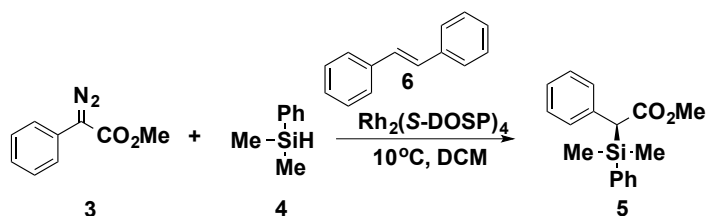


Figure 4.6: The heat flow of the reaction (mW) versus reaction time (min) for the reaction of **4** (1.2 M) with 0.2 mL injections of **3** (7.5 M) and additive **6** (7.5M) in the reaction mixture. The reaction is catalyzed by $\text{Rh}_2(\text{S-DOSP})_4$ (0.007 mol%) in dichloromethane at 10 °C. The equivalent of trans-stilbene added to the reaction mixture to determine if potential olefin coordination could increase the activity of the dirhodium(II) catalyst in the multiple injection studies. Addition of the olefin increased the overall activity, however, deactivation of the catalyst was still observed.

The results of the kinetic studies could be used to establish a mechanistic proposal for the Si-H insertion. The classical kinetic studies for Si-H insertion revealed a positive order in [Rh] and methyl phenyldiazoacetate. The silane substrate showed clear zero order kinetics, suggesting that there is no observed substrate coordination. These results are further evidence that N₂ extrusion is the rate-determining step. Based on the current kinetic experiments, we could not identify any off-reservoirs of the catalyst. While calorimetry experiments suggest that catalyst deactivation/decomposition does take place, the proposed catalytic cycle in Figure 4.7 does not explicitly denote off-cycle reservoirs of the catalyst. Furthermore, until further kinetic studies can be conducted on this system a full rate law will not be proposed.

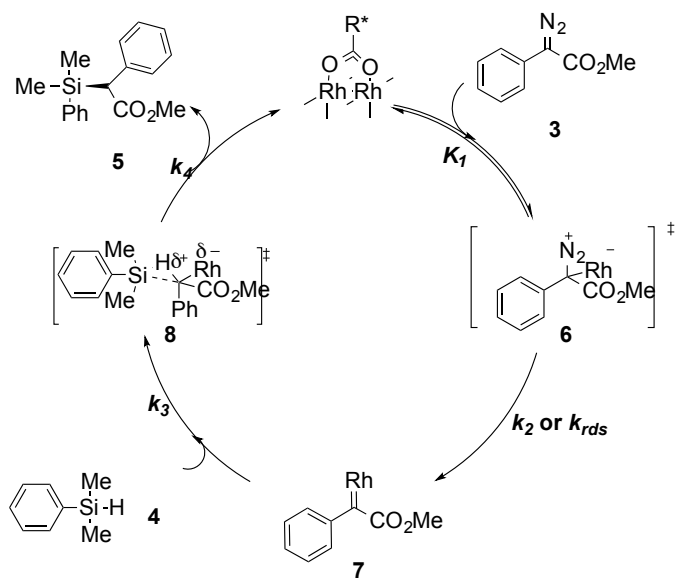


Figure 4.7: Potential reaction mechanism for dirhodium(II) carbenoid Si-H insertion into dimethylphenylsilane. Off-reservoirs of the catalyst are currently unknown, therefore the proposed mechanism is tentative and points out the lack substrate and product coordination to the catalyst

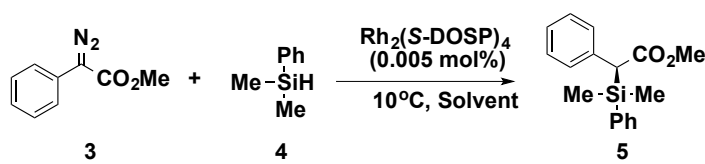
4.3.3 Further Kinetic Screening for Si-H Insertion

The kinetic information obtained from the Si-H insertion identified that the silane substrate had no influence over the rate of the reaction, rendering the reaction zero order in silane. Based on this result, we desired to further study factors contributing to deactivation of the dirhodium catalyst. Common C-H functionalization substrates, solvents, and “diazo decomposition products” were evaluated by ReactIR™. The initial rates, or first 5 seconds of the reactions, were compared to evaluate the relative rates of diazo decomposition.

The first study explored the influence of solvent on the rate of the reaction. The results are described in Table 4.3. As expected, common hydrocarbon solvents have little to no

influence over the relative rates of the reaction. Aromatic solvents, however, tend to afford a rate depression. This result is in line with spectroscopic studies conducted by Drago and coworkers with dirhodium(II) butyrate.^{15,16} In these early studies of dirhodium(II) carboxylates, Drago proposed that benzene can coordinate through weak interactions with the axial sites of the catalysts. Of particular interest was the affect of ethyl acetate. Recent studies have found that high asymmetric induction can be observed using ethyl acetate as a solvent.¹⁷ We believe coordination to the rhodium carbenoid via the acetate carbonyl incites a more robust metal carbenoid. Kinetic results suggest some type of catalyst/carbenoid interaction with ethyl acetate, as the rate of the reaction decreased in the presence of ethyl acetate.

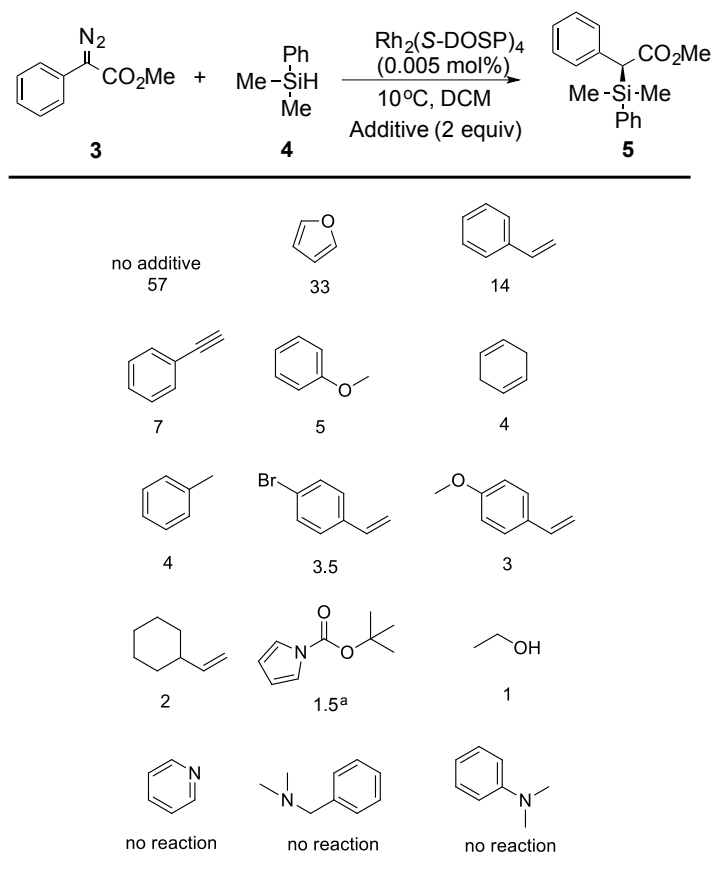
Table 4.3: Influence of solvent over the relative rate of the reaction of **3** (0.3 M) with silane **4** (1.2 M) catalyzed by $\text{Rh}_2(\text{S-DOSP})_4$ (0.005 mol%) in the appropriate solvent at 10 °C.



Entry	Solvent	Relative Rate
1	DCM	10
2	Hexanes	10
3	Pentane	10
4	Toluene	4
5	Ethyl Acetate	1

The next set of experiments, explored common substrates for C-H functionalization. A number of alkenes, alkynes, benzene derivatives and Lewis bases were tested for substrate coordination. In these reactions a 1:2 ratio of additive to dimethylphenyl silane was used. Based on N₂ extrusion as the rate determining state, additive coordination to the catalyst could induce rate depression or acceleration. We envision that the catalyst would be in equilibrium with the substrate bound catalyst; however, only the free catalyst would be available for carbenoid formation. Relative rates are detailed in Table 4.4. Again, rates were derived from the slope of the reaction profile over the first 5 sec of the reaction. Additives with Lewis basic sites strongly coordinate to the catalyst and shut down all catalytic activity. N-Boc pyrrole hindered catalytic activity for several minutes before slow decomposition of the diazo compound was observed, leading to the formation of the Si-H insertion product. While aromatic substrates coordinated, unactivated olefins tend to have stronger coordination, as seen with vinyl cyclohexane.

Table 4.4: Relative Rates for common substrates for C-H functionalization for the reaction of **3** (0.3 M) with silane **4** (1.2 M) catalyzed by $\text{Rh}_2(\text{S-DOSP})_4$ (0.005 mol%) doped with 2 equiv (0.5 M) of additive in DCM at 10 °C



^a No reaction for 2 minutes

In robust catalytic reactions, the diazo compound will decompose to form the rhodium carbenoid, and the carbenoid will then react to form the desired product. However, there are a number of other diazo compound decomposition products that are commonly observed as side products of less reactive C-H functionalization reactions. The most notable are the diazo compound azine, formed via reaction of the diazo compound with the rhodium carbenoid and pyrazole, which can spontaneously form from vinyl

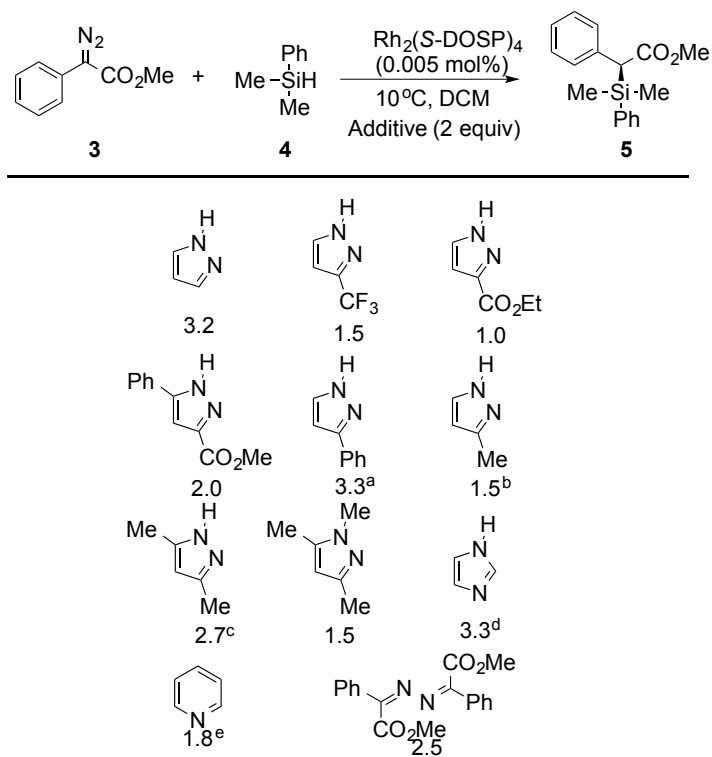
diazo compounds via nitrogen attack at the terminal end of the olefin, followed by a 1,5 proton shift. We believe in most vinylcarbenoid reactions a small amount of pyrazole can form, resulting in lower reaction yield. A common pyrazole formed from methyl phenylvinyl diazoacetate, as well as, a number of commercially available pyrazoles were tested for their effect on the reaction rate. Additionally, imidazole, pyridine, and the diazo compound azine were tested to investigate the influence of the nitrogenous additives on the rate of the reaction.

Experiments were conducted with a sub-stoichiometric amount of the heterocycle additives, due to the strong coordination Lewis basic sites can have to the dirhodium(II) catalyst. Catalyst and additive were premixed prior to addition to the reaction mixture. Upon mixture a quick solution color change took place. In most instances the catalyst changed from a bright green to a variant of blue or purple. This color change suggests that the additive is now coordinated to the catalyst in a 1:1 or 1:2 catalyst to adduct fashion.

The relative rates for additive addition are in table 4.5. Pyrazoles with electron deficient substituents in the 3-position tend to have a drastic effect on the rate of diazo compound decomposition. Relative rates 13x slower than the additive free system were observed. Interestingly, electron rich substituents in the 3-position caused an initial delay of 5-15s in catalytic activity before diazo compound decomposition. While the cause of the delay is currently unknown, it is possible that the N-H and 3-position CH₃ are hydrogen bonding to the carboxylate ligand preventing initial catalytic activity. Protection of the N-H with CH₃ (3,5 dimethyl pyrazole vs 1,3,5 trimethyl pyrazole)

resulted in no delay in catalytic activity; however, a slower relative rate was recorded. Imidazole and pyridine both caused a delay in catalytic activity. It is well known that pyridine strongly binds to dirhodium catalysts, as it has been used as a scaffold for polymer supported dirhodium catalysts. It is expected that imidazole would part-take in cooperative association to the catalyst similar to electron rich pyrazoles.

Table 4.5: Relative Rate of Si-H insertion with heterocycle additive for the reaction of **3** (0.3 M) with silane **4** (1.2 M) catalyzed by a 1:1 solution of $\text{Rh}_2(\text{S-DOSP})_4$ (0.005 mol%) and additive (0.005 mol%) in DCM at 10 °C



^a No reaction for 5 seconds

^b No reaction for 20 seconds

^c No reaction for 13 seconds

^d No reaction for 10 seconds

^e No reaction for 25 seconds

4.4 Discussion and Conclusions

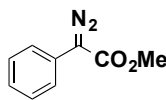
In summary, kinetic analysis has led to a more in depth understanding of factors that contribute to catalyst deactivation for dirhodium catalyzed carbenoid Si-H insertions. The exothermic nature of the reaction complicated the ability to conduct RPKA experiments, therefore initial rates were used to gain some kinetic insight. The initial rate data illustrated that the silane has a zero order dependence on the reaction, while diazo compound and catalyst are key driving-forces. Reaction calorimetry demonstrated that the catalyst deactivates but this deactivation can be alleviated with the addition of a “dummy olefin”. Moreover, solvent, substrate, and diazo compound side products can all lead to inhibition of the catalytic cycle.

4.5 Experimental

4.5.1 General Considerations

All reactions were carried out in oven-dried glassware under inert atmosphere. All chemicals were purchased, or found in the Davies Group Diazo Compound Library unless otherwise stated. All solvents used were either distilled or retrieved out of the solvent system and degassed 15 minutes prior to usage. Flash column chromatography was performed on silica gel. ^1H NMR Spectra were recorded at 400 and 600 MHz on a Varian 400, Inova 400, and Inova 600. ^{13}C NMR was recorded at 100 MHz on a Varian and Inova 400.

4.5.2 Characterization of Known Diazo Compounds



1

See Chapter 2.4.2 compound **1a**.

4.5.3 General procedure for kinetic measurements on ReactIRTM for Si-H Reactions

Experiments were carried out with a Mettler Toledo ReactIRTM 45m instrument equipped with a 9.5mm x 12" AgX 1.5m SiComp probe. Stock solutions of diazo compounds and Rh (II) catalysts in the appropriate solvent were prepared. To a dry round bottom flask was added a stir bar, trap, solvent and an aliquot of diazo compound solution. Unless otherwise noted, the reaction was cooled to 10 °C (*p*-dioxane, CO_{2(s)} bath) or 0 °C (ice/water bath) and allowed to equilibrate for 30 minutes. The ReactIRTM

probe was then inserted and the instrument set up for a continuous scan experiment. The scan was started and, at $t_0 = 20$ s, an aliquot of the catalyst solution was injected by syringe in one movement with vigorous stirring.

The reaction rates for the kinetic experiments herein were determined from the initial rates of the reaction. Due to the rapid decomposition of the diazo compound **1**, the first 5 seconds of the reaction was utilized to determine a reaction rate. This method was consistently used for all of the kinetic experiments in this chapter. An example of raw data extracted from a kinetic experiment for the reaction of **3** (0.3 M) with **4** (1.2 M) catalyzed by $\text{Rh}_2(\text{S-DOSP})_4$ (0.005 mol%) in dichloromethane at 10 °C can be found in Figure 4.8.

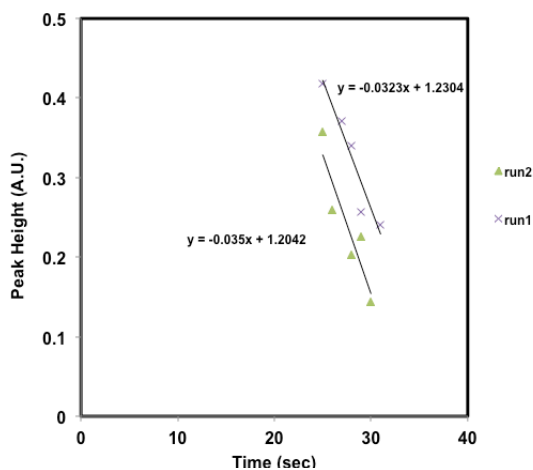
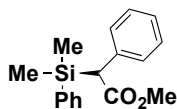


Figure 4.8: Two runs of Peak Height (A.U.) versus time (sec) for the first 5 seconds in the reaction of **4** (1.2 M) and **3** (0.4 M) catalyzed by $\text{Rh}_2(\text{S-DOSP})_4$ (0.0005 mol%) in dichloromethane at 10 °C.

4.5.4 Characterization Data of Known C-H functionalization Products



3

methyl (*R*)-2-(dimethyl(phenyl)silyl)-2-phenylacetate

See Chapter 3.9.4 compound 7.

4.5.5 Representative Kinetic Plots, Equations, and Rate Derivation

Calibration Curve for Methyl Phenyl diazoacetate (**1**)

See Chapter 2.4.6.

4.5.6 Multiple Injection Kinetic Experiments

See Chapter 2.4.8

4.5.7 General Procedure for Reactions Doped with Common C-H insertion Substrates:

Stock solutions of $\text{Rh}_2(\text{S-DOSP})_4$ (7.1 mg, 0.00374 mmol) were prepared 5.0 mL volumetric flasks in dichloromethane. In a separate 5.0 mL volumetric flask, **3** (0.810 mL, 1.5 mmol) and 2 equiv of C-H insertion substrate was added and dissolved in dichloromethane. To a 2-neck 25 mL flask fit with ReactIRTM probe and stir bar, the solution of **3** is added and cooled to 10 °C. The solution is allowed to equilibrate for 30 minutes. The ReactIRTM software is started for 5 sec scanning over 30 min. A stable signal is established (5 min) then at $t = 20$ sec the catalyst solution is added in one shot.

The reaction is monitored until completion. The raw data is then imported into Excel and processed.

4.5.8 General Procedure for Reactions Doped with Common Dirhodium(II) Posions:

Stock solutions of $\text{Rh}_2(\text{S-DOSP})_4$ (7.1 mg, 0.00374 mmol) and heterocycle additive (0.00374 mmol) were prepared 5.0 mL volumetric flasks in dichloromethane. The solution was allowed to equilibrate at 25 °C for 30 min – 1 hr prior to use. In a separate 5.0 mL volumetric flask, **3** (0.810 mL, 1.5 mmol) was added and dissolved in dichloromethane. To a 2-neck 25 mL flask fit with ReactIR™ probe and stir bar, the solution of **3** is added and cooled to 10 °C. The solution is allowed to equilibrate for 30 min. The ReactIR™ software is started for 5 sec scanning over 30 min. A stabile signal is established (5 min) then at $t = 20$ sec the catalyst/heterocycle solution is added in one shot. The reaction is monitored until completion. The raw data is then imported into Excel and processed.

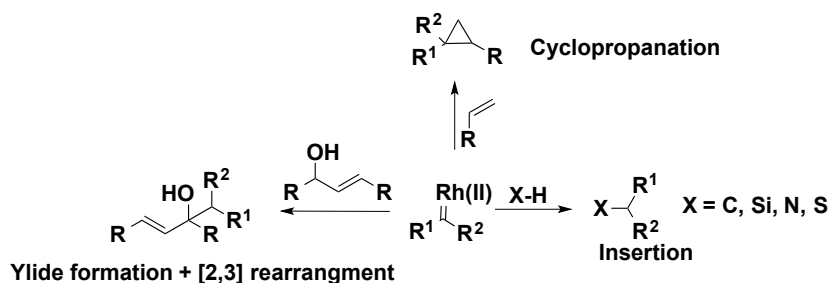
- (1) Bagheri, V.; Doyle, M. P.; Taunton, J.; Claxton, E. E. *J. Org. Chem.* **1988**, *53*, 6158.
- (2) Buck, R. T.; Doyle, M. P.; Drysdale, M. J.; Ferris, L.; Forbes, D. C.; Haigh, D.; Moody, C. J.; Pearson, N. D.; Zhou, Q. L. *Tetrahedron Lett.* **1996**, *37*, 7631.
- (3) Davies, H. M. L.; Hansen, T.; Rutberg, J.; Bruzinski, P. R. *Tetrahedron Lett.* **1997**, *38*, 1741.
- (4) Davies, H. M. L. *Curr. Org. Chem.* **1998**, *2*, 463.
- (5) Doyle, M. P. *Enan.* **1999**, *4*, 621.
- (6) Lee, J.; Panek, J. S. *Org. Lett.* **2011**, *13*, 502.
- (7) Wu, J.; Panek, J. S. *J. Org. Chem.* **2011**, *76*, 9900.
- (8) Zhu, K.; Panek, J. S. *Org. Lett.* **2011**, *13*, 4652.
- (9) Wu, J.; Zhu, K. C.; Yuan, P. W.; Panek, J. S. *Org. Lett.* **2012**.
- (10) Wu, J.; Chen, Y.; Panek, J. S. *Org. Lett.* **2010**, *12*, 2112.
- (11) Hu, T.; Takenaka, N.; Panek, J. S. *J. Am. Chem. Soc.* **2002**, *124*, 12806.
- (12) Wang, J.; Liang, F.; Chen, B. *J. Org. Chem.* **1998**, *63*, 8589.
- (13) Qu, Z.; Shi, W.; Wang, J. *J. Org. Chem.* **2001**, *66*, 8139.
- (14) Wong, F. M.; Wang, J.; Hengge, A. C.; Wu, W. *Org. Lett.* **2007**, *9*, 1663.
- (15) Drago, R. S.; Tanner, S. P.; Richman, R. M.; Long, J. R. *J. Am. Chem. Soc.* **1979**, *101*, 2897.
- (16) Drago, R. S.; Long, J. R.; Cosmano, R. *Inorg. Chem.* **1981**, *20*, 2920.
- (17) Qin, C. M.; Boyarskikh, V.; Hansen, J. H.; Hardcastle, K. I.; Musaev, D. G.; Davies, H. M. L. *J. Am. Chem. Soc.* **2011**, *133*, 19198.

CHAPTER 5

Kinetic Studies for the Dirhodium(II) Mediated Reactions of a Chemically Non-equivalent Bis-Diazo Compound

5.1: Background

The variety of reactions mediated by dirhodium(II) carbenes displays the versatility afforded by these highly reactive and selective intermediates.^{1,2} C-H Insertion,³ cyclopropanation,⁴⁻⁷ ylide formation,^{8,9} [2+3], [3+2], and [3+4] annulations,¹⁰⁻¹³ as well as, Si-H^{14,15} and vinylogous carbenoid reactions^{16,17} have been used as the foundation of new synthetic methods (Scheme 5.1). One of the key developments in dirhodium(II) carbene chemistry is the advent of chiral dirhodium(II) catalysts.



Scheme 5.1: Reactions that can be conducted with dirhodium(II) carbenoids

Recent studies conducted by Davies and coworkers have given greater insight into the synthetic utility of chiral catalyst $\text{Rh}_2(\text{S-DOSP})_4$.¹⁸ In the presence of donor/acceptor carbene precursors, the catalyst can achieve extremely high TON's, while much lower TON's are achieved with the traditional carbene precursors lacking a donor group. Combined with theoretical calculations, this recent work has created a strong argument for the increased selectivity of donor/acceptor carbenoids compared to the traditional dirhodium(II) acceptor-only

and acceptor/acceptor carbenoid. A challenge, however, is to control the selectivity of two chemically non-equivalent dirhodium(II) carbene precursors within the same molecule. While such “bis-diazo” compounds have been synthesized, their utility has been limited and no one, to our knowledge, has conducted a kinetic study to predict the reactivity of bis-diazo compounds for natural product synthesis (Figure 5.1).

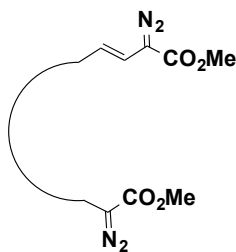
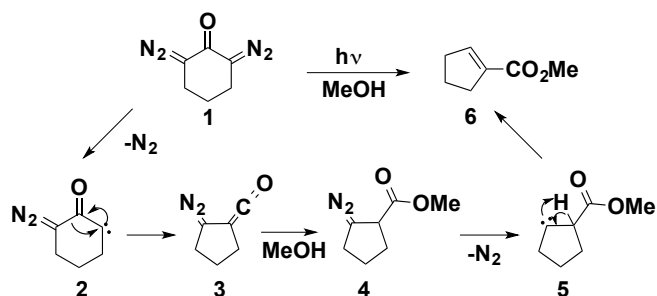


Figure 5.1: Generic Bis-Diazo Compound

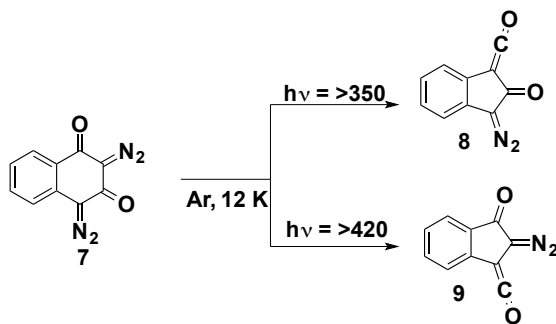
5.1.1: Bis-Diazo Compounds

The synthesis of highly functionalized organic molecules from bis-diazo compounds has a rich history in thermal, photochemical and transition-metal carbene chemistry.¹⁹⁻²⁹ There are several notable examples of complex molecules generated from bis-diazo compounds. One of the first examples of a photo-controlled decomposition of a bis-diazo compound was by Kirmise.¹⁹ Kirmise illustrated the photochemical ring contraction of the bis-diazo cyclohexanone **1** via a Wolff rearrangement to yield the cyclopentene **6** (Scheme 5.2).



Scheme 5.2: Kirmise's photochemical ring constriction of a bis-diazo compound.

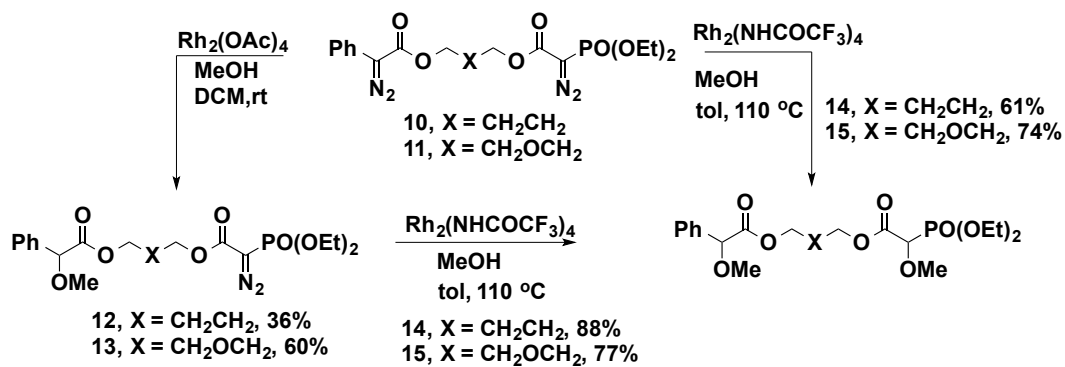
The early work with thermal and photochemical bis-diazo compounds focused on chemically equivalent diazo compounds, however, chemically non-equivalent bis-diazo compounds have also been extensively explored. In chemically non-equivalent bis-diazo compounds, one diazo moiety can often be selectively decomposed due to the differences in reactivity. Carva²⁰, Fields²¹ and Tomioka³⁰ have all demonstrated the utility of chemically non-equivalent bis-diazo compounds in synthesis. In particular, Tomioka has illustrated photocontrolled Wolff rearrangement of **7** can be controlled by attenuating the wavelength of the light exposed to the bis-diazo compound (Scheme 5.3).



Scheme 5.3: Tomioka's approach to photochemical selective photochemical decomposition of a bis-diazo compound.

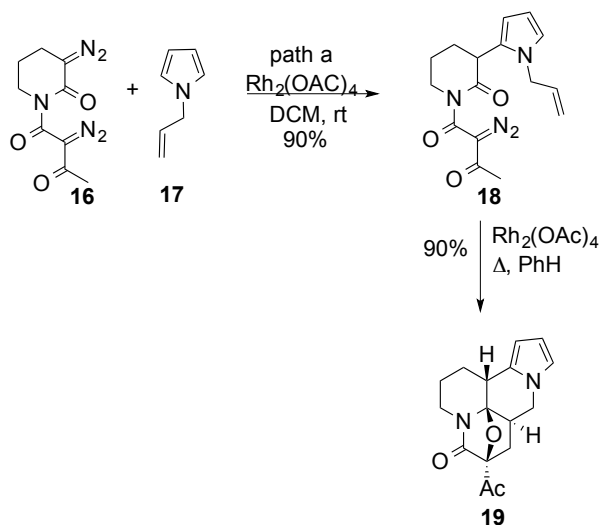
Transition metal mediated decomposition of bis-diazo compounds has been of particular interest in the chemical community due to the enhanced reactivity and selectivity of metal carbenoids.² Serratosa³¹, McKervey³², Doyle³³, Che³⁴ and Liu³⁵ have all demonstrated notable work with bis-diazo compounds. The majority of their efforts, however, have focused on compounds containing two chemically equivalent diazoacetates. Only recently, work by Moody³⁶ and Muthusamy³⁷ has illustrated synthetic efforts towards generating complex molecules from chemically non-equivalent diazoacetates.

Moody and coworkers have illustrated that selective decomposition can be achieved in chemically non-equivalent diazo compounds.³⁶ In the synthesis of **14** and **15**, Moody demonstrated the differences between utilizing a phosphonate flanked acceptor/acceptor diazoacetate compared to a donor/acceptor diazoacetate. In the presence of methanol and $\text{Rh}_2(\text{OAc})_4$, the selective decomposition of the donor/acceptor portion was afforded **12** and **13** (Scheme 5.4). $\text{Rh}_2(\text{NHCOCF}_3)_4$ and methanol were then used to afford decomposition of the acceptor/acceptor diazo compound. Alternatively, $\text{Rh}_2(\text{NHCOCF}_3)_4$ could induce simultaneous decomposition of both diazoacetates. This work illustrates the control that can be asserted with non-equivalent bis-diazo compounds as well as influence of the dirhodium(II) catalyst over the reactivity.



Scheme 5.4: Moody's selective decomposition of non-equivalent diazo compounds within a bis-diazo compound.

Muthusamy and coworkers have demonstrated the ability to conduct carbenoid and ylide chemistry within the same molecule, utilizing bis-diazoimide **16** (Scheme 5.5).³⁷ Treatment with N-allylpyrrole and $\text{Rh}_2(\text{OAc})_4$ resulted in the selective decomposition of the acceptor diazo portion and formation of **18** in 90 % yield. The mono-functionalized product can then be exposed to $\text{Rh}_2(\text{OAc})_4$ in refluxing benzene to give the polycyclic compound **19**, as a single diastereomer.



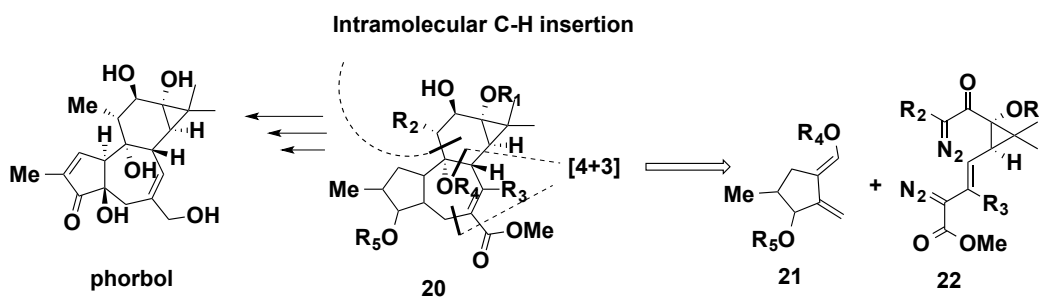
Scheme 5.5: Muthusamy's selective C-alkylation and cycloaddition.

5.2 Dr. Guzman's Results

The development and synthesis of bis-diazo compounds for use in natural product synthesis requires a understanding of the individual reactivity of each diazo compound, as well as the ability to accurately predict how the reactivity of the compounds will be affected by factors such as substrate, catalyst, solvent, and temperature. While synthetic efforts and reaction development the bis-diazo compounds are addressed in the thesis of Dr. Pablo Guzman,³⁸ herein, we will discuss a study on understanding the reactivity of the diazo compounds via reaction rates and catalyst inhibition.

In situ spectroscopic FTIR (ReactIRTM) was utilized to monitor the decomposition of the diazo compounds and calculate observed rate values. Using the method of initial rates, qualitative and quantitative information on donor/acceptor and traditional acceptor/acceptor diazo compounds is gathered in order to predict the reactivity of the bis-diazo compounds.

The plant-derived compound phorbol (Scheme 1) is a member of the diterpene family Tigliane.³⁹⁻⁴¹ Efforts to synthesize phorbol have been undertaken by a number of research groups including Wender and Cha.⁴²⁻⁴⁵ Additionally, several other groups have explored, “core-generating” methodologies.⁴²⁻⁵⁴ Former Davies graduate student, Dr. Pablo Guzman developed a retro-synthesis for Phorbol utilizing a chemically non-equivalent bis-diazo compound to build the core structure (Scheme 5.6). The retro-synthesis requires the bis-diazo compound to undergo two dirhodium(II) carbenoid mediated reactions, cyclopropanation/cope rearrangement and C-H insertion. Davies and coworkers have extensively studied the two dirhodium(II) carbenoid reactions proposed for the bis-diazo compound independently and high selectivity and enantioselectivity are routinely observed. The challenge Dr. Guzman faced, however, was the selective decomposition of one diazo compound in the presence of another.



Scheme 5.6: Retrosynthesis of phorbol

To probe the viability of bis-diazo inspired synthesis, model bis-diazo substrates **23** and **24** were synthesized by Dr. Guzman (Figure 5.2).³⁸ Based upon initial kinetic screenings by Dr. Guzman, it was predicted that in the presence of a Rh(II) catalyst and diene the donor/acceptor portion of **23/24** will first react in a [3+4] annulation fashion, followed by an intramolecular C-H

insertion by the acceptor/acceptor portion of the bis-diazo compound. This sequence of reactivity would afford a backbone similar to phorbol.

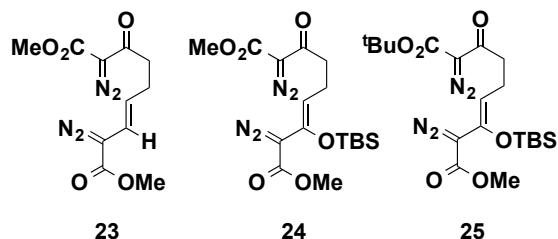
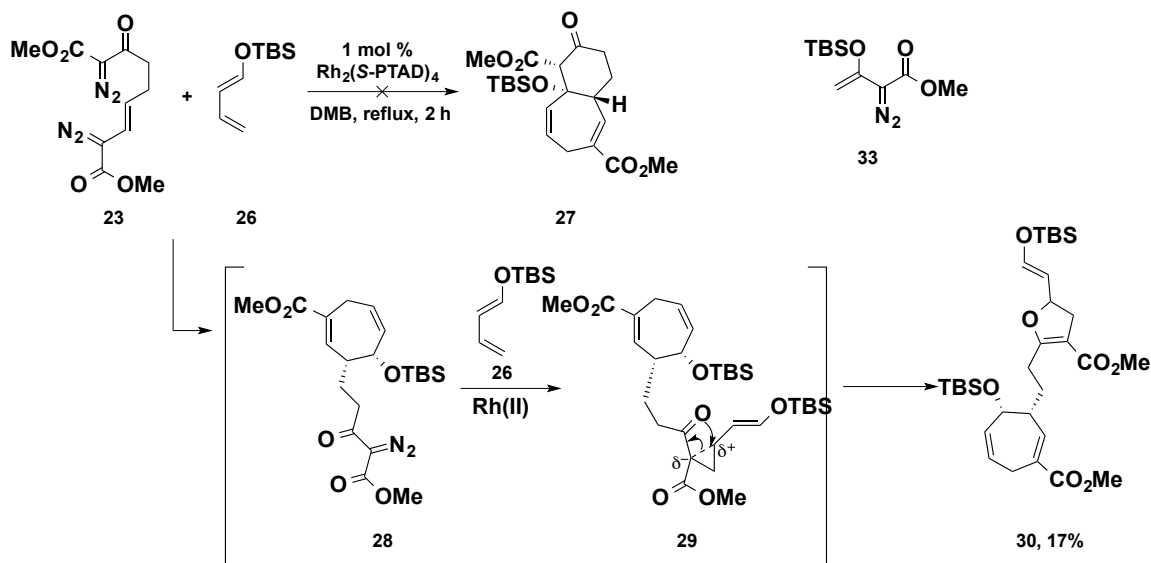


Figure 5.2: Bis-diazo compounds synthesized by Dr. Guzman for model study

However, in the presence of $\text{Rh}_2(\text{S-PTAD})_4$ and diene **26**, bis-diazo **23** did not form the expected cyclic product **27**. Instead the undesired product **30** was formed in 17%.³⁸ It is proposed that following the tandem cyclopropanation/Cope rearrangement the acceptor/acceptor portion reacted with the diene to give adduct **30** (Figure 5.7). The result suggested that the rates of reactivity for each diazo compound were too close to control selectivity, therefore, further kinetic studies were proposed to determine relative rates of reaction of the two diazo functionality.



Scheme 5.7: Reactivity of **23** with acyclic diene **26**

5.3 Goals of This Work

To study conditions suitable for the bis-diazo reaction, we set out to determine the relative reactivity profile of the diazoacetates in Figure 5.3 with competition studies as well as rates of decomposition for the individual diazo compounds. The cyclic diene, furan would be used in the majority of competition studies, due to its availability. The acyclic diene **26**, synthesized by Dr. Guzman, would be studied in a select number of reactions, after determining general reactivity profiles with furan. It was proposed that by studying the rate of decomposition for each diazo compound, we could learn how the catalyst interacted with diazo compound. Additionally, competition studies would assess the reactivity of the diazo compounds in the presence of each other.

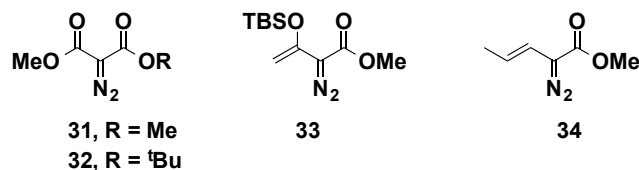


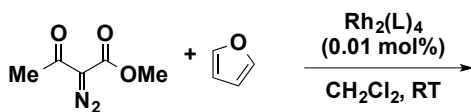
Figure 5.3: Diazo compounds explored in this study

5.4 Results

5.4.1 Kinetic Experiments of Diazo Compounds **31** and **32**

The unexpected reactivity observed with bis-diazo compound **24** sparked an interest in the activity of the acceptor/acceptor diazo compound. In particular, we were interested in how the steric bulk of the diazo compound and activity of the catalyst could influence the rate of diazo decomposition. Therefore, we set out to investigate the kinetic activity of two acceptor/acceptor diazo compounds with various dirhodium(II) catalysts. While $\text{Rh}_2(\text{S-PTAD})_4$ would be the optimum catalyst for a highly asymmetric cyclopropanation/cope rearrangement, we explored other catalysts to gain insight into the general activity of the diazo compounds. Additionally, we decided to explore increasing the bulk of the ester grouping from a methyl to a *t*-butyl group. We proposed, the increased steric bulk could potentially decrease the rate of decomposition. Studies of two acceptor/acceptor diazo compounds **31** and **32** were completed with furan in the presence of various chiral and achiral catalysts (Figure 5.4 and 5.5). A nonpolar, noncoordinating solvent CH_2Cl_2 was used to eliminate issues of solvation and unproductive catalyst-solvent binding. Finally, 0.01 mol% of catalyst was utilized to acquire reliable kinetic data.

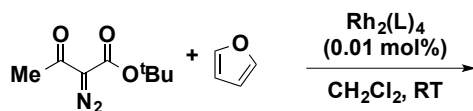
The relative rates of the diazo compound decomposition for **31** can be found in Table 5.1. Stark differences were observed between $\text{Rh}_2(\text{S-DOSP})_4$, which gave no decomposition, and $\text{Rh}_2(\text{S-PTAD})_4$, which displayed the fastest reaction rate. The achiral catalyst $\text{Rh}_2(\text{Piv})_4$ displayed an identical rate to $\text{Rh}_2(\text{S-PTAD})_4$. Their rates were 40x faster than the slowest catalyst $\text{Rh}_2(\text{TPA})_4$. The bridging achiral catalyst $\text{Rh}_2(\text{esp})_4$ and achiral catalyst $\text{Rh}_2(\text{Oct})_4$ both displayed significantly slower rates.

Table 5.1: Observed Rates for Diazo Compound **31**

Entry	L	Relative Rate
1	S-DOSP	NR
2	S-PTAD	44
3	Oct	2.5
4	Piv	44
5	Esp	12.5
6	TPA	1

The next set of experiments set out to explore the influence of ester size could have on the rate of decomposition. Therefore, ester of the diazo compound was modified increase steric bulk. Table 5.2 illustrates the rate observed for diazo compound **32**. Overall, slower rates were observed compared to the methyl ester diazoacetate **31**. $\text{Rh}_2(\text{S-DOSP})_4$, $\text{Rh}_2(\text{S-PTAD})_4$, and $\text{Rh}_2(\text{esp})_2$ displayed identical reaction rates. While, $\text{Rh}_2(\text{TPA})_4$ and $\text{Rh}_2(\text{Piv})_4$ demonstrated rates that were 6.5 times slower. $\text{Rh}_2(\text{Oct})_4$ fell in the middle with a rate a little more than half of $\text{Rh}_2(\text{S-DOSP})_4$, $\text{Rh}_2(\text{S-PTAD})_4$, and $\text{Rh}_2(\text{esp})$.

Table 5.2: Observed Rates for Diazo Compound **32**

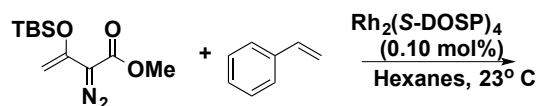


Entry	L	Relative Rate
1	S-DOSP	6.5
2	S-PTAD	6.5
3	Oct	3.8
4	Piv	1
5	Esp	6.5
6	TPA	1

Diazo compound **33** was initially studied with cyclopropanation of styrene, however it was discovered that the rate of the diazo compound could not be accurately determined due to variability in the reaction rate. Table 5.3 illustrates the results of a screening with diazo compound **33**. The time scale refers to the age of the diazo compound. As displayed in the table the older the diazo compound is the slower the reaction time. Re-purifying the diazo compound can bring back some of the activity (entries 3 and 4), however, the reaction time is not consistent. To overcome this challenge, competition studies between diazo compound **31** and **33** and **32** and **33** were conducted.

The competition reactions were conducted with freshly synthesized diazo compound to avoid any issues with diazo compound impurities. In retrospect, a standard test reaction should have been run prior to each kinetic experiment to ensure reproducibility, however, such a control reaction was not conducted. Instead, each competition reaction was conducted twice to verify the results. The goal of these reactions was to gain some qualitative information about the reactivity of the system. The ReactIR™ 3D plots were used as a visual description of the diazo compound decomposition. Competition reactions were completed in the presence of $\text{Rh}_2(\text{S-PTAD})_4$, because it is well established that $\text{Rh}_2(\text{S-PTAD})_4$ is an effective catalyst for the [4+3] annulation.

Table 5.3: Differences in reaction time for diazo compound **33**



Entry	Time	Reaction Time
1	1 hr	15 s
2	4 hr	36 s
3	14 days	20 min
4 ^a	14 days	5 min
5	6 months	1 hr, 38 min

^a Diazo compound was washed with $\text{NH}_4\text{Cl}(\text{aq})$ and dried with MgSO_4

5.4.2 Competition Studies

A competition reaction between **31** (0.6 M) and **33** (0.6 M) with furan (6.0 M) in the presence of 0.01 mol% $\text{Rh}_2(\text{S-PTAD})_4$ was conducted. The reaction was observed via ReactIR™ over a 16 h period (Figure 5.4), then allowed to stir without *in situ* monitoring for an additional 8 h. Slight decomposition of the donor/acceptor diazo compound **33** is observed, while the acceptor/acceptor diazo compound remained in tact.

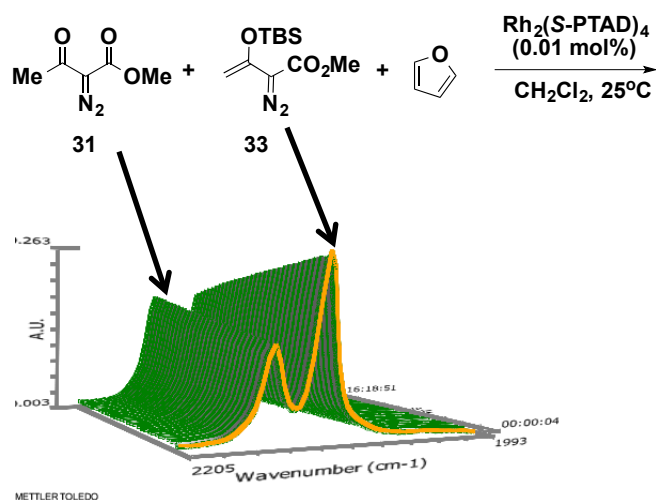


Figure 5.4: Plot of Abs versus Time for **31** (0.6 M) and **33** (0.6 M) in the presence of furan (6.0 M) and $\text{Rh}_2(\text{S-PTAD})_4$ (0.01 mol%). Slight decomposition of the donor/acceptor diazo compound **33** is observed, while no reactivity of **31** is displayed.

The reaction of **32** (0.6 M) and **33** (0.6 M) with furan (6.0 M) illustrated similar reactivity. In the presence of 0.01 mol% $\text{Rh}_2(\text{S-PTAD})_4$ no decomposition of the t-butyl diazo compound **32** was observed, while full decomposition was observed of the donor/acceptor diazo compound **33** (Figure 5.5).

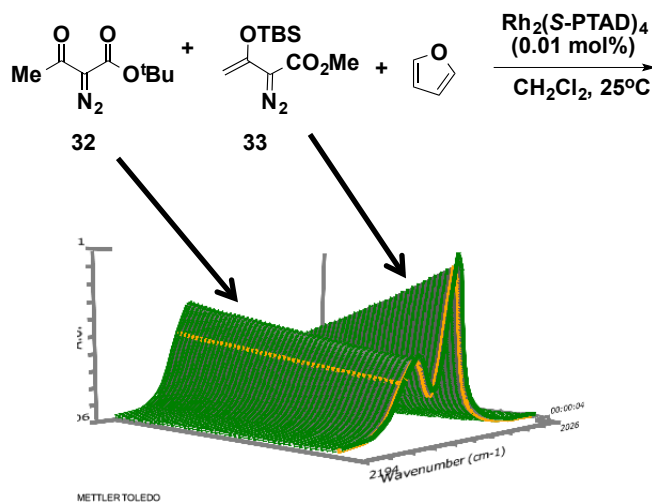


Figure 5.5: The competition reaction between **32** (0.6 M) and **33** (0.6 M) with furan (6.0 M) in the presence of $\text{Rh}_2(\text{S-PTAD})_4$ (0.01 mol%). Decomposition of the donor/acceptor diazo compound **33** is observed, while **32** remains untouched.

The activity of vinyl diazo **34** in the presence of the acceptor/acceptor diazo compounds **31** and **32** was additionally explored. Vinyl diazoacetates are known to be capable of rearrangement to pyrazoles. The influence of pyrazoles on dirhodium(II) catalyst activity has been discussed in chapter 4. The competition experiments were conducted in the presence of 0.01 mol% $\text{Rh}_2(\text{S-PTAD})_4$ and 10 equiv. of furan. The reaction of diazo compounds **34** and **31** with furan resulted in decomposition of the donor/acceptor diazo compound and no decomposition of the acceptor/acceptor diazo compound (Figure 5.6).

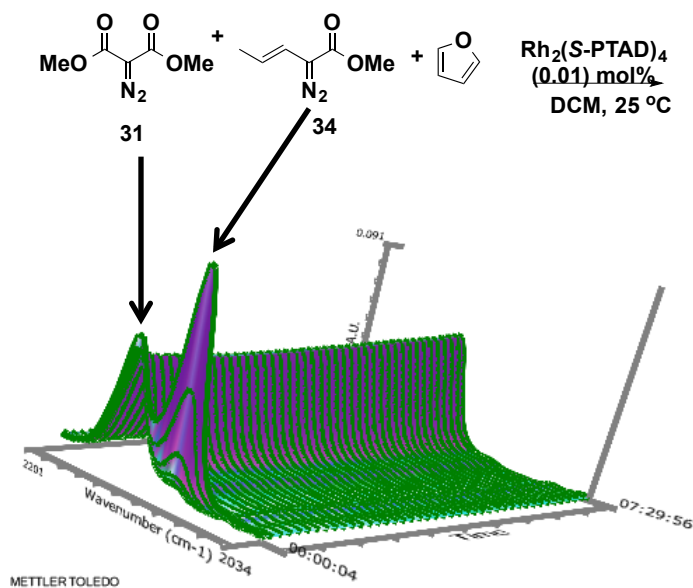


Figure 5.6: The competition reaction between **31** (0.6 M) and **34** (0.6 M) in the presence of furan (6.0 M) and $\text{Rh}_2(\text{S-PTAD})_4$ (0.01 mol%). Full decomposition of **34** is observed, while **31** remains untouched.

In the presence of the sterically bulkier diazo compound **32** similar reactivity was observed (Figure 5.7). Addition of 0.01 mol% catalyst to **32**, **34** and furan resulted in decomposition of the donor/acceptor diazo compound **34**. The bulky acceptor/acceptor diazo compound remained intact over the course of the reaction.

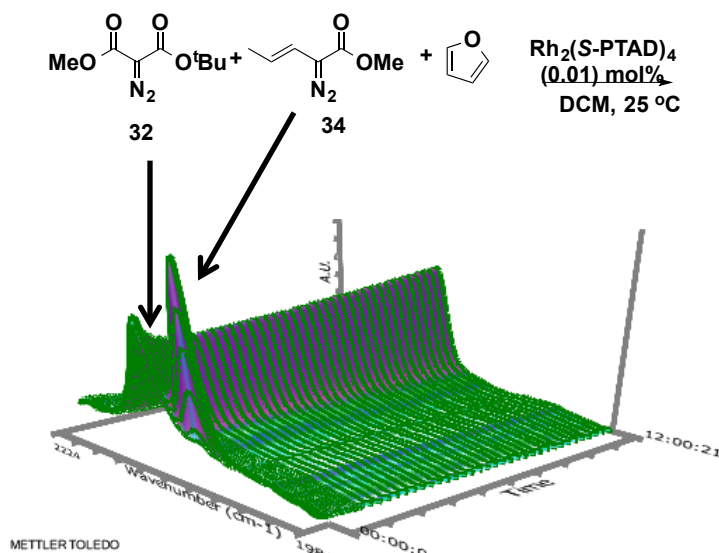


Figure 5.7: The competition reaction between 0.6 M **32** and 0.6 M **34** in the presence of 6.0 M furan and 0.01 mol% Rh₂(S-PTAD)₄. Full decomposition of **34** is observed, while **32** remains untouched.

In the model study conducted by Dr. Guzman, the acyclic diene **26** was utilized; therefore, a competition reaction was conducted with 6.0 M (10 equiv.) of diene **26** and 0.6 M diazo compounds **34** and **31**, respectively (Figure 5.8). In the presence of 0.01 mol% of $\text{Rh}_2(\text{S-PTAD})_4$, the decomposition of both diazo compounds was observed, however, diazo compound **34** demonstrated a significantly faster rate of decomposition than **31**. In the actual bis-diazo complex, Dr. Guzman observed decomposition of both diazo compounds as well, however selective reactivity of the acceptor/acceptor diazo compound for intramolecular C-H insertion could not be achieved, due to competitive intermolecular reactivity with diene **26**. To circumvent this problem a the competition reaction in the presence of a catalyst inhibitor was conducted to explore selective decomposition of the donor/acceptor diazo compound

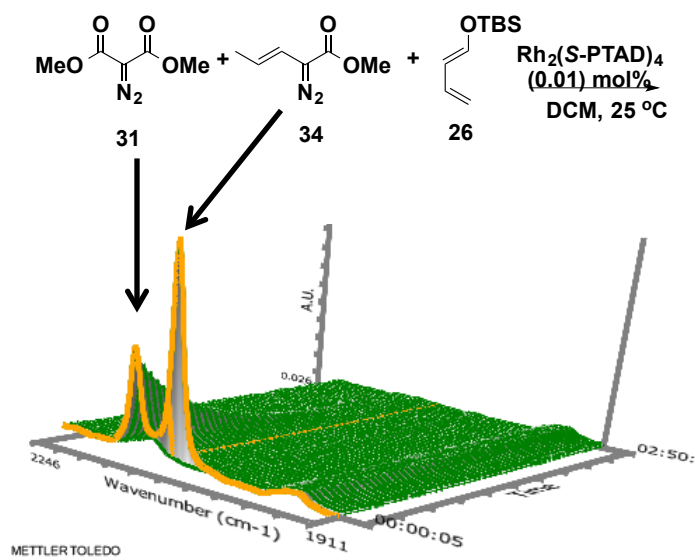
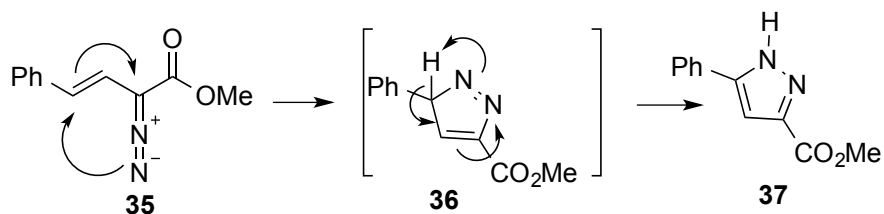


Figure 5.8: The competition reaction between **31** (0.6 M) and **34** (0.6 M) in the presence of diene **26** (6.0 M) and $\text{Rh}_2(\text{S-PTAD})_4$ (0.01 mol%). Full decomposition of both diazo compounds is observed.

In chapter 4, common dirhodium(II) catalyst inhibitors were explored to understand the influence such interactions can have over the rate of diazo decomposition. One of the inhibitors explored were the heterocycle pyrazole. Pyrazoles are commonly formed from vinyl diazo compounds, therefore, it is proposed that a small amount of pyrazole may be present in many reactions of vinyl diazo compounds (Scheme 5.8). Our goal in this study was to utilize a pyrazole as an inhibitor of the catalyst. It was proposed that if the catalyst was slightly inhibited only the most reactive carbenoid reaction would take place. Therefore pyrazole **37**, which is commonly formed from donor/acceptor diazo compound **35**, was tested in a competition study between **34** and **31** with 10 equiv of diene **26** and $\text{Rh}_2(\text{S-PTAD})_4$.



Scheme 5.8: Formation of the pyrazole from donor/acceptor carbenoid **35**.

Figure 5.9 depicts the results of pyrazole addition to the reaction mixture. The catalyst and inhibitor were premixed to a 1:1 ratio and allowed to equilibrate for 1-h prior to addition. To a solution of 0.6 M **34**, 0.6 M **31** and 6.0M diene **26**, the catalyst/pyrazole solution was added in one shot. Selective decomposition of donor/acceptor carbenoid was observed, while acceptor/acceptor diazo compound remained untouched. Dr. Guzman then utilized the conditions established by the competition study to afford selective decomposition of the donor/acceptor compound portion of bis-diazo compound **23**.

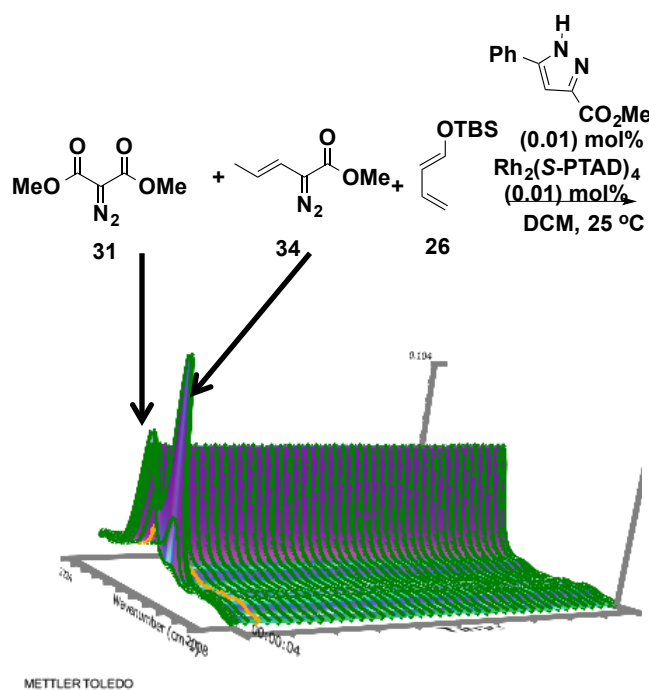


Figure 5.9: The competition reaction between diazo compound **31** (0.6 M) and **34** (0.6 M) in the presence of **26** (6.0 M), and 0.01 mol% 1:1 $\text{Rh}_2(\text{S-DOSP})_4$: pyrazole solution. Full decomposition of **34** is observed while **31** remains untouched.

5.4.3 Kinetic Studies of the Bis-Diazo Compounds

Based on the results from the competition studies, a goal of the bis-diazo project became to influence selective decomposition of the donor/acceptor compound. From there a second solution of catalyst could be used to induce decomposition of the acceptor/acceptor diazo compound. The thesis of Dr. Pablo Guzman explores the second decomposition study, however, here we will discuss a preliminary runs conducted with bis-diazo compound **24** and **25**.

Exposure of bis-diazo compound **24** to $\text{Rh}_2(\text{S-PTAD})_4$ and 10 equivalents of furan resulted in full decomposition of both diazo compounds. The result was unexpected, considering that competition studies suggested that sole decomposition of the donor/acceptor diazo compound should be observed. To circumvent the issue, however, a 1:1 solution of catalyst: pyrazole (0.01 mol%) solution was utilized. Under the modified conditions, selective decomposition of the donor/acceptor diazo compound was observed, compound **25** was purified and characterized by Dr. Pablo Guzman.

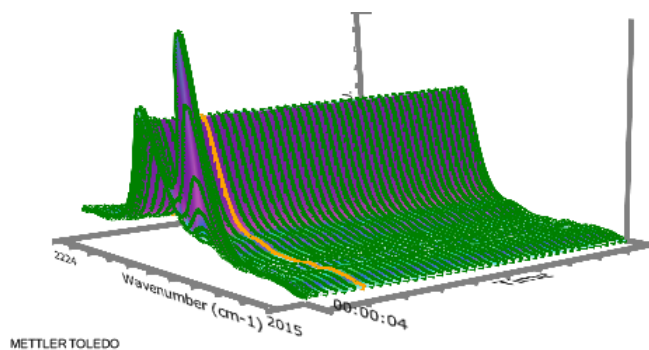
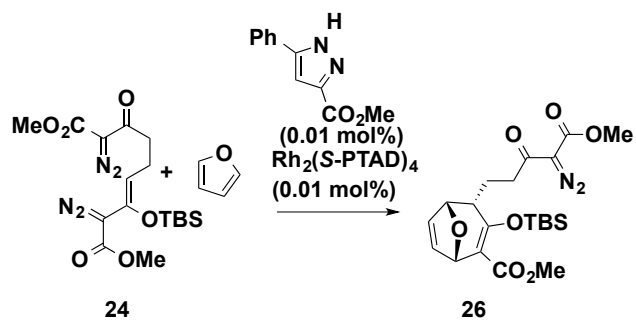


Figure 5.10: Reaction of the bis-diazo compound **24** (0.3 M) with furan (3.0 M) in the presence of a 1:1 solution $\text{Rh}_2(\text{S-PTAD})_4$ (0.01 mol%) and pyrazole additive (0.01 mol%). Decomposition of the donor/acceptor portion is observed, while the acceptor/acceptor portion remains untouched.

The initial catalyst screening of diazo compound **31** in reaction with furan demonstrated significant rate differences between $\text{Rh}_2(\text{S-DOSP})_4$ and $\text{Rh}_2(\text{S-PTAD})_4$ (Table 5.1). The cause for such apparent rate differences is not straightforward. Based on the result in Figure 5.10, however, we became curious about the activity bis-diazo compound **24** would display in the presence of $\text{Rh}_2(\text{S-DOSP})_4$. Therefore, **24** (0.3M) was reacted with furan (3.0M) in the presence of $\text{Rh}_2(\text{S-DOSP})_4$ (0.01 mol%) to yield selective decomposition of the donor/acceptor portion of the diazo compound to yield **25** (Figure 5.11). The result confirms that $\text{Rh}_2(\text{S-DOSP})_4$ and $\text{Rh}_2(\text{S-PTAD})_4$ have significantly different reactivity profiles for compounds containing diazo malonate moieties, however the basis of this behavior remains unknown.

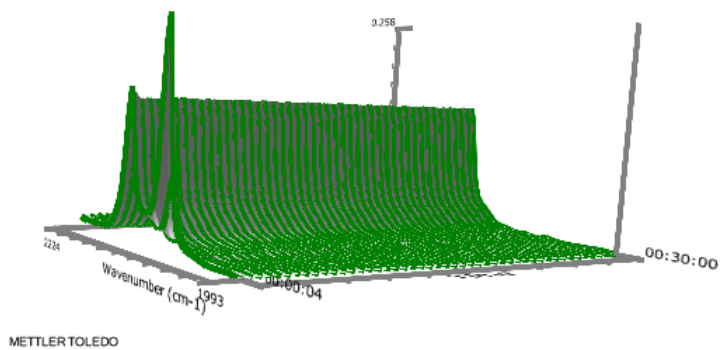
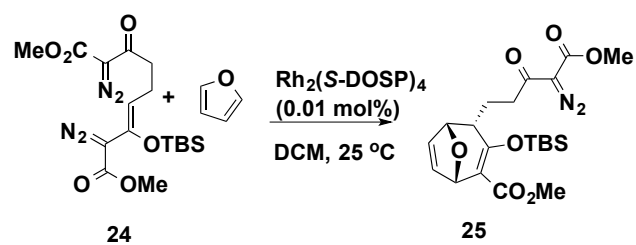


Figure 5.11: Reaction of the bis-diazo compound **24** (0.3 M) with furan (3.0 M) in the presence of $\text{Rh}_2(\text{S-DOSP})_4$ (0.01 mol%). Decomposition of the donor/acceptor portion is observed, while the acceptor/acceptor portion remains untouched.

Finally, to assess the reactivity of the t-butyl ester bis-diazo compound **25** (0.3 M), a reaction with 10 equivalents of furan catalyzed by $\text{Rh}_2(\text{S-PTAD})_4$ (0.01 mol%) was conducted. The experiment resulted in full decomposition of donor/acceptor portion, while the acceptor/acceptor portion remained in tact (Figure 5.12). The reaction gave adduct **27**, isolated by Dr. Guzman.

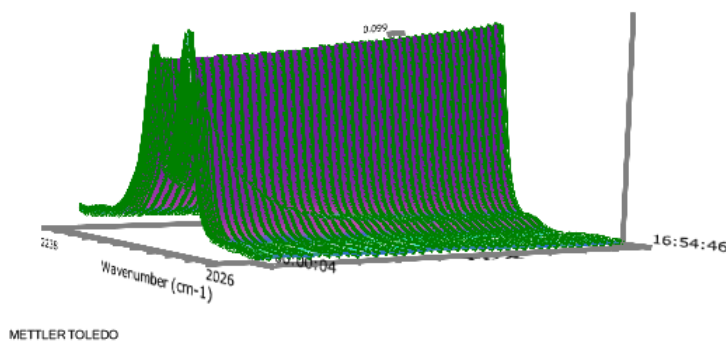
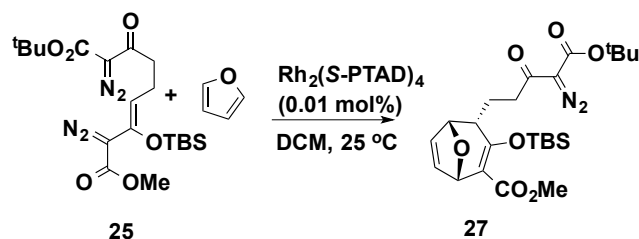


Figure 5.12: Reaction of the bis-diazo compound **25** (0.3M) with furan (3.0 M) in the presence of $\text{Rh}_2(\text{S-DOSP})_4$ (0.01 mol%). Decomposition of the donor/acceptor portion is observed, while the acceptor/acceptor portion remains untouched.

5.5 Discussion and Conclusions

The present study revealed the initial rates for diazo compounds **31** and **32**. While we were not able to make an inference on how the catalyst structure directly affected the rate of the reaction, based on the data presented, we can state that more sterically hindered diazo compounds afford slower rates. These rate differences are related to how the ester grouping interacts with the ligands on the catalysts. Computational studies could complement this hypothesis, by giving us a theoretical analysis of how the diazo compound approaches the catalyst, as well as, how the carbenoid sits in the coordination site.

As stated previously, it is not straightforward why such large rate differences are observed for the diazo compound **31** in the presence of $\text{Rh}_2(\text{S-DOSP})_4$ and $\text{Rh}_2(\text{S-PTAD})_4$ (Table 5.1). However, these results proved to be consistent when studying the model bis-diazo compound **24**. If anything, the result may suggest that $\text{Rh}_2(\text{S-DOSP})_4$ is more sensitive to structural changes than other dirhodium(II) catalysts.

Diazo compound **33** proved to be rather interesting. Throughout the study, irreproducible rates were observed due to some unknown catalyst inhibition. Is it worth noting that the reactions in this chapter are conducted with a large excess of substrate and that the substrate itself could potentially act as an inhibitor. While the issue of substrate coordination has been explored in Chapter 4, one could postulate that in the case of diazo compound **33**, both the substrate and the diazo compound are competitively binding to the catalyst, therefore the diazo compound itself is acting as an inhibitor. Another possibility is that the diazo is forming some impurity with a high binding affinity to the catalyst. While Pirrung and coworkers suggest that the diazo binding should be stronger and more favored than any weak Lewis acid impurity, the structure and

identity of the impurity present in our system is currently unknown; therefore, it is possible that this unknown impurity could have a greater binding affinity for the catalyst than the diazo compound. If this is the case, then the impurity would have a significant effect on catalyst deactivation.

The competition reactions proved to be insightful. In most cases, the competition reactions were able to predict the reactivity of the bis-diazo compound **24**. The method fell short, however, for the reaction of **24** in the presence furan catalyzed by of $\text{Rh}_2(\text{S-PTAD})_4$. In that case a pyrazole additive was necessary to control the reactivity of the acceptor/acceptor diazo portion.

Pyrazole inhibitor was capable of preventing the decomposition of the acceptor/acceptor diazo compound in reactions that demonstrated reactivity of both diazo compounds. The influence was exhibited in both competition reactions, as well as, the model bis-diazo compound **24**. The result suggests that inhibitors can have a significant influence over the decomposition of acceptor/acceptor diazo compounds. Additionally, the addition of additives to bis-diazo compound **24** is an attractive route toward building complex structures, which is further discussed in the thesis of Dr. Pablo Guzman.

The goal of this study was to understand the controlling factors for manipulating a chemically non-equivalent bis-diazo compound toward synthetic use based on reaction rates. The study has illustrated that sterics and the inherent differences between donor/acceptor and acceptor/acceptor diazo compounds have a significant influence over the reaction rate. In summary, low catalyst loading (0.01 mol %) and doping the catalyst with additives exert a large effect over the product distribution and rate. Studies by Dr. Pablo Guzman have expanded and exploited this chemistry in approaches to the synthesis of complex natural products.

5.6 Experimental

5.6.1 *General procedure for kinetic measurements on diazo acetates 31 and 32:* Experiments were carried out with a Mettler Toledo ReactIR™ 45m instrument equipped with a 9.5mm x 12” AgX 1.5m Si Comp probe. Stock solutions of Diazo Compounds and Rh(II) in CH₂Cl₂ were prepared. To a dry round bottom flask was added a stir bar, furan (10 equiv.), CH₂Cl₂ and an aliquot of diazoacetate solution (1.0 equiv, 0.6 M). The ReactIR probe was then inserted and the instrument set up for a continuous scan experiment. The scan was started and, at $t_0 = 20$ s, an aliquot of the catalyst solution was injected by syringe in one movement with vigorous stirring.

The percent conversion, η , was estimated from the following formula:

$$\eta = (|A_t - A^\circ| / |A_0 - A^\circ|) * 100\%$$

Where: A_t = Absorbance at time t .

A° = Absorbance at full conversion.

A_0 = Initial absorbance before reaction was started.

5.6.2 Example of Kinetic Data

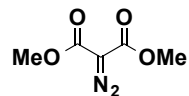
Only a single example is shown for the initial 3 minutes of the reaction of **31** (0.6M) with furan (6.0 M) and 0.01 mol % of $\text{Rh}_2(\text{S-DOSP})_4$:

Time (sec)	Peak Height	Time (sec)	Peak Height	Time(sec)	Peak Height
19	0.15334	79	0.129306	135	0.115945
23	0.148281	83	0.127611	139	0.116392
28	0.145122	87	0.127499	143	0.114345
33	0.139349	91	0.127452	147	0.115303
38	0.139625	95	0.125256	151	0.114614
42	0.139488	99	0.125287	155	0.112955
47	0.136333	103	0.123665	159	0.110625
52	0.136161	107	0.123116	163	0.111248
56	0.135191	111	0.121976	167	0.110666
61	0.134801	115	0.121123	171	0.109992
66	0.133117	119	0.121329	175	0.108303
71	0.132595	123	0.119857	179	0.106555
75	0.131038	127	0.118513	183	0.106741
79	0.129306	131	0.118323	187	0.106306

5.6.3 General procedure for kinetic measurements for competition studies: Experiments were carried out with a Mettler Toledo ReactIR™ 45m instrument equipped with a 9.5mm x 12” AgX 1.5m Si Comp probe. Stock solutions of Diazo Compounds and Rh(II) in CH_2Cl_2 were prepared. Stock solutions of Rh(II) in CH_2Cl_2 was prepared in a 5.0 mL volumetric flask (in cases where pyrazole are used, the catalyst solution is a 1:1 ratio of Rh(II) catalyst to pyrazole, the solution is allowed to equilibrate for 1 hour prior to use).. To a dry 2-neck round bottom flask fit with ReactIR™ probe was added a stir bar, furan (10 equiv.), CH_2Cl_2 and an aliquot of each diazoacetate solution (1.0 equiv, 0.6 M). The ReactIR™ software was set up for a continuous

scan experiment. The scan was started and, at $t_0 = 20$ s, an aliquot of the catalyst solution was injected by syringe in one movement with vigorous stirring.

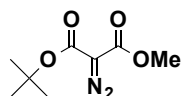
5.6.4 Synthesis of Known Diazo Compounds



31

methyl 2-diazo-3-oxobutanoate

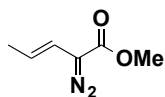
Et₃N (11.18 mL, 84.5 mmol, 1.2 equiv) was added to a solution of the methyl acetylacetate (7.60 mL, 70.4 mmol, 1.0 equiv) and the p-ABSA (18.50 g, 77 mmol, 1.1 equiv) in 150 mL of acetonitrile and stirred for 16 hr at rt. The formed precipitate was filtered off and the reaction mixture was quenched with 50 mL of saturated NH₄Cl solution and extracted with Et₂O (100 mL). The combined ether extracts were dried with MgSO₄ and filtered. The residue was concentrated and purified by flash chromatography using 20% Et₂O/hexanes to yield the desired product as a yellow oil. ¹H NMR (400 MHz, CDCl₃) δ 3.80 (s, 3H), 2.46 (s, 3H). The spectroscopic data are consistent with previously reported data.⁵⁵



32

***tert*-butyl 2-diazo-3-oxobutanoate**

Et₃N was added to a solution of the *t*butyl acetylacetate and the *p*-ABSA in 150 mL of acetonitrile and stirred for 16 hr at rt. The formed precipitate was filtered off and the reaction mixture was quenched with 50 mL of saturated NH₄Cl solution and extracted with Et₂O (100 mL). The combined ether extracts were dried with MgSO₄ and filtered. The residue was concentrated and purified by flash chromatography using 20% Et₂O/hexanes to yield the desired product as a yellow oil. 11.70 g (59% yield). ¹H NMR (400 MHz, CDCl₃) δ 2.46 (s, 3H), 1.534 (s, 9H). The spectroscopic data are consistent with previously reported data.⁵⁵

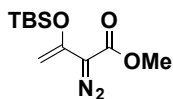


34

Methyl (E)-2-diazo-3-pentenoate

To a stirred solution of *trans*-pent-3-enoic acid (3.0 g, 30.0 mmol) in methanol (20 mL) was added concentrated H₂SO₄ (1 mL). The reaction mixture was stirred for 12 h at room

temperature and then slowly neutralized with saturated sodium bicarbonate (NaHCO₃). The aqueous layer was extracted with dichloromethane and the combined organic layers were washed with brine and dried (Na₂SO₄). The solvent was removed under reduced pressure and the remaining clear oil (3.30 g, 96% yield) was used for the next step, without further purification. To a stirred solution of methyl trans-pent-3-enoate (1.0 g, 8.76 mmol) and p-ABSA (3.15 g, 13.1 mmol) in CH₃CN (20 mL) cooled to 0°C, was added DBU (2.66 g, 17.5 mmol) in one portion. The reaction mixture was allowed to warm to room temperature over 7 h then quenched with saturated ammonium chloride (NH₄Cl). The aqueous layer was extracted with diethyl ether and the combined organic layers were washed with brine and dried (Na₂SO₄). The solvent was removed under reduced pressure and the residue was purified by flash chromatography (SiO₂, pentane) to give the title compound (0.80 g, 65% yield) as an orange oil, which was stored in pentane below -10°C until ready for use. ¹H NMR (400 MHz, CDCl₃) δ 5.77-5.74 (d, 1H, J = 16.0 Hz), 5.37-5.33 (m, 1H), 3.82 (s, 3H), 1.86-1.84 (d, 3H, J = 6.0 Hz). The spectroscopic data are consistent with the previously reported data.⁵⁶



33

***tert*-butyl 3-((*tert*-butyldimethylsilyl)oxy)-2-diazobut-3-enoate**

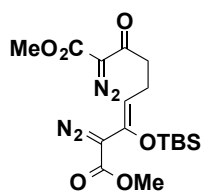
Et₃N (11.18 mL, 84.5 mmol, 1.2 equiv) was added to a solution of the methyl acetylacrylate (7.60 mL, 70.4 mmol, 1.0 equiv) and the p-ABSA (18.50 g, 77 mmol, 1.1 equiv) in 150 mL of acetonitrile and stirred for 16 hr at rt. The formed precipitate was filtered off and the reaction

mixture was quenched with 50 mL of saturated NH_4Cl solution and extracted with Et_2O (100 mL). The combined ether extracts were dried with MgSO_4 and filtered. The residue was concentrated and purified by flash chromatography using 20% Et_2O /hexanes to yield the desired product as a yellow oil. The yellow oil is dissolved in 100 mL of DCM and cooled to 0 °C. Triethylamine (9.0 mL, 65.3 mmol, 1.4 equiv.) is slowly added followed by slow addition (over 5 minute period) of tertbutyldimethylsilyl triflate (12 mL, 51.3 mmol, 1.2equiv.). The reaction mixture was allowed to stir at 0 °C for 1 hour then diluted with 100 mL of hexanes. The organic solution is washed with 100 mL of dilute NaHCO_3 . The organic layer is dried with MgSO_4 , and concentrated to yield a dark orange oil. This oil was purified via flash chromatography on silica in 9:1 Pentane: Ether eluent to give 70% yield of an orange oil. ^1H NMR (400 MHz, CDCl_3) δ NMR (400J= 2, 1H), 4.21 (d, J = 2, 1H), 3.80 (s, 3H), 0.98 (s, 9H), 0.21 (s, 6H). The spectroscopic data are consistent with previously reported data.⁵⁵

5.6.5 *General procedure for kinetic measurements for reactions with compound 24 and 25:*

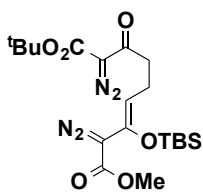
Experiments were carried out with a Mettler Toledo ReactIR™ 45m instrument equipped with a 9.5mm x 12” AgX 1.5m Si Comp probe. A 0.00075 M (7.1 mg, 0.0000375 mmol) Stock solutions of Rh(II) in CH_2Cl_2 was prepared in a 5.0 mL volumetric flask (in cases where pyrazole are used, the catalyst solution is a 1:1 ratio of Rh(II) catalyst to pyrazole, the solution is allowed to equilibrate for 1 hour prior to use). In a separate 5.0 mL volumetric flask **24** (1.5 mmol) and furan (30 mmol) are added and dissolved in DCM. To a 2-neck, dry round bottom flask fit with ReactIR™ probe was added a stir bar, and 5.0 mL solution of furan and **24**. The ReactIR™ software was then set up for a continuous scan experiment (rapid collect, 30 min). The scan was started and, at $t_0 = 20$ s, an aliquot of the catalyst solution was injected by syringe in one movement with vigorous stirring.

5.6.7 Compounds Characterized by Dr. Pablo Guzman³⁸



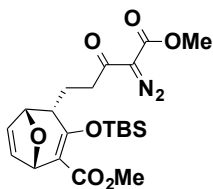
24

(Z)-dimethyl 3-((tert-butyldimethylsilyl)oxy)-2,8-bis(diazo)-7-oxonon-3-enedioate³⁸



25

(Z)-9-tert-butyl 1-methyl 3-((tert-butyldimethylsilyl)oxy)-2,8-bis(diazo)-7-oxonon-3-enedioate³⁸

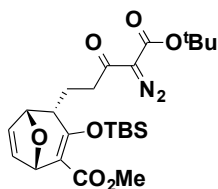


205

26

methyl (1*S*,4*S*,5*R*)-3-((*tert*-butyldimethylsilyl)oxy)-4-(4-diazo-5-methoxy-3,5-dioxopentyl)-8-oxabicyclo[3.2.1]octa-2,6-diene-2-carboxylate³⁸

38



27

(1*R*,4*R*,5*S*)-methyl 4-(5-(*tert*-butoxy)-4-diazo-3,5-dioxopentyl)-3-((*tert*butyldimethylsilyl)oxy)-8-oxabicyclo[3.2.1]octa-2,6-diene-2-carboxylate³⁸

- (1) Davies, H. M. L.; Manning, J. R. *Nature*. **2008**, *451*, 417.
- (2) Doyle, M. P.; McKervey, M. A.; Ye, T. *Modern Catalytic Methods for Organic Synthesis with Diazo Compounds: From Cyclopropanes to Ylides*; Wiley, 1998.
- (3) Davies, H. M. L.; Morton, D. *Chem. Soc. Rev.* **2011**, *40*, 1857.
- (4) Doyle, M. P. *Modern Rhodium-Catalyzed Organic Reactions* **2005**, 341.
- (5) Ventura, D. L.; Li, Z. J.; Coleman, M. G.; Davies, H. M. L. *Tetrahedron* **2009**, *65*, 3052.
- (6) Nadeau, E.; Ventura, D. L.; Brekan, J. A.; Davies, H. M. L. *J. Org. Chem.* **2010**, *75*, 1927.
- (7) Wang, H. B.; Guptill, D. M.; Varela-Alvarez, A.; Musaev, D. G.; Davies, H. M. L. *Chem. Sci.* **2013**, *4*, 2844.
- (8) Parr, B. T.; Li, Z. J.; Davies, H. M. L. *Chem. Sci.* **2011**, *2*, 2378.
- (9) Li, Z. J.; Parr, B. T.; Davies, H. M. L. *J. Am. Chem. Soc.* **2012**, *134*, 10942.
- (10) Davies, H. M. L.; Hu, B. H. *Tetrahedron Lett.* **1992**, *33*, 453.
- (11) Davies, H. M. L.; Matasi, J. J.; Hodges, L. M.; Huby, N. J. S.; Thornley, C.; Kong, N.; Houser, J. H. *J. Org. Chem.* **1997**, *62*, 1095.
- (12) Davies, H. M. L.; Kong, N.; Churchill, M. R. *J. Org. Chem.* **1998**, *63*, 6586.
- (13) Lian, Y. J.; Davies, H. M. L. *J. Am. Chem. Soc.* **2010**, *132*, 440.

- (14) Davies, H. M. L.; Hansen, T.; Rutberg, J.; Bruzinski, P. R. *Tetrahedron Lett.* **1997**, *38*, 1741.
- (15) Buck, R. T.; Doyle, M. P.; Drysdale, M. J.; Ferris, L.; Forbes, D. C.; Haigh, D.; Moody, C. J.; Pearson, N. D.; Zhou, Q. L. *Tetrahedron Lett.* **1996**, *37*, 7631.
- (16) Valette, D.; Lian, Y. J.; Haydek, J. P.; Hardcastle, K. I.; Davies, H. M. L. *Angew. Chem. Int. Ed.* **2012**, *51*, 8636.
- (17) Smith, A. G.; Davies, H. M. L. *J. Am. Chem. Soc.* **2012**, *134*, 18241.
- (18) Hansen, J.; Autschbach, J.; Davies, H. M. L. *J. Org. Chem.* **2009**, *74*, 6555.
- (19) Kirmse, W. *Angew. Chem. Int. Ed.* **1959**, *71*, 381.
- (20) Cava, M. P.; Glamkows.Ej; Weintrau.Pm *J. Org. Chem.* **1966**, *31*, 2755.
- (21) Borch, R. F.; Fields, D. L. *J. Org. Chem.* **1969**, *34*, 1480.
- (22) Rubin, M. B.; Bargurie, M.; Kosti, S.; Kaftory, M. *J. Chem. Soc. Perk. T. 1.* **1980**, 2670.
- (23) Tosi, G.; Cardellini, L.; Pellicciari, R.; Fringuelli, R. *Gazz. Chim. Ital.* **1981**, *111*, 379.
- (24) Maas, G.; Ganster, O.; Regitz, M.; Eistert, B. *Chem. Ber.-Recl.* **1982**, *115*, 435.
- (25) Sugawara, T.; Bethell, D.; Iwamura, H. *Tetrahedron Lett.* **1984**, *25*, 2375.
- (26) Bethell, D.; Gallagher, P.; Bott, D. C. *J. Chem. Soc. Perk. T. 2.* **1989**, 1097.
- (27) Bethell, D.; Gallagher, P.; Self, D. P.; Parker, V. D. *J. Chem. Soc. Perk. T. 2.* **1989**, 1105.
- (28) Koga, N.; Matsumura, M.; Noro, M.; Iwamura, H. *Chem. Lett.* **1991**, 1357.
- (29) Sung, D. D.; Park, Y. M.; Kim, K. C.; Park, D. K. *B Kor. Chem. Soc.* **1993**, *14*, 335.

- (30) Tomioka, H.; Okuno, A.; Sugiyama, T.; Murata, S. *J. Org. Chem.* **1995**, *60*, 2344.
- (31) Font, J.; Valls, J.; Serratosa, F. *Tetrahedron* **1974**, *30*, 455.
- (32) Kulkowit, S.; Mckervey, M. A. *Chem. Comm.* **1978**, 1069.
- (33) Doyle, M. P.; Hu, W. H.; Phillips, I. M.; Wee, A. G. H. *Org. Lett.* **2000**, *2*, 1777.
- (34) Li, G. Y.; Che, C. M. *Org. Lett.* **2004**, *6*, 1621.
- (35) Xiao, L.; Liao, L.; Liu, L.; Li, Y. *New. J. Chem.* **2013**, *37*, 1874.
- (36) Moody, C. J.; Miller, D. J. *Tetrahedron* **1998**, *54*, 2257.
- (37) Muthusamy, S.; Gunanathan, C.; Nethaji, M. *J. Org. Chem.* **2004**, *69*, 5631.
- (38) Davies, H. M. L.; Hubby, N. J. S. *Tetrahedron Lett.* **1992**, *33*, 6935.
- (39) Nishizuka, Y. *Natur.* **1984**, *308*, 693.
- (40) Evans, F. J. *Naturally Occuring Phorbol Esters*; CRC Press: Boca Raton, 1986.
- (41) Rosfjord, E. C.; Maemura, M.; Johnson, M. D.; Torri, J. A.; Akiyama, S. K.; Woods, V. L.; Dickson, R. B. *Exp. Cell. Res.* **1999**, *248*, 260.
- (42) Wender, P. A.; Kogen, H.; Lee, H. Y.; Munger, J. D.; Wilhelm, R. S.; Williams, P. D. *J. Am. Chem. Soc.* **1989**, *111*, 8957.
- (43) Wender, P. A.; McDonald, F. E. *J. Am. Chem. Soc.* **1990**, *112*, 4956.
- (44) Wender, P. A.; Rice, K. D.; Schnute, M. E. *J. Am. Chem. Soc.* **1997**, *119*, 7897.
- (45) Lee, K.; Cha, J. K. *J. Am. Chem. Soc.* **2001**, *123*, 5590.
- (46) Rigby, J. H.; Kierkus, P. C.; Head, D. *Tetrahedron Lett.* **1989**, *30*, 5073.
- (47) Harwood, L. M.; Ishikawa, T.; Phillips, H.; Watkin, D. *Chem. Comm.* **1991**, 527.
- (48) Shigeno, K.; Sasai, H.; Shibasaki, M. *Tetrahedron Lett.* **1992**, *33*, 4937.
- (49) Dauben, W. G.; Dinges, J.; Smith, T. C. *J. Org. Chem.* **1993**, *58*, 7635.

- (50) McMills, M. C.; Zhuang, L. H.; Wright, D. L.; Watt, W. *Tetrahedron Lett.* **1994**, *35*, 8311.
- (51) Paquette, L. A.; Sauer, D. R.; Edmondson, S. D.; Friedrich, D. *Tetrahedron* **1994**, *50*, 4071.
- (52) Carroll, G. L.; Little, R. D. *Org. Lett.* **2000**, *2*, 2873.
- (53) Ovaska, T. V.; Roses, J. B. *Org. Lett.* **2000**, *2*, 2361.
- (54) Page, P. C. B.; Hayman, C. M.; McFarland, H. L.; Willock, D. J.; Galea, N. M. *Synlett* **2002**, 583.
- (55) Davies, H. M. L.; Ahmed, G.; Churchill, M. R. *J. Am. Chem. Soc.* **1996**, *118*, 10774.
- (56) Davies, H. M. L.; Smith, H. D.; Hu, B. H.; Klenzak, S. M.; Hegner, F. J. *J. Org. Chem.* **1992**, *57*, 6900.